United States Nuclear Regulatory Commission
Protecting People and the Environment

NUREG/CR-6428, Rev. 1
ANL/EVS-17/3

Effects of Thermal Aging on Fracture Toughness and Charpy-Impact Strength of Stainless Steel Pipe Welds

Office of Nuclear Regulatory Research

AVAILABILITY OF REFERENCE MATERIALS IN NRC PUBLICATIONS

NRC Reference Material

As of November 1999, you may electronically access NUREG-series publications and other NRC records at NRC's Library at www.nrc.gov/reading-rm.html. Publicly released records include, to name a few, NUREG-series publications; *Federal Register* notices; applicant, licensee, and vendor documents and correspondence; NRC correspondence and internal memoranda; bulletins and information notices; inspection and investigative reports; licensee event reports; and Commission papers and their attachments.

NRC publications in the NUREG series, NRC regulations, and Title 10, "Energy," in the *Code of Federal Regulations* may also be purchased from one of these two sources.

1. **The Superintendent of Documents**
   U.S. Government Publishing Office
   Washington, DC 20402-0001
   Internet: bookstore.gpo.gov
   Telephone: (202) 512-1800
   Fax: (202) 512-2104

2. **The National Technical Information Service**
   5301 Shawnee Road
   Alexandria, VA 22312-0002
   www.ntis.gov
   1-800-553-6847 or, locally, (703) 605-6000

A single copy of each NRC draft report for comment is available free, to the extent of supply, upon written request as follows:

Address: **U.S. Nuclear Regulatory Commission**
Office of Administration
Multimedia, Graphics, and Storage & Distribution Branch
Washington, DC 20555-0001
E-mail: distribution.resource@nrc.gov
Facsimile: (301) 415-2289

Some publications in the NUREG series that are posted at NRC's Web site address www.nrc.gov/reading-rm/doc-collections/nuregs are updated periodically and may differ from the last printed version. Although references to material found on a Web site bear the date the material was accessed, the material available on the date cited may subsequently be removed from the site.

Non-NRC Reference Material

Documents available from public and special technical libraries include all open literature items, such as books, journal articles, transactions, *Federal Register* notices, Federal and State legislation, and congressional reports. Such documents as theses, dissertations, foreign reports and translations, and non-NRC conference proceedings may be purchased from their sponsoring organization.

Copies of industry codes and standards used in a substantive manner in the NRC regulatory process are maintained at—

The NRC Technical Library
Two White Flint North
11545 Rockville Pike
Rockville, MD 20852-2738

These standards are available in the library for reference use by the public. Codes and standards are usually copyrighted and may be purchased from the originating organization or, if they are American National Standards, from—

American National Standards Institute
11 West 42nd Street
New York, NY 10036-8002
www.ansi.org
(212) 642-4900

Legally binding regulatory requirements are stated only in laws; NRC regulations; licenses, including technical specifications; or orders, not in NUREG-series publications. The views expressed in contractorprepared publications in this series are not necessarily those of the NRC.

The NUREG series comprises (1) technical and administrative reports and books prepared by the staff (NUREG–XXXX) or agency contractors (NUREG/CR–XXXX), (2) proceedings of conferences (NUREG/CP–XXXX), (3) reports resulting from international agreements (NUREG/IA–XXXX), (4) brochures (NUREG/BR–XXXX), and (5) compilations of legal decisions and orders of the Commission and Atomic and Safety Licensing Boards and of Directors' decisions under Section 2.206 of NRC's regulations (NUREG–0750).

United States Nuclear Regulatory Commission

Protecting People and the Environment

NUREG/CR-6428, Rev. 1
ANL/EVS-17/3

Effects of Thermal Aging on Fracture Toughness and Charpy-Impact Strength of Stainless Steel Pipe Welds

Manuscript Completed: February 2017
Date Published: August 2018

Prepared by:
Omesh K. Chopra

Argonne Associate
Argonne National Laboratory
Argonne, IL 60439

Appajosula S. Rao, NRC Project Manager

Office of Nuclear Regulatory Research

ABSTRACT

The effect of thermal aging on the degradation of fracture toughness and Charpy-impact properties of austenitic stainless steel (SS) welds has been characterized at reactor temperatures. The solidification behavior and the distribution and morphology of the ferrite phase in SS welds are described. Thermal aging of the welds results in moderate decreases in Charpy-impact strength and fracture toughness. The upper-shelf Charpy-impact energy of aged welds decreases by 50–80 J/cm^2. The decrease in fracture toughness J-R curve, or J_{Ic} is relatively small. Thermal aging has minimal effect and the welding process has a significant effect on the tensile strength. Fracture properties of SS welds are controlled by the distribution and morphology of second-phase particles. Failure occurs by the formation and growth of microvoids near hard inclusions. Differences in fracture resistance of the welds arise from differences in the density and size of inclusions. However, the existing data are inadequate to accurately establish the effect of the welding process on fracture properties of SS welds. Consequently, the approach used for evaluating thermal and neutron embrittlement of austenitic SS welds relies on establishing a lower-bound fracture toughness J-R curve for unaged and aged, and non-irradiated and irradiated, SS welds. The existing fracture toughness J-R curve data for SS welds have been reviewed and evaluated to define lower-bound J-R curve for austenitic SS welds in the unaged and aged conditions. Thermal aging decreases the fracture toughness by about 20%. The potential combined effects of thermal and neutron embrittlement of austenitic SS welds are also described. Lower-bound curves are presented that define the change in coefficient C and exponent n of the power-law J-R curve and the J_{Ic} value for SS welds as a function of neutron dose. The potential effects of reactor coolant environment on the fracture toughness of austenitic SS welds are also discussed.

FOREWORD

Stainless steel welds are used in light water reactor (LWR) systems. These welds have a duplex structure consisting of austenite and ferrite phases. The ferrite phase increases tensile strength and improves resistance to stress corrosion cracking. However, these austenitic SS welds are susceptible to thermal aging. This is because the ferrite phase suffers from thermal embrittlement after extended operation at reactor operating temperatures. In addition, these welds, when exposed to neutron irradiation for extended periods, tend to degrade due to changes in their microstructure and microchemistry. As a result, the weld fracture properties will change because of neutron embrittlement and their susceptibility to irradiation-assisted stress corrosion cracking.

The purpose of the original NUREG/CR-6428 (1996) was to compile and evaluate the thermal embrittlement on austenitic SS welds. NUREG/CR-6428 Rev.1 updates the fracture properties of SS welds following a thorough review of available open literature results on Charpy-impact energy, tensile properties, and fracture toughness J-R curves of thermally aged and neutron irradiated welds. NUREG/CR-6428 Rev.1 also documents the potential combined effects of both thermal and neutron embrittlement and revises the lower-bound fracture-toughness J-R curves for austenitic SS welds during service in LWRs, using a much larger database.

Thermal aging of austenitic SS welds generally increases their hardness and tensile strength, while decreasing weld ductility, impact strength and fracture toughness. Thermal aging of welds decreases the Charpy upper-shelf energy and increases the Charpy energy transition temperature. Long term operation degrades the fracture toughness of austenitic SS welds due to thermal aging and the extent of degradation depending on the welding process. This is because the welding process and conditions influence both the weld composition and weld microstructure.

The results of NUREG/CR-6428 Rev.1 may be used to: (a) determine when active aging management of reactor primary pressure boundary and reactor vessel internal components manufactured using SS weld materials is needed for license renewal (LR) of LWRs under 10 CFR Part 54; (b) inform technical content in the subsequent license renewal guidance documents NUREG-2191 and NUREG-2192; (c) determine appropriate inspection and flaw disposition procedures for reactor vessel internals for use in American Society of Mechanical Engineers (ASME) code development, and for developing appropriate staff positions for Title 10, Section 50.55a,"Codes and Standards," of the Code of Federal Regulations (10 CFR 50.55a); and (d) identify technical issues related to screening criteria for the lower bound value of the delta ferrite limit at which significant loss of the fracture toughness of the SS welds could potentially occur during the normal operation of the nuclear power plants.

TABLE OF CONTENTS

LIST OF FIGURES

LIST OF TABLES

EXECUTIVE SUMMARY

Background

Austenitic stainless steels (SSs) are used extensively as structural alloys in light water reactor (LWR) systems, including reactor primary pressure boundary and core internal components, because of their excellent ductility, high notch toughness, corrosion resistance, and good formability. Although wrought SSs are completely austenitic, welded SSs have a duplex structure consisting of austenite and ferrite phases. The ferrite phase increases tensile strength and improves resistance to stress corrosion cracking (SCC). However, structural materials such as austenitic SS welds and cast austenitic stainless steel (CASS) are susceptible to thermal embrittlement of the ferrite phase after extended operation at reactor operating temperatures. In addition, exposure of these materials to neutron irradiation for extended periods, changes their microstructure (radiation hardening) and microchemistry (radiation-induced segregation), which degrades their fracture properties and increases their susceptibility to irradiation-assisted stress corrosion cracking (IASCC).

The scope of this report is to compile and evaluate the thermal and neutron embrittlement data on austenitic SS welds obtained after NUREG/CR-6428 (1996) was published, and (a) update the results presented earlier in the report on Charpy impact energy, tensile properties, and fracture toughness J-R curves, (b) establish the effects of thermal embrittlement on the degradation of fracture properties, and (c) evaluate the potential combined effects of thermal and neutron embrittlement. The lower-bound fracture-toughness J-R curves for austenitic SS welds during extended service in LWRs have been revised to incorporate the effects of thermal and neutron embrittlement using a much larger database. These curves bound the experimental fracture-toughness data on austenitic SS welds reviewed in this study. The potential effects of reactor coolant environment on fracture-toughness J-R curves are also discussed.

Material Characterization

Austenitic SS welds have a duplex structure, with ferrite being the minor phase distributed in various forms in the austenite matrix. Typically, the ferrite content in commercial AISI 300 series austenitic SSs welds varies between a couple of percent to 20 percent (%) depending on the material composition and to some extent on weld cooling rate. The solidification mode of SSs can be predicted based on the Cr_{eq}/Ni_{eq} ratio using the Schaeffer equation. For the austenite/ferrite mode, the Cr_{eq}/Ni_{eq} ratio is generally between 1.49 and 1.95. The various phase transformations that occur during solidification of austenitic SS welds, involve extensive solute redistribution. Based on the weld composition and weld process conditions these transformations result in four different ferrite morphologies in the weld.

Vermicular ferrite is the most commonly observed in austenitic SS welds containing 5 to 15% ferrite. The word vermicular means the markings, motion, or tracks of worms. It appears as an aligned skeletal network of ferrite. Lacy ferrite is observed in welds with 13 to 15% ferrite. The lacy form of ferrite is characterized by long columns of interlaced ferrite oriented along the growth direction in an austenite matrix. Acicular ferrite is observed in the crown passes of a weld and has no directionality, and does not conform to any substructure. It is observed in weld containing about 14% ferrite. Globular ferrite is in the form of globules, randomly distributed in a matrix of austenite. Globular ferrite is formed because of thermal instability of any of the other forms of ferrite, particularly the acicular form. Methods for estimating or measuring the ferrite content is austenitic SS welds are discussed.

Thermal Embrittlement

Thermal aging of austenitic SS welds, generally, increases their hardness and tensile strength, and decreases ductility, impact strength, and fracture toughness. The degradation of fracture properties occurs due to a combination of the strengthening of the ferrite matrix by spinodal decomposition and the weakening of grain/phase boundaries because of the presence of second phase particles. Fracture occurs along the delta ferrite regions where the second phase particles initiate voids/cracks either by decohesion of the ferrite/austenite interphase or particle cracking. The kinetics of thermal embrittlement are discussed.

Thermal aging of welds decreases the Charpy upper-shelf energy and increases the Charpy energy transition temperature. The effect of thermal aging increases with increasing ferrite content in the weld. Charpy impact energy at reactor temperatures is greater then at room temperature, but the difference decreases with thermal aging. The effect of thermal aging on tensile properties is to increase the yield and ultimate tensile stress and decrease the ductility. The effect on ultimate tensile stress is greater then on the yield stress. However, the effect is insignificant on welds with <10% ferrite.

Thermal aging also degrades the fracture toughness of austenitic SS welds; the welding process has a significant effect. The effect on submerged arc (SA) and shielded metal arc (SMA) welds is greater than on the gas tungsten arc (GTA) welds. However, since the composition and microstructure of welds varies with the welding process and conditions, it is difficult to estimate the change in fracture toughness as a function of time and temperature of aging. Therefore, the approach adopted in this report is to establish the effect of thermal embrittlement on the fracture toughness of SS welds and define the lower bound values of fracture toughness parameters, such as, J_{Ic} and coefficient "C" and exponent "n" of the power-law J-R curve. Separate lower bound values are presented for SA/SMA and GTA welds for unaged and aged SS welds. However, the SS weld data used in this evaluation, for which the weld ferrite content was known, contained less then or equal to 12% ferrite. Therefore, the applicability of these results to welds containing higher ferrite content needs to be evaluated.

Combined Effects of Thermal and Neutron Embrittlement

The fracture toughness of austenitic SS welds decreases with increasing neutron irradiation dose. The extent of embrittlement depends on the amount and morphology of the ferrite phase in the weld. The mechanism of neutron embrittlement is briefly discussed. The point defects produced by neutron irradiation strengthen the material, resulting in an increase in tensile strength and a reduction in ductility and fracture toughness. The yield strength of austenitic SSs and welds can increase significantly. The extent of irradiation hardening and the increase in yield stress depend on the material composition, heat treatment and irradiation temperature. Correlations have been developed for estimating the tensile properties as a function of neutron dose by the Materials Reliability Program (MRP).

The fracture toughness of nonirradiated austenitic SSs is known to decrease as the test temperature is increased. The J_{Ic} values of austenitic SS and welds either nonirradiated or irradiated to relatively low doses, decrease with increasing test temperature. However, for SSs irradiated to 12 dpa or more, test temperature has no effect on fracture toughness. Available data are inadequate to accurately establish the effect of irradiation temperature on fracture toughness of SS welds. Similar to the effect of thermal embrittlement, lower bound values of J_{Ic} and coefficient C and exponent n of the fracture toughness J-R curve are defined as a function of neutron dose.

ACKNOWLEDGMENT

This work is sponsored by the Office of Nuclear Regulatory Research, U.S. Nuclear Regulatory Commission, under Job Code V6455; Program Manager: Appajosula S. Rao.

ABBREVIATIONS AND ACRONYMS

AMP	aging management program
ANL	Argonne National Laboratory
ASME	American Society of Mechanical Engineers
ASTM	American Society for Testing and Materials
AWS	American Welding Society
BWR	boiling water reactor
CASS	cast austenitic stainless steels
CMTR	certified material test record
CNSR	Chevron notch short rod
CR	composition ratio
CW	cold worked
CT	compact tension
DBTT	ductile-brittle transition temperature
DO	dissolved oxygen
dpa	displacements per atom
EdF	Electricité de France
EPFM	elastic-plastic fracture mechanics
EPRI	Electric Power Research Institute
FN	ferrite number
FRA	Framatome
GALL	Generic Aging Lessons Learned
GF	George Fischer
GTA	gas tungsten arc
HAZ	heat-affected zone
IASCC	irradiation-assisted stress corrosion cracking
J-R	J-integral resistance
LEFM	linear-elastic fracture mechanics
LWR	light water reactor
MHI	Mitsubishi Heavy Industry, Ltd.
MIG	Metal inert gas
MMA	manual metal arc
MRP	Materials Reliability Program
MSIP	mechanical stress improvement process
NP	National Power
NRC	Nuclear Regulatory Commission
PIFRAC	pipe fracture (database)
PWR	pressurized water reactor
RIS	radiation-induced segregation
SA	submerged arc
SCC	stress corrosion cracking
SMA	shielded metal arc
SS	stainless steel

SWC	Shutdown water chemistry
TIG	Tungsten inert gas

NOMENCLATURE

a	Crack length
b	Uncracked ligament of Charpy specimen
d	Neutron dose in dpa
B	Specimen thickness
C	Coefficient of the power-law J-R curve
Cr_{eq}	Chromium equivalent for the material
C_V	Room-temperature “normalized” Charpy-impact energy, i.e., Charpy-impact energy per unit fracture area, at any given service and aging time (J/cm^2). The fracture area for a standard Charpy V-notch specimen (ASTM Specification E 23) is 0.8 cm^2. The value of impact energy in J has been divided by 0.8 to obtain “normalized” impact energy in J/cm^2.
da	Increment in crack length
dJ	Increment in J
E	Elastic modulus
F	Ferrite content
J	J integral, a mathematical expression used to characterize the local stress-strain field at the crack tip region (parameter J represents the driving force for crack propagation)
K	Stress intensity factor
K_{Ic}	Critical stress intensity factor
K_{Jc}	Equivalent critical stress intensity factor
n	Exponent of the power-law J-R curve
Ni_{eq}	Nickel equivalent for the material
P	Aging parameter, i.e., the log of the time of aging at 400°C
P_m	Yield load for instrumented Charpy specimen
P_y	Maximum load for instrumented Charpy specimen
Q	Activation energy for the process of thermal embrittlement (kJ/mole)
R	Load ratio
t	Service or aging time
T	Tearing modulus or temperature
W	Specimen width
δ_c	Ferrite content calculated from the chemical composition of a material (%)
υ	Poisson ratio
σ_f	Flow stress, defined as the average of yield and ultimate stress
σ_u	Ultimate stress
σ_y	Yield stress

In this report, all values of impact energy have been normalized with respect to the actual cross sectional area of the Charpy impact specimen. Thus, for a standard Charpy-V-notch specimen per ASTM Specification E 23 (i.e., 10 x 10-mm cross section and 2-mm V notch), impact energy value in J has been divided by 0.8 cm^2 to obtain impact energy in J/cm^2. Impact energies obtained on subsize specimens were normalized with respect to the actual cross-sectional area and appropriate correction factors were applied to account for size effects. Similarly, impact energies from other standards such as U-notch specimen were converted to a Charpy-V-notch value by appropriate correlations.

SI units of measurements have been used in this report. Conversion factors for measurements in British units are as follows:

To convert from	to	multiply by
in.	mm	25.4
J*	ft·lb	0.7376
kJ/ m^2	in.–lb/in.^{2}	5.71015
kJ/mole	kcal/mole	0.239

* When impact energy is expressed in J/cm^2, first multiply by 0.8 to obtain impact energy of a standard Charpy V–notch specimen in J.

1 INTRODUCTION

Austenitic stainless steels (SSs) are used extensively as structural alloys in light water reactor (LWR) systems, including reactor primary pressure boundary and core internal components, because of their excellent ductility, high notch toughness, corrosion resistance, and good formability. Although wrought SSs are completely austenitic, welded SSs have a duplex structure consisting of austenite and ferrite phases. The ferrite phase increases tensile strength and improves resistance to stress corrosion cracking (SCC). Furthermore, the ferrite phase is desired in austenitic SS welds for controlling the weld solidification behavior and inhibiting the formation of low melting point compounds such as sulfides and phosphides, which promote microfissuring [1].

However, materials with a duplex structure such as austenitic SS weld and cast austenitic SS (CASS), are susceptible to thermal embrittlement after extended operation at reactor operating temperatures [1–27], typically 282°C (540°F) for boiling water reactors (BWRs), 288–327°C (550–621°F) for pressurized water reactor (PWR) primary coolant piping, and 343°C (650°F) for PWR pressurizers. In addition, exposure to neutron irradiation for extended periods changes the microstructure (radiation hardening) and microchemistry (radiation-induced segregation, or RIS) [28–32] of these duplex materials, degrades their fracture properties [33–47], and increases their susceptibility to irradiation-assisted stress corrosion cracking (IASCC) [46–55]. A critical assessment of the susceptibility of austenitic SSs to IASCC and neutron embrittlement was presented in NUREG/CR-7027 and two review articles [45,47,55]. The existing data were evaluated to establish the effects of material parameters (such as composition, thermo-mechanical treatment, microstructure, microchemistry, yield strength, and stacking fault energy) and environmental parameters (such as water chemistry, irradiation temperature, dose, and dose rate) on IASCC susceptibility and neutron embrittlement. The results indicate that for the same irradiation conditions, the fracture toughness of thermally aged CASS material and austenitic SS weld metal is lower than that of the HAZ of SS base materials, which, in turn, is lower than that of solution-annealed SS base materials. The combined effects of thermal and neutron embrittlement on the fracture toughness of CASS materials, has also been investigated [56,57].

For embrittled materials, a fracture mechanics methodology, such as elastic-plastic fracture mechanics (EPFM) or linear-elastic fracture mechanics (LEFM) is needed for analysis of structural integrity and development of inspection guidelines. The former involves the use of J integral-resistance (J-R) curve approach, where failure is caused by plastic deformation. The J integral is a mathematical expression used to characterize the local stress-strain field at the crack tip region (parameter J represents the driving force for crack propagation), and the J-R curve characterizes the resistance of the material to stable crack extension. The fracture toughness of such materials is represented by fracture mechanics parameters such as J_{Ic}, the value of J near the onset of crack extension, and the tearing modulus, T, which characterizes the slope of the J-R curve. The tearing modulus is expressed as

$$T = (dJ/da)(E/\sigma_f^2), \qquad (1)$$

where E is the elastic modulus, "a" is the crack length, and σ_f is the flow stress defined as the average of the yield stress (σ_y) and ultimate stress (σ_u), i.e., $\sigma_f = (\sigma_y+\sigma_u)/2$.

The LEFM methodology is used where failure involves negligible plastic deformation. The fracture toughness of such materials is represented by the parameter K_{Ic} (i.e., plane strain fracture toughness), which characterizes the resistance of the material to unstable crack extension. For small-scale yielding (e.g., deep cracks in bending in a large specimen), the fracture toughness can be characterized by J_{Ic}. For convenience, the fracture toughness J_{Ic} is represented in terms of a parameter K_{Jc}, which has the units of K_{Ic} and is determined from the relationship

$$K_{Jc} = (E' J_{Ic})^{1/2}, \tag{2}$$

where the normalized elastic modulus is given by $E' = E/(1 - \upsilon^2)$, E is the elastic modulus, and υ is the Poisson ratio. K_{Jc} is equal to the critical stress intensity K_{Ic} only in cases where LEFM is applicable.

The thermal embrittlement of CASS materials and austenitic SS welds has been investigated at Argonne National Laboratory (ANL) and the results were published in several NRC reports [22–27]. A procedure and correlations have been developed at ANL for estimating fracture toughness, tensile, and Charpy-impact properties of CASS components during service in LWRs from known material information. The ANL estimation scheme originally described in NUREG/CR-4513 Rev. 1 [24] is applicable to compositions within the American Society for Testing and Materials (ASTM) Specifications A351 for Grades CF-3, CF-3A, CF-8, CF-8A, and CF-8M.

In the ANL methodology for estimating thermal embrittlement of CASS materials, embrittlement is characterized in terms of room temperature Charpy-impact energy. The extent or degree of thermal embrittlement at “saturation” (i.e., the minimum impact energy that can be achieved for a material after long-term aging) is determined from the chemical composition of the material [24]. Charpy-impact energy as a function of the time and temperature of reactor service is estimated from the kinetics of thermal embrittlement, which are also determined from the chemical composition. The fracture toughness J-R curve for the aged material is then obtained by correlating room temperature Charpy-impact energy with fracture-toughness parameters. Tensile yield and flow stresses, and Ramberg/Osgood parameters are estimated from the flow stress of the unaged material and the kinetics of embrittlement [26].

However, the NUREG/CR-4513 Rev. 1 [24] methodology for estimating loss of fracture toughness due to thermal embrittlement in LWR environments was limited to CASS materials with ferrite contents up to 25%, and the synergistic effects of thermal and neutron embrittlement were not evaluated. Limited data suggest that the concurrent exposure to neutron irradiation during reactor service can result in a combined effect wherein the service-degraded fracture toughness can be less than that predicted for either thermal or neutron irradiation embrittlement independently [56]. The ANL methodology was later updated to include CASS materials with up to 40% ferrite. In addition, procedure for estimating the combined effects of thermal and neutron embrittlement on loss of fracture toughness of CASS materials was also included. The results were presented in NUREG/CR-4513, Rev. 2 [58].

Although austenitic SS welds have a duplex structure and their chemical compositions are similar to those of CASS materials, their fracture toughness is lower than that of the wrought SSs and most CASS materials. Typically, austenitic SS welds exhibit ductile dimpled fracture morphology at temperatures up to 550°C (1022°F) [27]. Because of a high density of inclusions in the weld, the dimples are relatively small and shallow, and often associated with inclusions. The overall fracture toughness of SS welds is controlled by the density and morphology of second-phase inclusions in these materials, which varies with the welding process. For example, gas tungsten arc (GTA) welds exhibit the highest toughness; shielded metal arc (SMA) welds have intermediate toughness; and submerged arc (SA) welds have the lowest toughness [1]. The median value of

J_{Ic} is 492 kJ/m^2 (2809 in.-lb/in.^{2}) for GTA welds and 147 kJ/m^2 (839 in.-lb/in.^{2}) for SA welds at temperatures up to 125°C (257°F).

In addition, welding of austenitic SSs results in a heat affected zone (HAZ) adjacent to the fusion zone, where the material microstructure and microchemistry are greatly altered because of the precipitation of chromium (Cr)-rich carbides at the grain boundaries. The formation of the carbides depletes Cr from the grain-boundary region thereby creating a region that is susceptible to SCC. However, the fracture toughness of HAZ material is generally superior to that of the weld metal and may be comparable to that of the base metal.

Because the microstructure and fracture behavior of austenitic SS welds is significantly different from that of CASS materials, the ANL fracture toughness estimation methodology for CASS materials is not applicable to austenitic SS welds. The NUREG/CR-4513 Rev. 2 correlations account for mechanical-property degradation of typical heats of CASS, but do not consider the effects of compositional or structural differences that may arise from various welding processes, all of which have a strong effect on the failure mechanism of weld materials. Consequently, the approach used for evaluating thermal and neutron embrittlement of austenitic SS welds, relies on establishing a lower-bound fracture toughness J-R curve for unaged and aged, and non-irradiated and irradiated SS welds.

The degradation of fracture toughness and Charpy-impact energy of several SS pipe welds was evaluated in NUREG/CR-6428 [27]. A few welds from the reactor coolant pressure boundary piping were aged for 7,000 to 10,000 h at 400°C (752°F) to simulate saturation conditions, the lowest impact energy that would be achieved by the material after long-term aging. The results were compared with data from other studies [1,12,13,59–77]. The results suggested that SS welds with poor fracture toughness (e.g., SMA or SA welds) appear to be relatively insensitive to thermal aging.

This earlier evaluation of fracture properties of austenitic SS welds due to thermal embrittlement as well as the potential degradation due to neutron embrittlement has recently been updated using a much larger database [78–96]. Most of the mechanical property data, particularly the fracture toughness J-R curve data (i.e., Δa vs. J data), were obtained by digitizing good quality plots from the reference documents. The combined effects of thermal and neutron embrittlement were also evaluated. The initial results were published in a journal article [97]. This report presents a revision of the original version of the NUREG/CR-6428 in its entirety. The lower bound fracture toughness J-R curves for austenitic SS welds during extended service in LWRs have been updated to incorporate the effects of thermal and neutron embrittlement using the larger database. These curves bound the experimental fracture-toughness data on austenitic SS welds reviewed in this study. The potential effects of reactor coolant environment on fracture toughness J-R curves are also discussed.

2 MATERIAL CHARACTERIZATION

2.1 Solidification Behavior and Ferrite Morphology

Austenitic SS welds have a duplex structure, with ferrite being the minor phase distributed in various forms in the austenite matrix. For commercial AISI 300 series austenitic SSs, the weld ferrite content varies in the range of 0 to about 20 volume percent (%) depending primarily on the material composition, and to a lesser extent on weld cooling rate [98–108]. However, the solidification behavior and subsequent solid-state transformation within the weld metal during cooling (shown in Figure 2-1 control the microstructural characteristics of the weld. Therefore, establishing the formation and distribution of different ferrite morphologies in the weld is rather difficult [105].

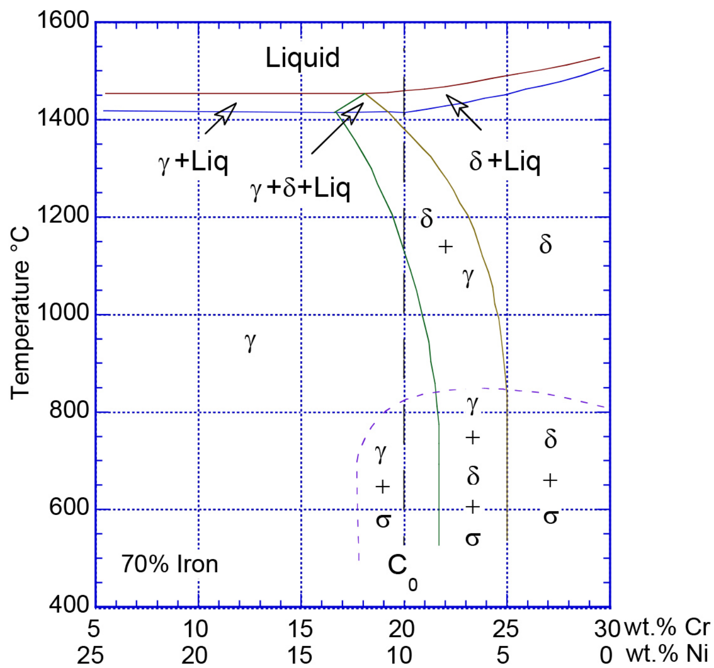

Figure 2-1 The 70% constant Fe vertical section of the Fe-Ni-Cr-system (Ref. 105).

In Figure 2-1, the structure of the equilibrium phase of composition C_o with Fe-20 wt.% Cr and 10 wt.% Ni (e.g., Type 304 SS base metal welded with Type 308 electrode) is ferrite at high temperatures [1380–1420°C (2516–2588°F)] and austenite at low temperatures (below 1120°C or 2048°F). Upon cooling from the δ-ferrite phase, this composition passes through a two-phase regime (δ+γ). The microstructures that result from changes in the various phases have been related to the weld material phase diagram [103] and to the ratio of the Cr and Ni equivalents (Cr_{eq}/Ni_{eq}) [99]. However, the microstructure is affected by the cooling rate [103,104]. In the primary ferrite solidification mode (i.e., Ni contents <10%), primary ferrite is first formed followed by solid-state transformation of ferrite (δ) to austenite (γ). In this case, the residual δ-ferrite is observed at the dendrite core [105]. On the other hand, in the primary austenite solidification mode (i.e., Ni contents ≥10%), the residual δ-ferrite is observed at the dendrite boundaries.

The solidification mode of SSs can be predicted based on the Creq/Nieq ratio using the Schaeffler equation [102,109]:

Austenite mode: $Cr_{eq}/Ni_{eq} \leq 1.48$ (3)

Ferrite/austenite mode: $1.48 \leq Cr_{eq}/Ni_{eq} \leq 1.95$ (4)

Ferrite mode: $1.95 \leq Cr_{eq}/Ni_{eq}$ (5)

where Cr_{eq} and Ni_{eq} are determined from the material composition in wt.%,

$$Cr_{eq} = Cr + 1.5Si + Mo + 0.5Nb + 2Ti \quad (6)$$

$$Ni_{eq} = Ni + 0.5Mn + 30C + 30(N – 0.06). \quad (7)$$

Because of the differences in the solidification behavior of the weld, both the morphology and composition of the δ-ferrite can vary significantly between the different modes of solidification. Note that Eqs. 6 and 7 are somewhat different than those used in the ASTM A800/800M methodology (based on the Schoefer diagram) discussed later [110,111]. Furthermore, due to differences in the Cr_{eq}/Ni_{eq} ratio of the base metal and weld compositions and solute segregation during solidification, the composition of welds of nominal composition C_o can vary significantly prior to any solid-state transformation.

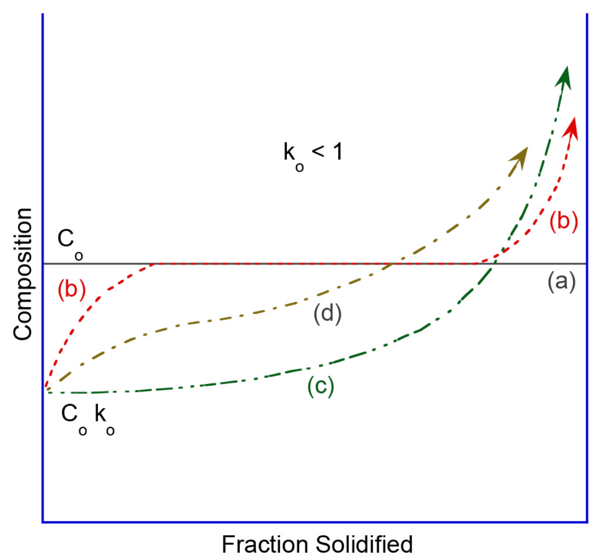

Figure 2-2 Solute distributions predicted by different models in a frozen bar from liquid of composition C_o: (a) equilibrium cooling, (b) solute mixing in the liquid by diffusion only, (c) complete mixing in the liquid, and (d) partial solute mixing in the liquid (Ref. 112 as reproduced in Ref. 105).

Davies [112] has summarized the composition profiles predicted by different models (shown in Figure 2-2) in a bar solidified from liquid of composition C_o. The shows a case in which equilibrium distribution coefficient k <1. The fraction of the melt of initial composition C_o, which has solidified is plotted along the x-axis. In Figure 2-2, line (a) represents the uniform composition profile C_o for equilibrium solidification. The other three cases are for no diffusion in the solid and equilibrium at the liquid-solid interface. The most common assumption in the solidification of castings or welds is complete mixing in the liquid; this condition is shown as curve (c) in the figure.

The final liquid solidifies at an invariant composition as an eutectic. In welds, this occurs within the interdendritic or intercell regions. Case (b) represents mixing in the liquid by diffusion only. This results in the formation of a solute-rich boundary layer at the liquid-solid interface, which depends on the solute distribution k, the diffusion coefficient in the liquid, and the solidification velocity. The case (d) represents some mixing in the liquid by convection in addition to diffusion. Note that in all cases, the initial solid to form at dendrite or cell core is of composition $C_o k_o$, where k_o is corresponds to the initial C_o.

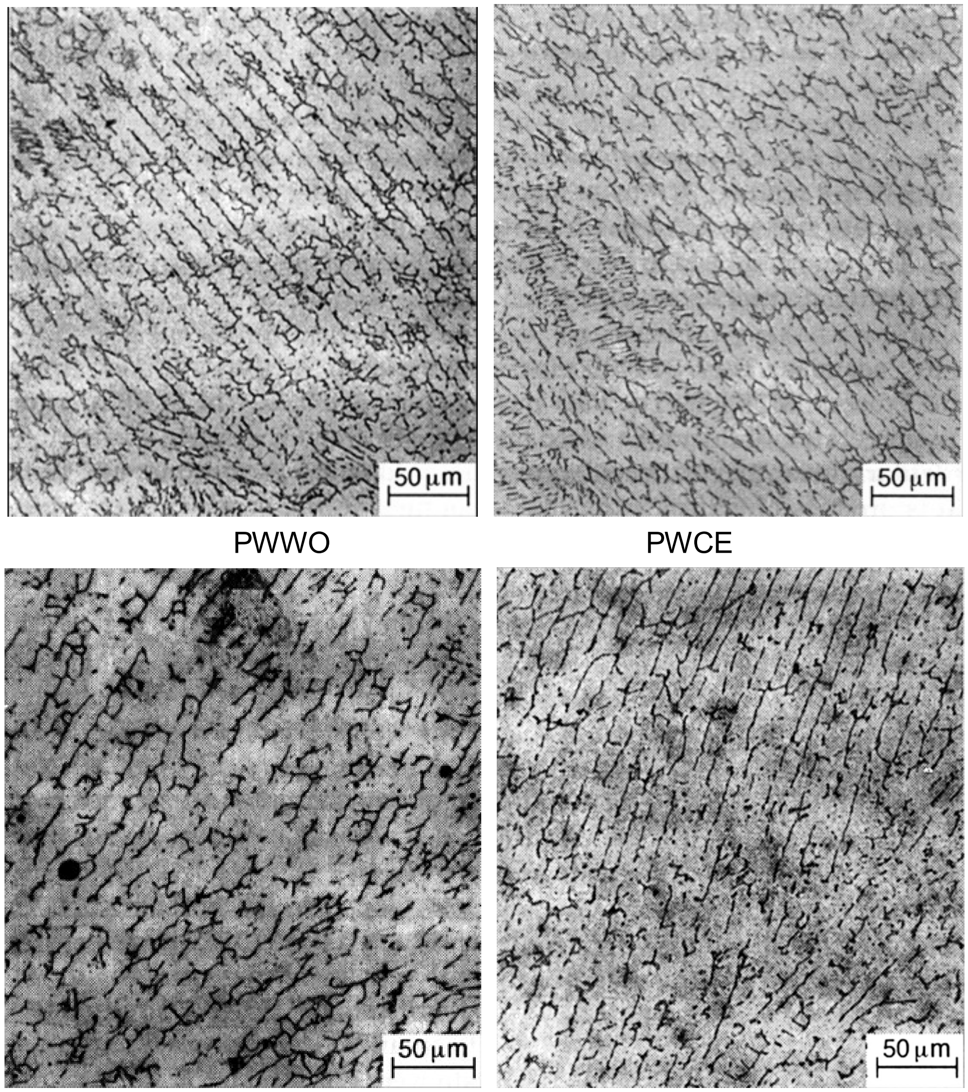

PWWO PWCE

PWDR PWMS

Figure 2-3 Typical ferrite morphology of four different welds (Ref. 27).

Examples of typical ferrite morphology of four different welds are shown in Figure 2-3. PWWO is a 0.305-m (12-in.) schedule 100 pipe mockup weld with overlays, PWCE is a 0.71-m (28-in.) Type 304 pipe-weld, PWDR is a 0.254-m (10-in.) Type 304 SS pipe weld after service in the Dresden reactor, and PWMS is a 0.71-m (28-in.) SS pipe weld treated by the Mechanical Stress Improvement Process (MSIP).

David [104] studied the ferrite morphology and variations in ferrite content in two Type 308 SS multipass welds and identified four distinct ferrite morphologies: vermicular, lacy, acicular, and globular. The welds were prepared by the GTA process with a 25-mm thick Type 304L SS plate containing a single-V butt joint. The compositions of the 304L plate and 308 filler metal were 0.019 C, 1.75 Mn, 0.63 Si, 0.029 P, 0.006 S, 10.0 Ni, 18.55 Cr, and balance Fe (wt.%) and 0.016 C, 1.95 Mn, 0.35 Si, 0.029 P, 0.004 S, 9.76 Ni, 20.14 Cr, and balance Fe (wt.%), and Cr_{eq}/Ni_{eq} = 1.66, respectively. One of the welds was made with the joint surfaces buttered with the weld metal and the other without buttering. Ferrite number, FN, was measured using a Magne-gage in accordance with American Welding Society A4.2-74 [113].

The average FNs of the root pass deposited in the buttered and not buttered weld were 13 and 8, respectively. The lower ferrite content of the weld prepared without buttering was attributed to weld-metal dilution with the base metal. The ferrite number of the root pass decreased further because of the dilution of ferrite from the thermal effects during the subsequent weld passes. Variations in ferrite content were also observed in both welds within a cross section of the bead, along the length and width of the weld. The FN values[1] at various weld locations varied from 9 to 13 and 5 to 14 for the buttered and not buttered welds, respectively. Based on the composition of the weld metal, the calculated ferrite content for the weld, without dilution, is 8.1% from Hull's equivalent factor [101], 5.9 from the ASTM A800/A800M methodology (based on the Schoefer diagram) [110,111], and about 13.8% from the modified Schaeffler (or Delong) diagram [114,115].

Note that the ferrite content determined using the ASTM A800 methodology is significantly lower than the average measured value of FN 11 for the buttered weld. However, since the ferrite content was measured using a Magne-gage, such instruments are very sensitive to surface roughness or surface curvature. Furthermore, phases other than ferrite and austenite may form at higher temperatures during welding, which may alter the magnetic response of the material such that the indicated ferrite content is quite different than of the same material not subjected to the welding process. It should also be mentioned that the variations in ferrite content in part might be due to differences in the N pickup during welding [104].

The results of the study by David indicate that the solidification sequences in Type 308 SS welds include primary crystallization of δ-ferrite with subsequent envelopment by austenite, followed by further transformations from liquid to γ and δ to γ [104]. As the sample cools below the solidus temperature, the transformation at the liquid-γ interface is completed, leaving behind a skeletal network of untransformed δ-ferrite along the cores of the primary and secondary dendrite arms. This residual ferrite is rich in Cr, which makes it very stable. However, primary ferrite, with lower average Cr content (24–25 wt.%), may transforms into Widmanstatten austenite and ferrite during rapid cooling. These two transformations involve extensive solute redistribution by diffusion; the results may be used to explain the various ferrite morphologies observed in SS welds [104]. The details regarding the four different morphologies are as follows.

Vermicular ferrite (i.e., skeletal ferrite morphology) was most commonly observed in austenitic SS welds with FN 5-15, and was predominantly observed in the weld root pass and the two subsequent passes. The vermicular (meaning the form, markings, motion, or tracks of worms) morphology, depending on the sectional cut viewed, appears as an aligned skeletal network of ferrite or as a curved skeletal form. The alignment is along the heat flow direction, which is also the primary dendrite growth direction. Studies by Fredricksson [116] indicated that the tip of the individual dendrites at the solidification front, where the temperature gradients were steep,

[1] FN values determined from the modified Schaeffler diagram.

transformed to a lathy-ferrite morphology. However, the core of the dendrite, where the cooling rate was much slower, consisted of vermicular ferrite morphology. Fredricksson concluded that the vermicular ferrite is formed by a diffusion controlled reaction in which Ni is partitioned to the austenite and Cr to the ferrite, leaving a Cr-rich Ni-depleted ferrite in the core of the ferrite dendrites (i.e., skeletal ferrite morphology). These results have been validated by Suutala et al. [102] and Lippold and Savage [103].

Lacy morphology was observed predominantly in the third pass of the weld; the ferrite content varied between FN 13 and 15. The lacy structure looked very regular and aligned. The lacy form of ferrite is characterized by long columns of interlaced ferrite oriented along the growth direction in an austenite matrix. Most likely, it forms by the transformation of primary δ-ferrite to Widmanstatten austenite and ferrite.

Acicular morphology was present in the sixth and crown passes of the weld; the ferrite content was about FN 14. However, unlike the previous two morphologies, the acicular structure had no directionality and did not conform to the solidification substructure in any way. This morphology is typical of weld metals with $Cr_{eq}/Ni_{eq} = 2$. It also forms by the low-temperature transformation of primary ferrite to austenite and ferrite.

Globular ferrite is in the form of globules, randomly distributed in a matrix of austenite. The structure has no directionality and is not related to the overall solidification substructure. It was commonly observed in weld passes 4, 5, and 6; the FN was ~10. Globular ferrite is formed because of thermal instability of any of the other forms of ferrite, particularly the acicular form.

Similar results were observed by Abe and Watanabe [109] in Type 316L SS welds that were prepared using two different filler metals, with 11.27 and 13.72 wt.% Ni. One weld solidified in primary ferrite mode and the other in primary austenite mode. The ferrite content of the two welds was 12.7% and 2.5%, respectively. The low-Ni, high ferrite weld showed predominantly a vermicular morphology with small amounts of lathy and acicular ferrite, while the high-Ni, low ferrite weld showed islands of δ-ferrite at the dendrite or cell boundaries. Note that these ferrite morphologies may appear continuous or discontinuous depending on the section of the weld viewed. Therefore, caution must be exercised in such characterization of the ferrite.

Note that for austenitic SS welds (or CASS materials) to be resistant to SCC in BWR environment, a minimum ferrite of 7.5% and a maximum C content of 0.035 wt.% is recommended in NRC NUREG-1801, The Generic Aging Lessons Learned (GALL) Report [117]. The GALL report identifies aging management programs (AMPs) that are determined to be acceptable to manage aging effects of systems, structures, and components in the scope of license renewal. These acceptable AMPs are described in Chapter XI of the report. The AMP for managing SCC of wrought and cast SSs and welds includes recommendations for selection of materials that are resistant to sensitization. These resistant materials are for new and replacement components, and include low-carbon grades of austenitic SS and weld metal with a maximum carbon of 0.035 wt.% and a minimum ferrite of 7.5% in weld metal and CASS materials.

2.2 Estimation of Ferrite Content

The ferrite content in austenitic SS welds is a function of the chemical composition and the welding process history. Typically, the ferrite content of duplex structures such as austenitic SS welds is determined from the (a) chemical composition, (b) magnetic response, or (c) metallographic examination of the material. Among the magnetic methods, the Magne-Gage and Ferritescope are the most commonly used instruments for measuring the ferrite content. The

Magne-Gage is a continuous-reading type instrument that utilizes a spring to measure the attraction between a magnet and the material of unknown ferrite content, and the response is compared with that of a calibrated sample. The Ferritescope operates on the magneto-induction principle measures the relative magnetic permeability of the specimen.

However, because the probes of these instruments are small, the surface roughness or curvature of the sample is an important parameter that can vary the magnetic linkage with the material being measured. In addition, phases other than ferrite and austenite may form in the material during service, which may alter the magnetic response of the material such that the indicated ferrite content is quite different from that of the same chemical composition that has undergone a different heat treatment.

Until 1973, ferrite contents in duplex structures such as CASS materials and austenitic SS welds were determined by metallographic examination of the structure. A sample of the material was polished and etched to reveal the ferrite and austenite phases and a grid was superimposed over the image of an optical microscope to determine by point counting the percentage of ferrite in the sample. The main drawback with this method is that the point count estimates of ferrite may vary with the etching technique used to reveal the ferrite phase, and with the number of grid points used in the measurements. Furthermore, it is tedious and obtaining metallographic samples from various regions of the weld may not be practical.

Although a quantitative metallographic method provides the most accurate estimate of ferrite content, determination of ferrite percent from chemical composition of the material offers the most useful and most common method for ferrite control during solidification of the metal from a melt during welding. However, the accuracy of these estimations depends on the accuracy of the chemical analysis procedure, and the degree of variability of composition within the weld. The most commonly used methods are described below.

2.2.1 Hull's Equivalent Factor

When a certified material test record (CMTR) is available, the ferrite content is calculated from chemical composition in terms of Hull's equivalent factors [101] for nickel and chromium given by

$$Cr_{eq} = Cr + 1.21(Mo) + 0.48(Si) - 4.99 \tag{8}$$

and

$$Ni_{eq} = (Ni) + 0.11(Mn) - 0.0086(Mn)^2 + 18.4(N) + 24.5(C) + 2.77, \tag{9}$$

where the concentrations of the various alloying and interstitial elements is in wt.%. The concentration of N is often not available in a CMTR; if not known, it is assumed to be 0.04 wt.%. The ferrite content δ_c is given by

$$\delta_c = 100.3(Cr_{eq}/ Ni_{eq})^2 - 170.72(Cr_{eq}/ Ni_{eq}) + 74.22. \tag{10}$$

The measured ferrite content and values calculated from Hull's equivalent factor for the various CASS heats used in studies at ANL [22], the Georg Fischer Co. (GF) [2], Electricité de France (EdF) [15], National Power (NP) [16], Framatome (FRA) [6], and the Electric Power Research Institute (EPRI) [7] are shown in Figure 2-4. For most heats, the difference between the estimated and measured values is ±6% ferrite. The results also indicate that the calculated ferrite content was generally lower than the measured values for CF-8M heats that contained ≥10% Ni.

2.2.2 ASTM A800/800M Methodology

In the ASTM A800/800M methodology [110,111] the ferrite content of the weld is estimated from the central line of the of the diagram at the composition ratio of chromium equivalent, Cr_{eq}, to nickel equivalent, Ni_{eq}, determined from the following formula:

$$(Cr_{eq}/Ni_{eq}) = (Cr + 1.5Si + 1.4Mo + Nb - 4.99)/(Ni + 30C + 0.5Mn + 26(N - 0.02) + 2.77) \qquad (11)$$

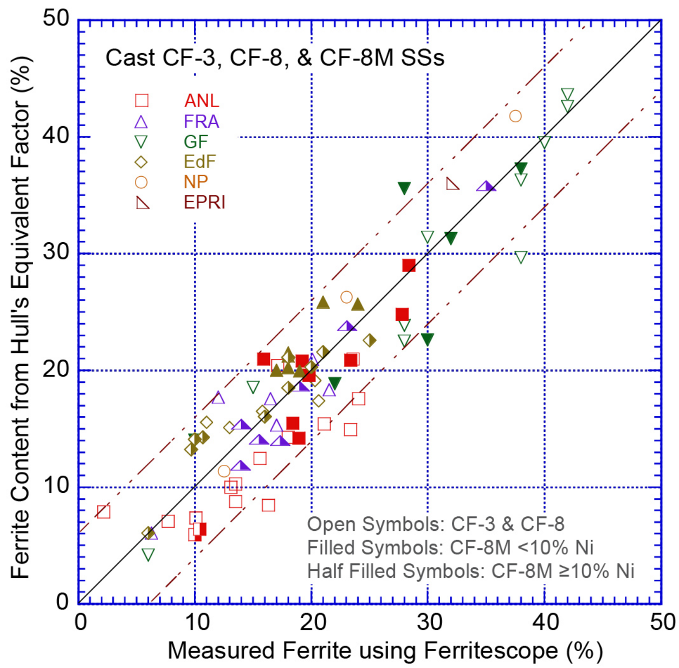

Figure 2-4 Plots of measured ferrite content and values calculated from Hull's equivalent factor for various CASS materials.

The values of the composition ratio (CR) for a given ferrite content (F), or vice versa, is then determined mathematically from the equation of the central line:

$$CR = 0.9 + 3.38883 \times 10^{-2}F - 5.58175 \times 10^{-4}F^2 + 4.22861 \times 10^{-6}F^3 \qquad (12)$$

The measured ferrite content and values calculated from ASTM A800/A800M methodology for the same heats of CASS materials plotted in Figure 2-4 are shown in Figure 2-5. The results indicate that for ferrite contents greater than 20%, the calculated ferrite content for several heats is lower than the measured values. Most of these heats with significantly lower calculated values contained 22.0-23.0 wt.% Cr and about 8.0-8.5 wt.% Ni. Compared to the ferrite content calculated from Hull' equivalent factor, the ASTM A800/A800M methodology under predicts the ferrite content for CASS materials with greater than 15% ferrite. The difference between the two methods can be seen clearly in Figure 2-6.

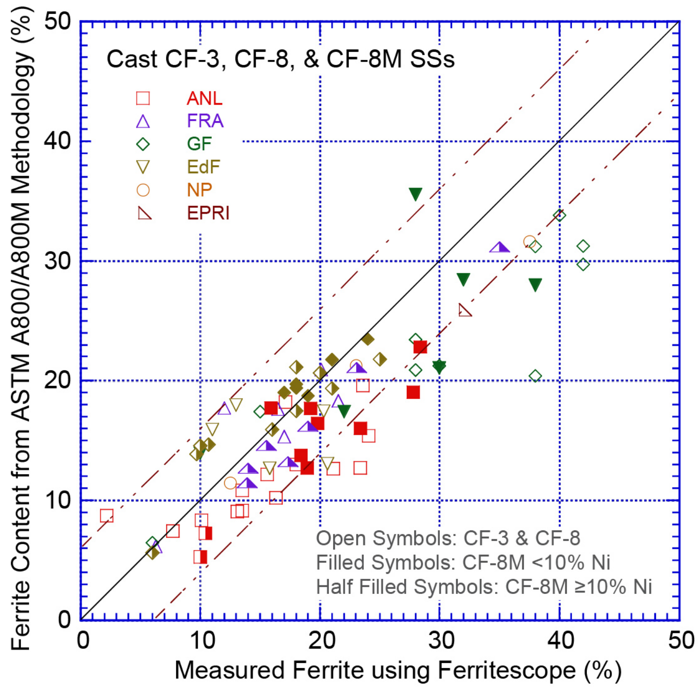

Figure 2-5 Plots of measured ferrite content and values calculated from the ASTM A800/A800M methodology for various CASS materials.

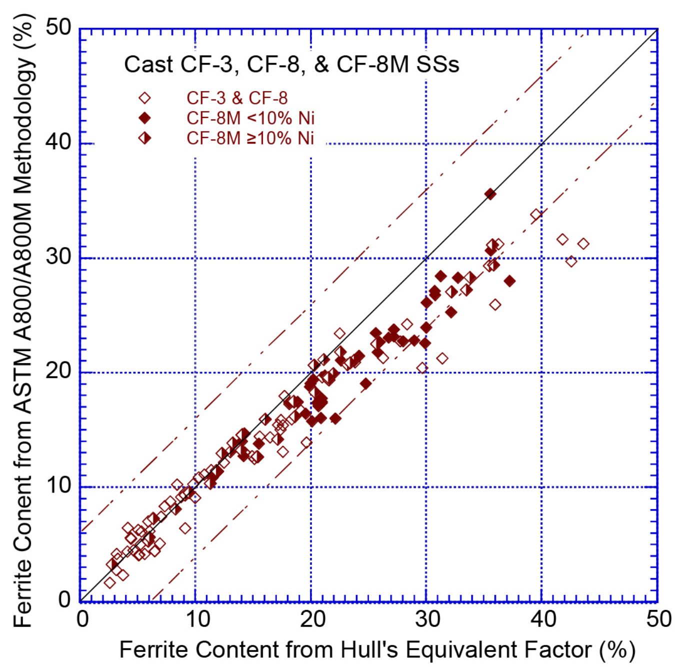

Figure 2-6 Plots of ferrite content calculated from Hull's equivalent factor and those estimated from the ASTM A800/A800M methodology for CASS materials.

The measured ferrite content and values calculated from Hull's equivalent factor or the ASTM A800/A800M methodology for several austenitic SS welds used in studies at ANL [27] and by Slama et al., [6] Mills [12], Lucas et al. [78,79] are plotted in Figure 2-7a and b, respectively.

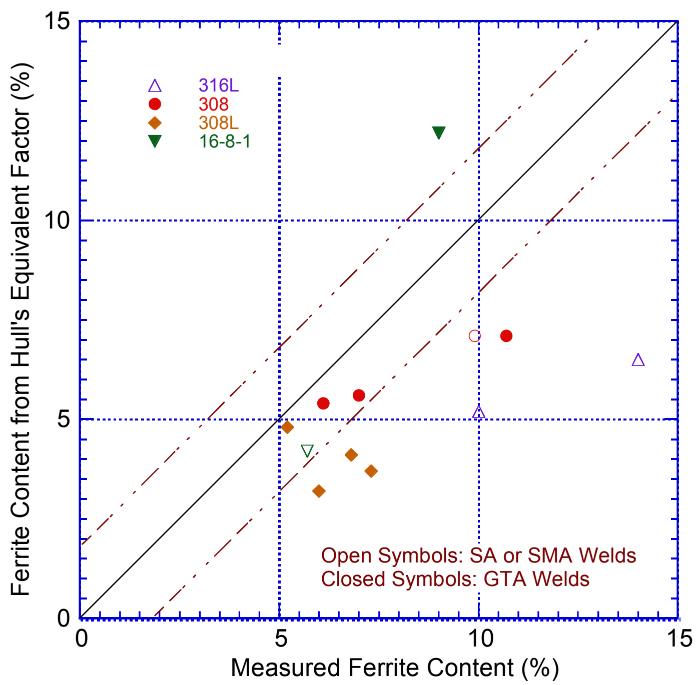

(a)

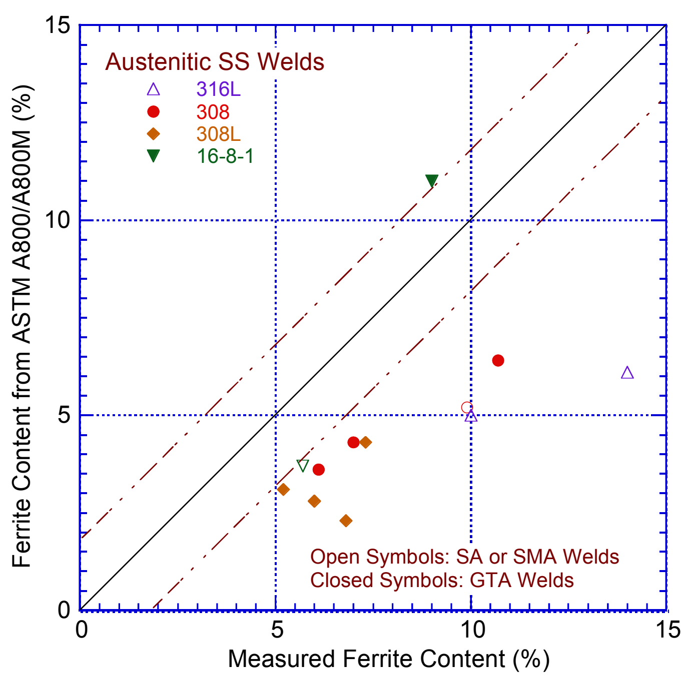

(b)

Figure 2-7 Plots of measured ferrite content and (a) values calculated from Hull's equivalent factor or (b) values calculated from ASTM A800/A800M methodology for various austenitic SS welds.

These limited data indicate that the measured ferrite contents are generally higher. For example, for welds with measured ferrite between 5 and 11%, the values calculated from Hull's equivalent factor range between 3 and 7%; the maximum difference is about 4% ferrite. Furthermore, as seen before for CASS materials, the difference between the measured values and those calculated from the ASTM A800 methodology is slightly larger.

3 THERMAL EMBRITTLEMENT OF AUSTENITIC SS WELDS

It is known that binary iron-chromium alloys and ferritic SSs are susceptible to severe embrittlement when exposed to temperatures in the range of 270 to 475°C (518 to 887°F) [118–121]. The potential for significant embrittlement of CASS materials, which consists of both austenite and ferrite phases, has been confirmed by studies at ANL [22–27] and elsewhere [2–6,14–16] on materials that were aged at temperatures of 290–450°C (554–842°F) for times up to 70,000 h (~8 yr). The results indicate that thermal aging of CASS materials (ASTM Specification A-351 for Grades[2] CF-3, CF-3A, CF-8, CF-8A, and CF-8M) at 270–350°C (518–662°F) increases their hardness and tensile strength; decreases ductility, impact strength, and fracture toughness; and shifts the Charpy transition curve to higher temperatures. The effect of thermal aging is observed to decrease at temperatures above 400°C (752°F). For example, the extent of thermal embrittlement in CASS materials aged at 450°C (842°F) is less than that in materials aged for similar times at 400°C (752°F) [46].

As mentioned earlier, in austenitic SS welds, the ferrite phase is desired for controlling the weld solidification behavior. Because the ferrite phase is brittle at low temperatures, austenitic SS welds also exhibit a ductile-brittle transition temperature (DBTT) phenomenon. However, at ambient and elevated temperatures, the ferrite phase shows a ductile deformation behavior. The fracture toughness of Type 304/308 and 316/16-8-2 welds is dependent on the weld process, but not composition [1]. For a given weld process, both these weld metals exhibit similar fracture toughness [12]. In general, GTA welds exhibit higher toughness than the SMA and SA welds. The J_{Ic} values for the latter are about one-third those for the GTA welds.

Austenitic SS welds generally contain 5–15% ferrite, but their mechanical properties differ from those of CASS materials. Studies conducted at ANL [27] indicated that, for a given ferrite content, the tensile strength of austenitic SS welds is higher and fracture toughness is lower than that of CASS materials. Experimental data [27] indicate that CASS materials with very poor fracture toughness are relatively insensitive to thermal aging. In these steels, failure is controlled by void formation near inclusions or other flaws in the material (i.e., by processes that are not sensitive to thermal aging). These results suggest that austenitic SS welds with poor fracture toughness (e.g., SA and SMA welds) should be relatively less sensitive to thermal aging than GTA welds; the GTA welds however, exhibit superior fracture properties.

3.1 Mechanism of Thermal Embrittlement

The overall fracture toughness of austenitic SS welds is controlled by the density and morphology of the second phase particles and to some extent on the ferrite content of the weld. The fracture toughness of welds is generally lower than that of wrought or cast SSs because of the higher density of inclusions. It depends on the weld process and not the composition [1]. For a given weld process, both 304/308 and 316/16-8-2 welds exhibit similar fracture toughness [12]. Among austenitic SS welds, the SA and SMA welds have poor fracture toughness relative to the GTA welds; they have a high density of manganese- and silicon-rich silicates and silicides. High silicon contents are generic to the SA and SMA welds because of silicon pickup from the flux. Typically

[2] The CF-3A and CF-8A grades represent high tensile strength material. The chemical composition of these grades is further restricted within the composition limits of CF-3 and CF-8, to obtain a ferrite/austenite ratio that results in higher ultimate and yield strengths. In this report, they are considered equivalent to CF-3 and CF-8 grades.

SA welds have 0.6-1.0% Si, SMA welds have 0.5-0.8% Si, and GTA welds have less than 0.5% Si [1].

Furthermore, in materials with a duplex structure (e.g., austenitic SS welds), the ferrite phase exhibits a ductile-to-brittle-transition temperature. Its plastic straining capacity is substantially decreased at low temperatures. However, the ferrite phase is ductile at room temperature and higher temperatures. Therefore, in the unaged condition, austenitic SS welds exhibit a ductile dimpled fracture. The transition temperatures of unaged materials are relatively low. The differences in the transition temperature for the various unaged heats and grades of CASS materials are due to the amount of ferrite and the differences in the mechanism of brittle fracture. The high-carbon CF-8 or CF-8M steels have a higher transition temperature than CF-3 steels because of the presence of phase boundary carbides. The carbides weaken the boundaries and lead to premature phase boundary separation with little or no strain hardening. For austenitic SS welds, because the ferrite volume fraction is typically less than 15%, the ferrite content has little effect on the overall fracture toughness of welds. However, the existing data indicate that the fracture toughness of welds is strongly influenced by specimen orientation.

The thermal aging of austenitic SS welds at 300–450°C (572–842°F) results in thermal embrittlement of the ferrite and, depending on the amount, morphology, and distribution of ferrite and second-phase particles, the ductile-to-brittle-transition temperature shifts to higher temperatures [1,22–26]. Thermal aging of austenitic SS welds leads to spinodal decomposition of the ferrite to form the α' phase, and formation of Ni- and Ti-rich silicides (the G phase, $Ti_6Ni_{16}Si_7$) in the ferrite, precipitation of $M_{23}C_6$ carbides on the phase boundaries, and limited M_6C carbides in the matrix [1]. The degradation of fracture properties occurs due to a combination of the strengthening of the ferrite matrix by spinodal decomposition and the weakening of grain/phase boundaries because of the presence of second phase particles. Fracture occurs along the delta ferrite regions where the second phase particles initiate voids/cracks either, by decohesion of the ferrite/austenite interphase or particle cracking [12]. The dominant failure-process is transgranular dimple fracture, and intergranular cracking is limited to a few isolated regions [1].

3.1.1 Kinetics of Thermal Embrittlement

The degree of thermal embrittlement of materials with duplex structures (e.g., CASS materials and austenitic SS welds) is characterized in terms of the Charpy-impact energy of notched toughness specimens. The "best estimates" of the degree of thermal embrittlement at reactor operating temperatures are determined from Arrhenius extrapolation of laboratory data obtained at higher temperatures (e.g., 400°C). The aging time to reach a given degree of embrittlement at different temperatures is determined from the following equation:

$$t = 10^P \exp\left[\frac{Q}{R}\left\{\frac{1}{T} - \frac{1}{673}\right\}\right], \tag{13}$$

where Q is the activation energy, R is the gas constant, T is the temperature, and P is an aging parameter that describes the combined effect of time and temperature on aging. It represents the degree of aging reached after 10^P h at 400°C (752°F). Thus, P = 1 for aging 10 h at 400°C. The aging parameter for any given aging condition is obtained by rewriting Eq. 13 so that,

$$P = \log(t) - \frac{1000Q}{19.143}\left(\frac{1}{T_s + 273} - \frac{1}{673}\right). \tag{14}$$

Information regarding the activation energy for the process of thermal embrittlement of austenitic SS welds is rather limited. However, the degree of thermal embrittlement of CF-3, CF-8, and CF-8M CASS materials has been investigated extensively at ANL [22–27]. The kinetics of thermal embrittlement of CASS materials are controlled by three processes: spinodal decomposition, precipitation and growth of phase boundary carbides, and precipitation of G phase in ferrite. Small changes in the composition cause the kinetics to vary significantly. The activation energies range from 65 to 230 kJ/mole (15 to 55 kcal/mole). The low values are most likely due to the formation of carbides/nitrides at the phase boundaries or G-phase and/or γ_2 precipitation in ferrite. The presence of Ni-Si-Mo clusters in the ferrite matrix of an unaged material is considered a signature of steels that show low activation energy (i.e., fast embrittlement). Such materials contain G-phase particles after aging.

Studies on low-temperature thermal aging of Types 304L and 316L SS welds containing about 10% ferrite yielded an activation energy of 113 kJ/mol for the thermal embrittlement of Type 304L weld in the range of 335–400°C [122]. For Type 316L weld, the activation energy was 148 kJ/mol in the aging temperature range of 365–400°C and 90 kJ/mol in the aging temperature range of 335–365°C, an average of 120 kJ/mol over the entire temperature range of 335–400°C. The welds were prepared by multi pass GTA welding process using Type 308L filler wire for the Type 304 SS plate and Type 316L filler wire for the Type 316L SS plate [122]. The material was aged up to 20,000 h at 335–400°C. Thermal aging of these welds at 400°C resulted in both spinodal decomposition and G-phase precipitation in the ferrite. However, aging up to 20,000 h at 335 and 365°C showed only spinodal decomposition [122]. The embrittlement rate determined by Charpy-impact and microhardness tests was considerably higher for the Type 316L weld compared to the Type 304L weld. The difference was attributed to the presence of Mo in the Type 316 SS, which increases the precipitation of G phase. These results for SS welds are consistent with the mechanism and kinetics of embrittlement observed in CASS materials.

3.2 Extent of Thermal Embrittlement

3.2.1 Charpy-Impact Energy

Nearly all of the initial studies on thermal embrittlement of austenitic SS welds and CASS materials (i.e., materials with duplex structures) consisted of Charpy V-notch impact test data, mostly at room temperature. A few studies included Charpy ductile-to-brittle-transition temperature data. In these studies, the transition temperature curves were represented by a hyperbolic tangent function of the form

$$C_V = K_o + B_{Ch}\left[1 - \tanh\left(\frac{T - C_{Ch}}{D_{Ch}}\right)\right], \tag{15}$$

where C_V is the normalized Charpy V-notch impact energy, K_o is the lower–shelf energy, T is the test temperature in °C, B_{Ch} is half the distance between the upper and lower shelf energy, C_{Ch} is the mid-shelf Charpy transition temperature in °C, and D_{Ch} is the half width of the transition region. The transition curves for a few austenitic SS welds are shown in Figure 3-1; the data for a SA-508 Class 3 low-alloy steel forging are also included for comparison [27,65]. The Charpy-impact data obtained at ANL for the thermally aged Type 304/308 pipe weld represent the saturation condition (i.e., the condition when the lowest impact strength is achieved by the material after long-term service at reactor temperatures). The results indicate that thermal aging increased the mid-shelf Charpy transition temperature by 47°C (i.e., from –105°C to –58°C), and decreased upper shelf

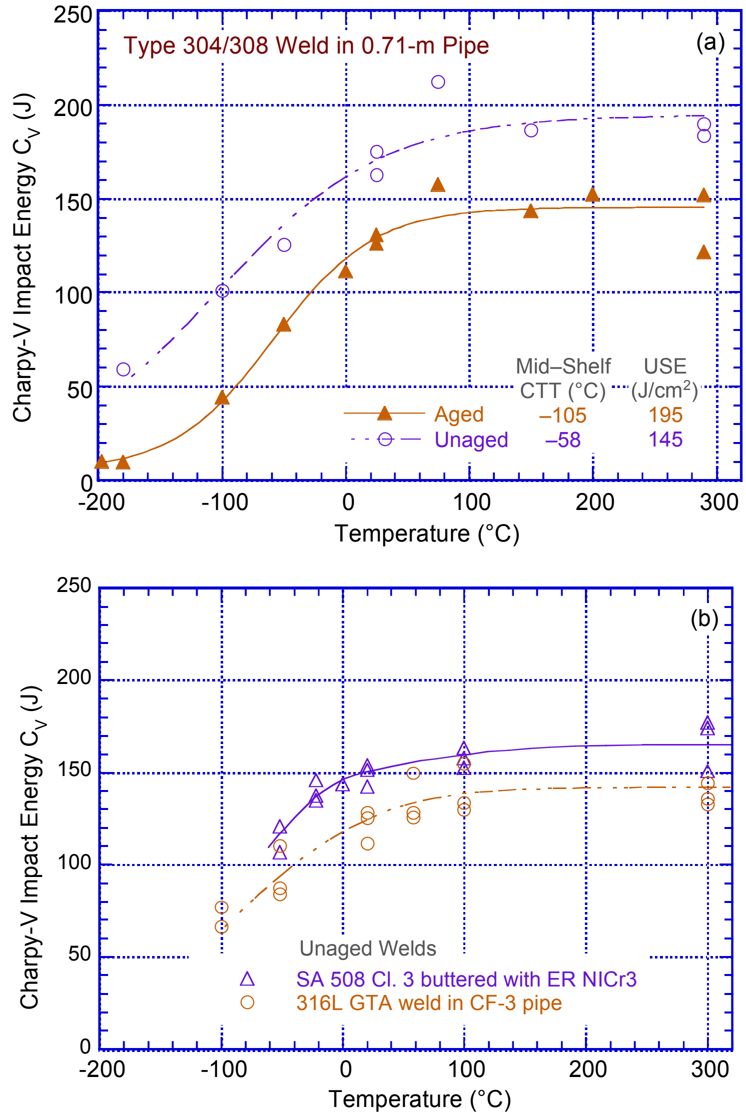

Figure 3-1 The Charpy transition temperature curves for (a) few austenitic SS welds and (b) SA 508 Class 3 low-alloy steel weld (Refs. 27,65).

energy by 50 J/cm^2 (30 ft·lb.) [27]. Similar behavior was observed for all welds; thermal aging resulted in moderate decreases in impact energy at both room temperature and 290°C [27]. The Charpy-impact upper-shelf energy decreased by 50–80 J/cm^2 (30–47 ft·lb) for the various welds.

Similar behavior was also observed in the recent study on thermal embrittlement of Type 308L and Type 316L GTA welds [122]. Aging for up to 20,000 h at 335 and 400°C increased DBTT transition temperature from –196°C to –115°C and –83°C, respectively, for the Type 304L weld, and from –196°C to –48°C and –54°C, respectively, for the Type 316L weld. The increase in DBTT was faster for the welds aged at 400°C. The upper shelf Charpy-impact energy decreased from about 200 J to 120 J for the Type 304L weld and from about 175 J to 115 J for the Type 316L weld.

Another study on thermal embrittlement of three multi pass SMA welds containing 4, 8, and 12% ferrite, showed increase in Charpy-impact transition temperature and decrease in upper shelf energy after thermal aging up to 50,000 h at 343°C [61]. The results are presented in Figure 3-2a and b. The effects increased as the ferrite content increased, and continues to increase with increasing aging time. The 12% ferrite weld exhibits a transition temperature increase of about 60°C, and a drop in upper-shelf energy of 34% after aging for 50,000 h. Microstructural examination of the aged welds indicated that the ferrite contains both heterogeneously and homogeneously nucleated G-phase and phase separation by spinodal decomposition into Fe-rich and Cr-rich regions. The authors concluded that the primary cause of the hardening and thus the property degradation of the welds were caused by spinodal decomposition of the ferrite rather than the G-phase precipitation.

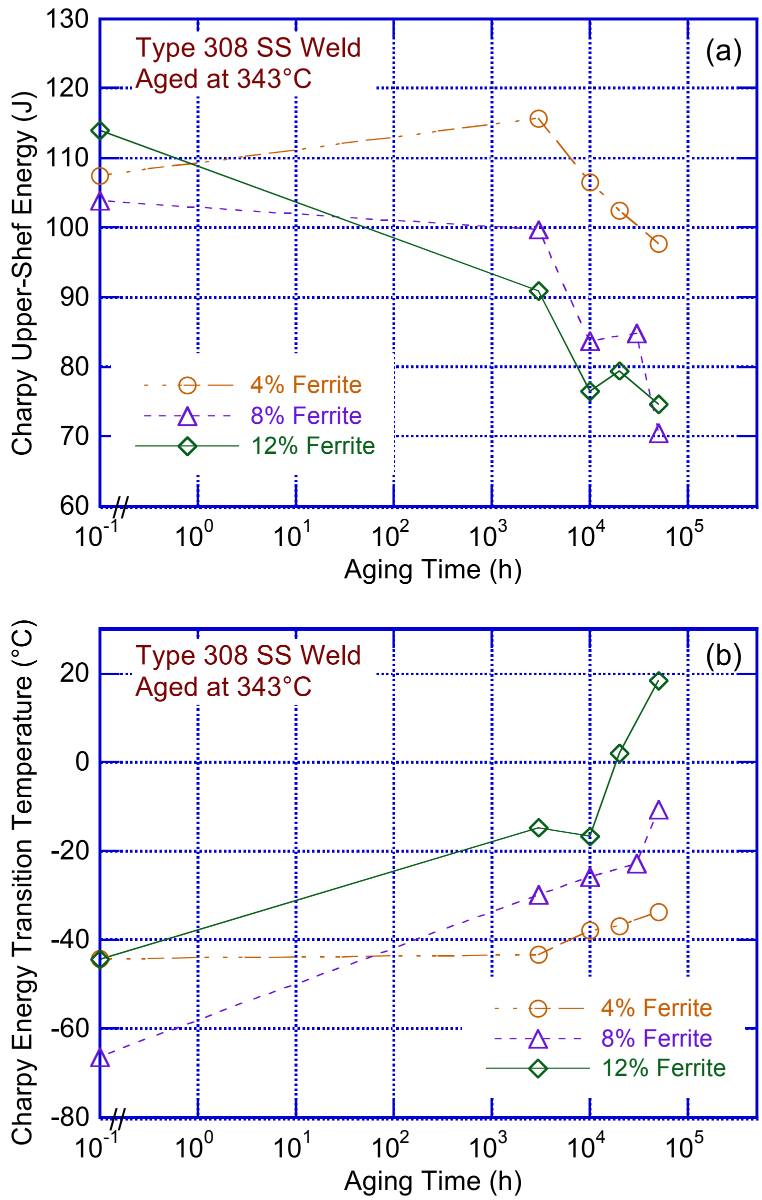

Figure 3-2 The change in (a) Charpy upper-shelf energy and (b) Charpy energy transition temperature for thermally aged Type 308 SMA weld (Ref. 61).

The Charpy-impact data for SMA, SA, and GTA welds prepared from Types 308 or 316 filler metal and in unaged and aged conditions, are shown in Figure 3-3 [1,12,13,27,59–74]. The results for the unaged welds show large variation. The Charpy-impact energy of some welds can be as low as 50 J (37 ft·lb). In general, the GTA welds exhibit higher impact strength than the SMA or SA welds. The impact energies of thermally aged welds [27,59–74] fall within the large scatter band of the unaged welds. The results indicate that the effect of thermal aging on Charpy-impact strength depends on the initial impact strength of the weld. Welds with relatively high impact strength (e.g., the GTA welds) show a significant decrease in impact energy whereas those with poor impact strength show minimal change. However, the data shown in Figure 3-3 indicate that even in the fully embrittled condition, austenitic SS welds have ≥50 J (37 ft·lb) impact energy.

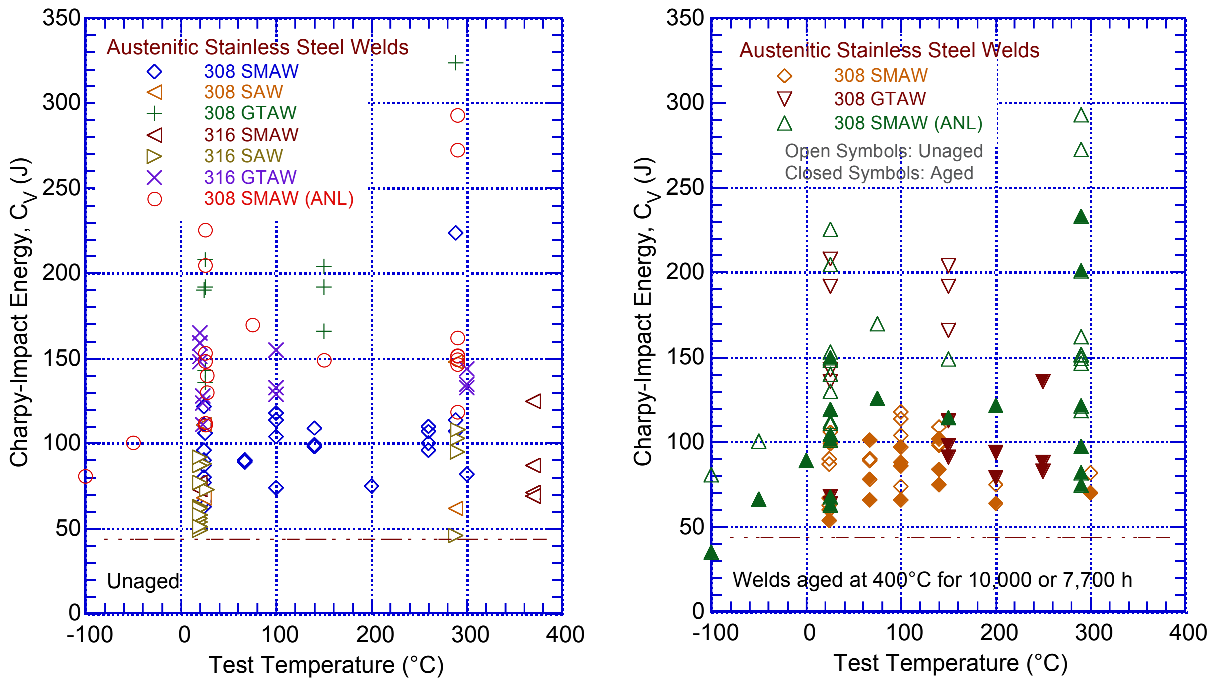

Figure 3-3 Plots of Charpy-impact energy of unaged (Refs. 1,12,13,27,59–74) and aged (Refs. 59–62) austenitic stainless steel welds as a function of temperature.

An example of the change in Charpy-impact energy, C_V, with test temperature as a function of ferrite content of welds, is shown in Figure 3-4 [69]. For an unaged Type 308 manual metal arc (MMA) weld, the difference between the value of C_V at room temperature and at the upper shelf is about 30 J/cm^2. The actual C_V values with increasing ferrite content first decreased when the ferrite increased from 5.2% to 14.0%, but increased back to the same level for the weld with 19.0% ferrite. Similar data for a Type 316 SA weld with 7.0–10.5% ferrite is also included in the figure for comparison. The C_V values for the SA weld are comparable to those for the MMA weld with 10.4% ferrite.

The potential effects of thermal aging on the Charpy-impact energy of a CF-3 pipe MMA orbital weld as a function of test temperature are shown in Figure 3-5 [75]. The results indicate that thermal aging for 3000 h at 300°C has no effect at reactor temperatures and the room temperature C_V is slightly increased. Aging for 1500 h at 400°C or 5000 h at 350°C deceased C_V by about 10 J/cm^2 at 300°C and only marginally at room temperature. However, the aging times at these temperatures are inadequate for estimating end-of-design-life changes. For example,

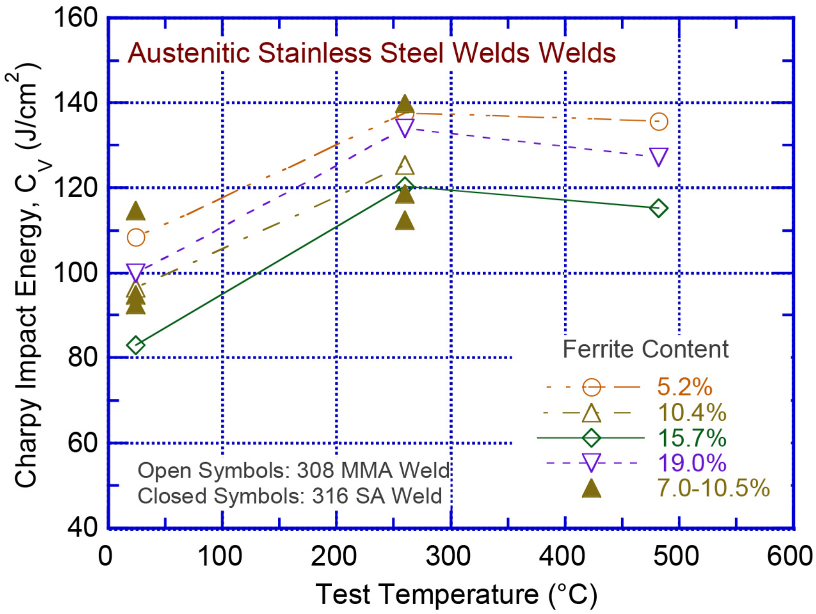

Figure 3-4 **The change in Charpy-impact energy C_V with temperature for austenitic stainless steel welds as a function of ferrite content (Ref. 69).**

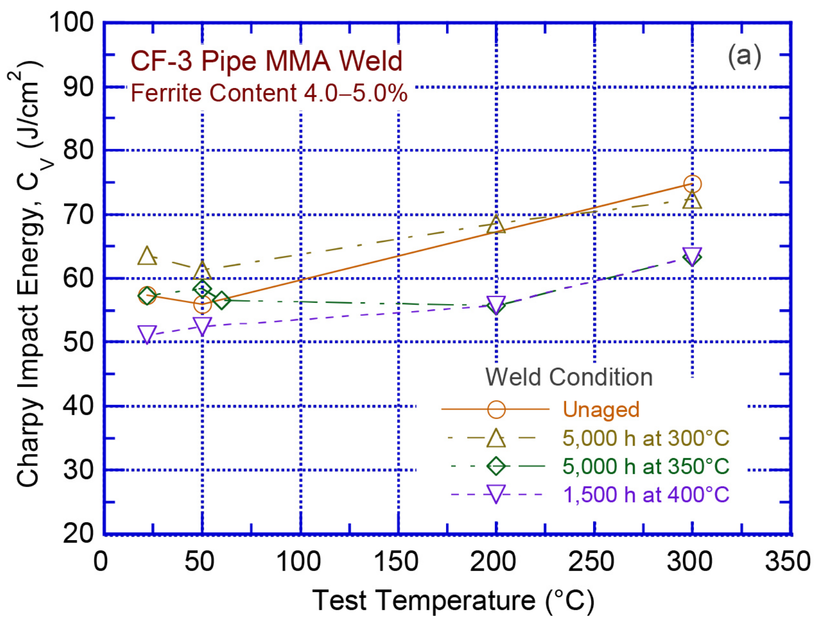

Figure 3-5 **The change in Charpy-impact energy C_V with temperature for an unaged or aged CF-3 pipe MMA orbital weld (Ref. 75).**

1500 h at 400°C is equivalent to about 4 years of reactor operation. Furthermore, the difference between the room temperature and upper-shelf Charpy-impact energy is small. However, the ferrite content of the weld is only 4.0–5.0%, and thermal aging effects are expected to be marginal.

The effect of thermal aging on the room temperature C_V for Type 308 MMA weld with 4, 8, and 12% ferrite and Type 316L GTA weld with 10 and 14% ferrite, are shown in Figure 3-6 and

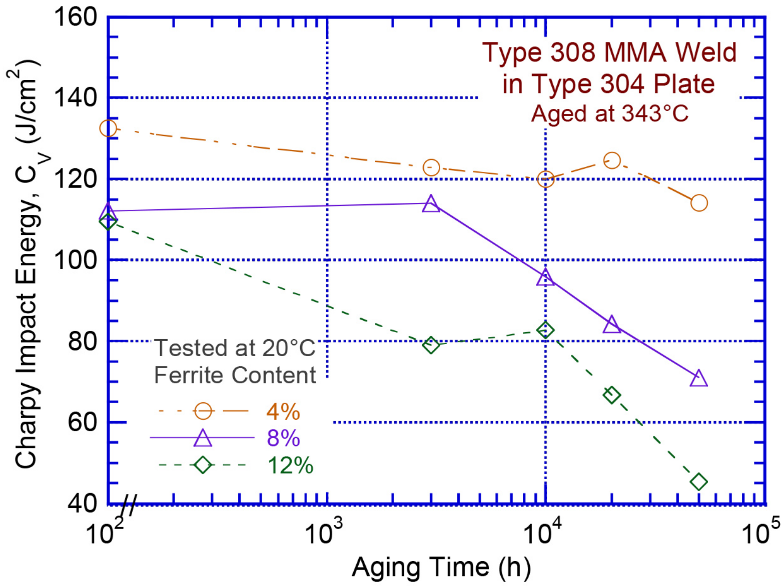

Figure 3-6 The effect of thermal aging on the Charpy-impact energy C_V at room temperature of Type 308 MMA welds with different ferrite content (Ref. 61).

Figure 3-7, respectively [61,78,79]. The results for thermal aging of Type 308 MMA weld at 343°C show that the room-temperature Charpy-impact energy decreases with increasing aging time, and the reduction in Charpy-impact energy increases with an increase in ferrite content of the weld [61]. At 343°C, the decrease in room temperature C_V starts after aging for about 500–1000 h.

The effect of thermal aging at 300 and 400°C, on the Charpy-impact energy, C_V, at 25 and 288°C, of Type 316L GTA weld with 10 or 14% ferrite as a function of aging time, is shown in Figure 3-7a and b [78,79]. Similar to the aging behavior of the Type 308 MMA weld, thermal aging at 300 or 400°C decreases the Charpy-impact energy of Type 316L GTA weld both at room temperature and at reactor temperature. The Charpy-impact energy of the GTA weld with 14% ferrite is greater then that of the weld with 10% ferrite. After long-term aging of the GTA welds at 400°C (i.e., more than about 3000 h) the impact energies of both welds at reactor temperature are the same as those at room temperature. The thermal aging behavior at 400°C of a CF-8M CASS material with 15.5% ferrite, is shown in Figure 3-7b for comparison. In general, the C_V values of the CASS material are lower. However, unlike the behavior of GTA welds, C_V continues to decrease even after 3000 h aging at 400°C.

Metallographic examination [27] of the fracture surface of unaged and aged weld metal Charpy-impact test specimens tested at room temperature indicate that the overall fracture behavior of the welds is controlled by the distribution and morphology of second-phase particles. All welds exhibit a dimple fracture. Photomicrographs of the fracture surface of Charpy specimens of a Type 308L SMA weld in the unaged and aged conditions and tested at room temperature are shown in Figure 3-8. Nearly every dimple is initiated by decohesion of an inclusion (most likely manganese silicide). Failure occurs by nucleation and growth of microvoids and rupture of the remaining ligaments. The hard inclusions in the weld resist deformation, and the buildup of high local stresses leads to decohesion of the particle/matrix interface. Inferior fracture resistance of the welds may be attributed to the higher density and larger size of inclusions. The ferrite phase seems to have little effect on the fracture properties of the welds. Cleavage of ferrite is typically not observed in the welds. However, cleavage of the ferrite phase may occur at very low temperatures, particularly for welds containing more than 10% ferrite.

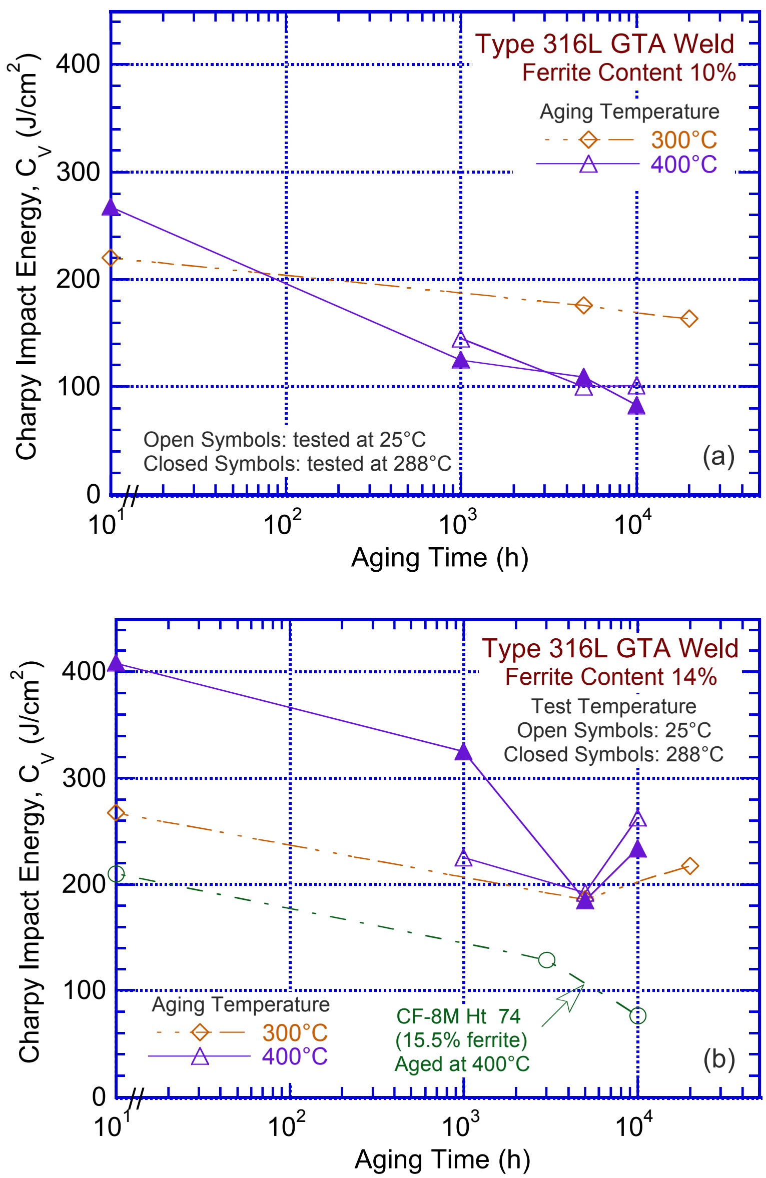

Figure 3-7 The change in Charpy-impact energy C_V with temperature for austenitic stainless steel welds as a function of ferrite content (Ref. 69).

3.2.2 Tensile Properties

The tensile yield and ultimate stresses for SMA, SA, and GTA welds prepared by using Types 308 or 316 filler metal, in the unaged and aged conditions, are shown as a function of test temperature in Figure 3-9 [1,12,13,27,59–74]. The tensile data at ANL were estimated from the instrumented Charpy-impact test results [27]. For a Charpy specimen, the yield stress σ_y is estimated from the expression

$$\sigma_y = C_1 P_y B/W b^2, \tag{16}$$

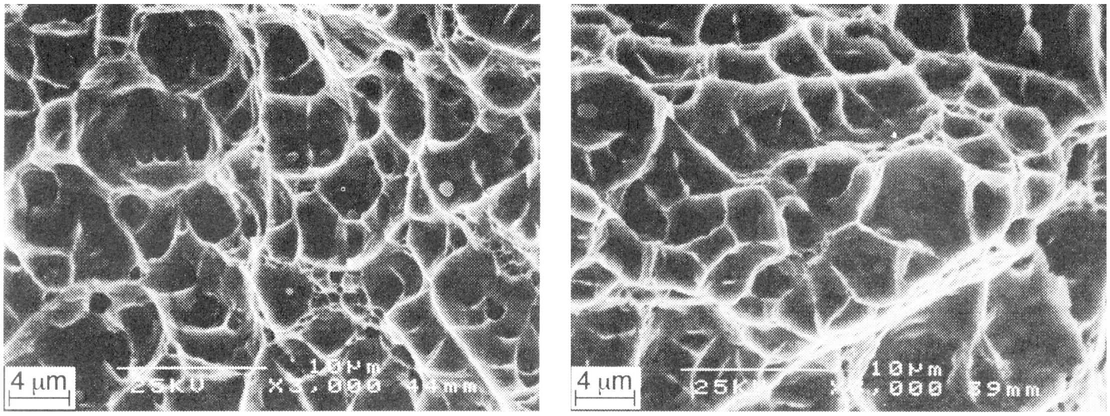

(a) (b)

Figure 3-8 Photomicrographs of the fracture surface of (a) unaged and (b) aged Type 308L SMA weld Charpy specimens tested at room temperature (Ref. 27).

and the ultimate stress σ_u is estimated from the expression

$$\sigma_u = C_2 P_m B/W b^2, \tag{17}$$

where P_y and P_m are the yield and maximum load, respectively; W is the specimen width; B is the specimen thickness; b is the uncracked ligament; and C_1 and C_2 are constants [123]. The yield and maximum loads were obtained from load-time traces of the instrumented Charpy-impact tests. The constants C_1 and C_2 were determined by comparing the Charpy-impact test results with existing tensile-property data for Type 308 and 316 weld metals. The best value of the constants was 2.2 for both C_1 and C_2. The estimated yield and ultimate stress for the various welds are compared with existing data for Type 308 or 316 welds in Figure 3-9. Average values of yield and ultimate stress for PWWO, PWCE, PWDR, and PWMS welds are listed in Table 3-1 [27]. Thermal aging has little or no effect on the tensile properties of Type 308 welds. These results are consistent with the data from several other studies [59–62].

Table 3-1 Tensile yield and ultimate stress of various stainless steel welds, estimated from Charpy–impact data.

			Room Temp.		290°C	
Material ID	Aging Temp. (°C)	Aging Time (h)	Yield Stress (MPa)	Ultimate Stress (MPa)	Yield Stress (MPa)	Ultimate Stress (MPa)
PWCE	–	–	425	643	315	430
	400	10,000	442	635	321	490
PWWO	–	–	472	633	349	446
	400	7,700	478	620	346	472
PWDR	–	–	437	608	289	421
	400	10,000	443	519	300	409
PWMS	–	–	471	650	327	456

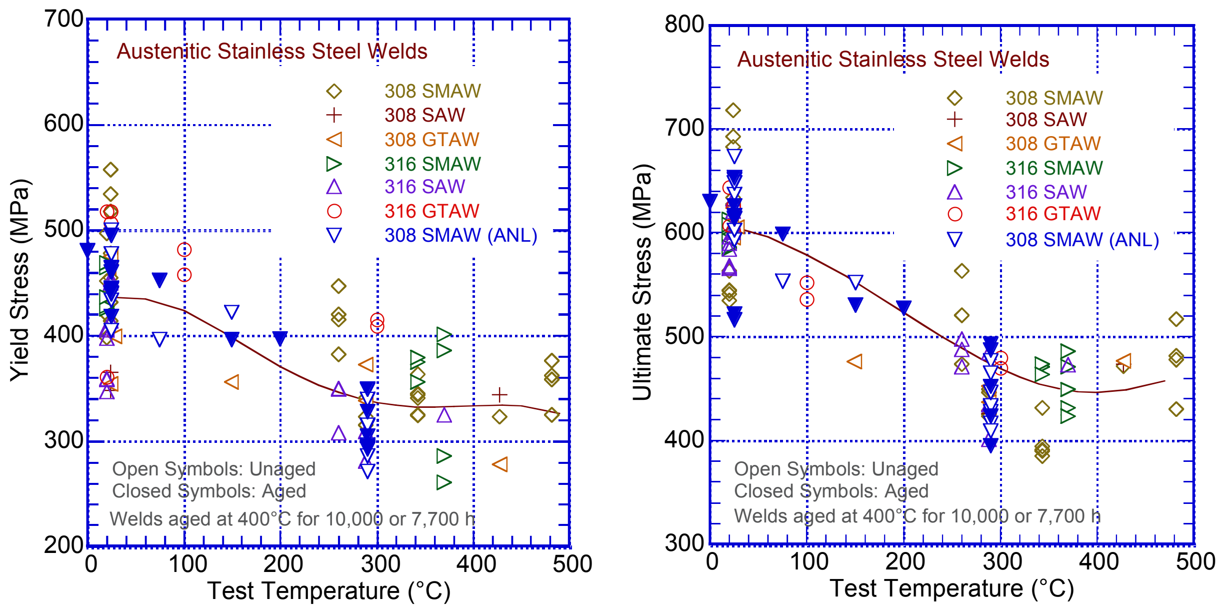

Figure 3-9 Tensile yield and ultimate stress of austenitic SS welds (Refs. 1, 12,13,27,59–74). Solid lines are the best fit to the data (Ref. 27).

The data in Figure 3-9 show significant scatter in the values of both yield and ultimate stresses. In general, both yield stress and ultimate tensile stress are lower at reactor temperatures than at room temperature. However, for some weak welds, the difference is insignificant, particularly for the yield stress. The limited data for aged welds show little or no effect of thermal aging (see open and closed inverted triangles in Figure 3-9). However, as discussed earlier, this is because of the relatively low ferrite content and thin vermicular ferrite morphology of these welds.

A few examples of the change in yield and ultimate tensile stress with temperature, of Type 308 MMA welds with different ferrite contents and a Type 316L GTA weld with 10% ferrite, are shown in Figure 3-10. The solid lines in the figure are the best-fit curve plotted in Figure 3-9; all of these welds are above the best-fit curve. The results indicate that both the yield and ultimate tensile stresses increase with the ferrite content of the weld. The yield stress of the Type 308 MMA and Type 316L GTA welds containing 10% ferrite are essentially the same, but the ultimate tensile stress of the Type 316L GTA weld is lower.

The difference is most likely due to the carbon content of the welds. Examples of the effect of thermal aging at 343°C on the tensile properties of Type 19-9L MMA weld with 5.0–9.0% ferrite, and a Type 308 SMA weld with different ferrite contents, are shown in Figure 3-11a and b. The tensile strength of austenitic SS welds increases with thermal aging at temperatures of 250–400°C. However, unlike the significant effect on Charpy impact energy, the change in tensile strength is relatively small. Thermal aging seems to have little or no effect on the yield stress and the ultimate tensile stress is slightly increased.

3.2.3 Fracture Toughness J-R Curves

The NRC sponsored fracture toughness J-R curve data compiled in the Pipe Fracture (PIFRAC) Database and from a few other sources [12,59–65], are shown in Figure 3-12 [27]. The database

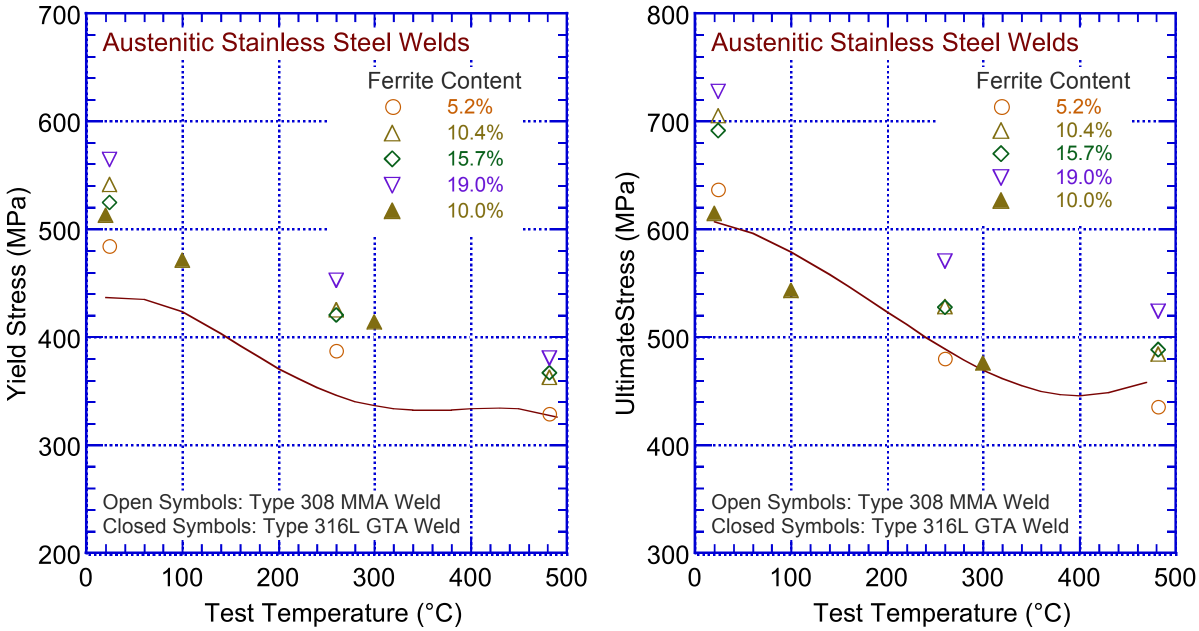

Figure 3-10 Tensile yield and ultimate stress of austenitic SS welds with different ferrite contents (Refs. 69). Solid lines from Figure 3-9.

PIFRAC3 [66–77] was originally compiled at Materials Engineering Associates, Inc. [80] and later updated by Battelle Memorial Institute [81]. The results indicate that fracture properties of austenitic SS welds are relatively insensitive to filler metal [12]. However, the welding process significantly affects fracture toughness [124]. In general, GTA welds exhibit higher fracture

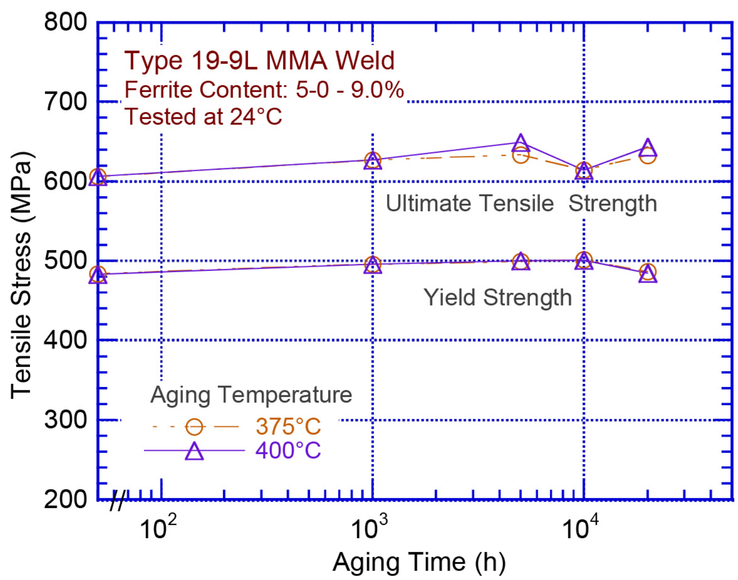

Figure 3-11 The effect of thermal aging on the room-temperature tensile properties of Type 19-9L and Type 308 SMA welds (Ref. 61,62).

[3] G. Wilkowski and N. Ghadiali, “Short Crack in Piping and Piping Welds,” in Technical Data CD-ROM, Battelle Columbus Division, Columbus, OH (May 1995).

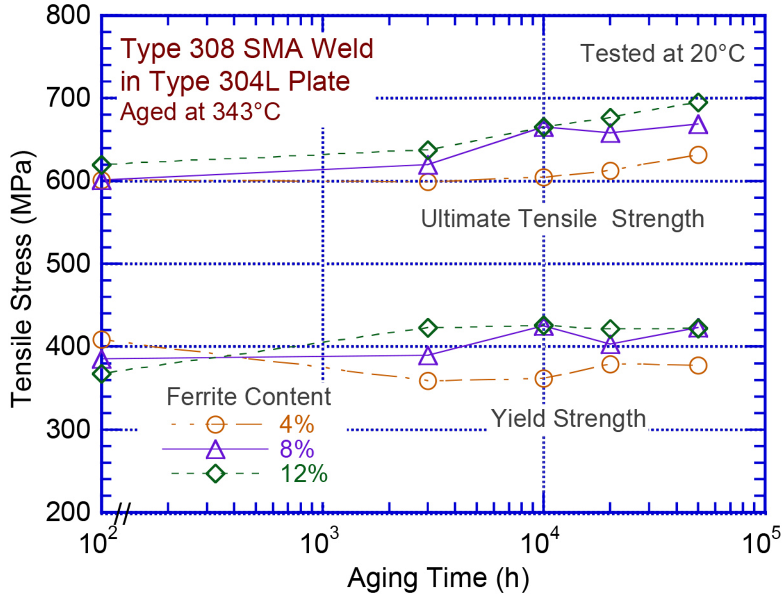

Figure 3-11 The effect of thermal aging on the room-temperature tensile properties of Type 19-9L and Type 308 SMA welds (Ref. 61,62) (Cont'd).

resistance than SA or SMA welds. The statistical differences in SA and SMA weld fracture toughness J-R curves have also been evaluated [82] and results indicate no difference between SA and SMA welds J-R curves. The results also indicate that, in general, the fracture toughness of austenitic SS welds is higher at room temperature than at reactor temperature. In the earlier study on thermal embrittlement of austenitic SS welds at ANL [27], the lower-bound fracture toughness J-R curve at 288°C for SS welds was represented by the expression proposed by Wilkowski in NUREG/CR-4878 and given by

$$J(\mathrm{kJ/m^2}) = 73.4 + 83.5\ \Delta a(\mathrm{mm})^{0.643}, \tag{18}$$

where 73.4 $\mathrm{kJ/m^2}$ is the fracture toughness J_{Ic}. The lower bound J-R curve given by Eq. 18 can also be represented in terms of the standard power law J-R curve expressed as

$$J(\mathrm{kJ/m^2}) = 138\ \Delta a(\mathrm{mm})^{0.45}. \tag{19}$$

The J-R curve data at 100–427°C for SA welds, MMA and SMA welds, and GTA, metal inert arc (MIG), and tungsten inert gas (TIG) welds from several studies [12,13,39,62–68,75–77,78,79, 83–85] and some of the significant results from earlier ANL study [27] are shown in Figure 3-13. The results indicate that fracture toughness of Type 316 welds is lower than that of Type 308 welds and that fracture toughness of low-C 316L and 308L welds, are lower than those of Type 316 and 308 welds, respectively. In addition, fracture toughness at room temperature is typically higher than at reactor temperatures. The results also indicate that the fracture toughness of GTA/MIG/TIG welds is generally superior to that of SA or SMA welds. The J value at 2.5-mm crack extension ($J_{2.5}$) is in the range of 600–1200 $\mathrm{kJ/m^2}$ for GTA/MIG/TIG welds, and 300–700 $\mathrm{kJ/m^2}$ for SMA welds. The lower-bound J-R curves in Eqs. 18 and 19 essentially represent the SA and SMA weld data; it is quite conservative for GTA or TIG weld fracture toughness data.

Based on the fracture toughness data evaluated in this study, the lower-bound power-law J-R curve for unaged GTA/MIG/TIG welds may be represented by

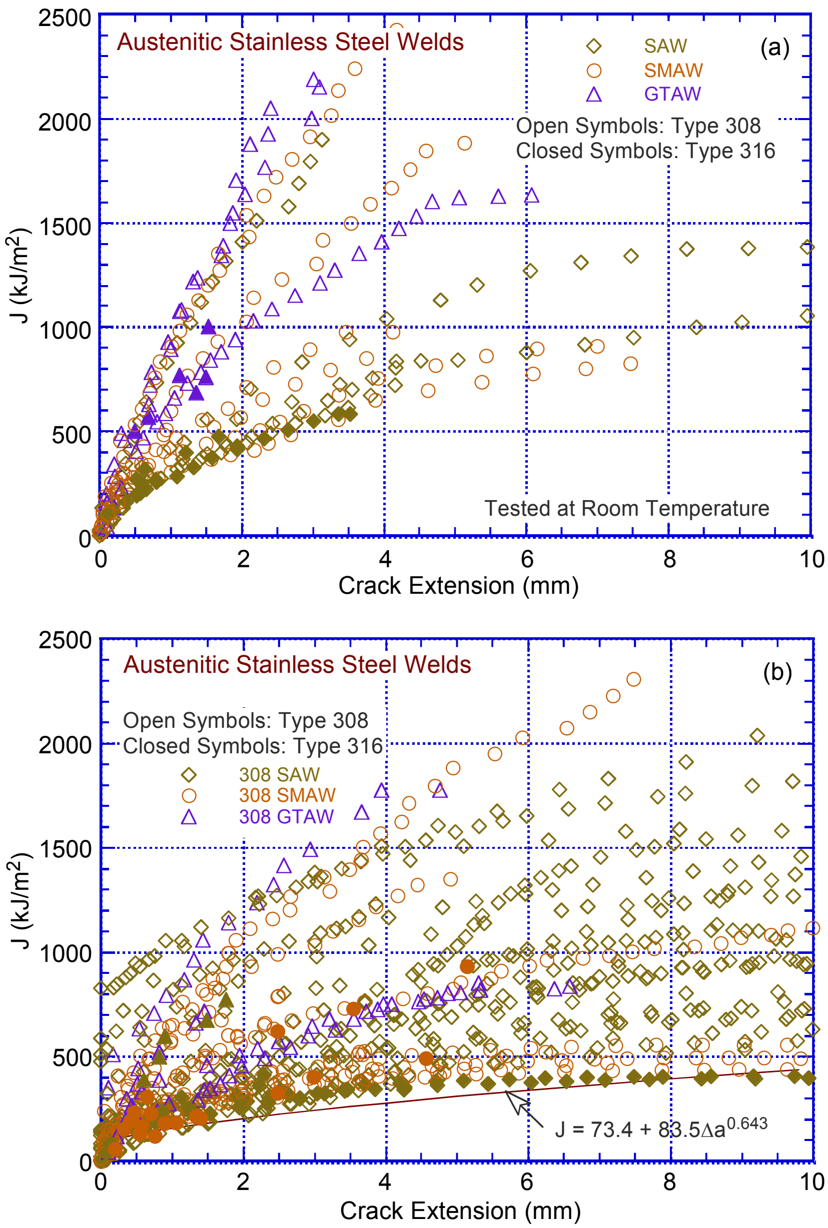

Figure 3-12 Fracture toughness J-R curves for SS welds at (a) room temperature and (b) 288–427°C. Solid line represents lower-bound curve (Ref. 27).

$$J(\text{kJ/m}^2) = 330\ \Delta a(\text{mm})^{0.45}. \tag{20}$$

However, additional data are needed to validate this lower bound curve for GTA/MIG/TIG welds. Note that the fracture toughness J-R data obtained by Lucas et al. [78,79] were not considered in establishing the above lower bound J-R curve because they are considered an outlier. For the two GTA welds (with FNs of 10 and 14) investigated by Lucas et al., the fracture toughness J-R curves at 288°C were comparable to the lower-bound J-R curve for SA/SMA welds (i.e., Eq. 19). Furthermore, the reported J_{Ic} values (in the range of 130–155 kJ/m^2) were determined using a slope of two times the flow stress, which is inappropriate for high toughness, ductile, and strain hardening materials. The analytical procedures described in the ASTM Specifications for J_{Ic} determination are not applicable for such materials; they significantly over predict crack extension and, therefore, yield nonconservative values of J_{Ic} [32,125]. For austenitic SSs, a value of four times the flow stress better defines the blunting line. The recalculated values of J_{Ic} using a steeper slope for the blunting line are in the range of 100–120 kJ/m^2. These results are unusual for GTA welds.

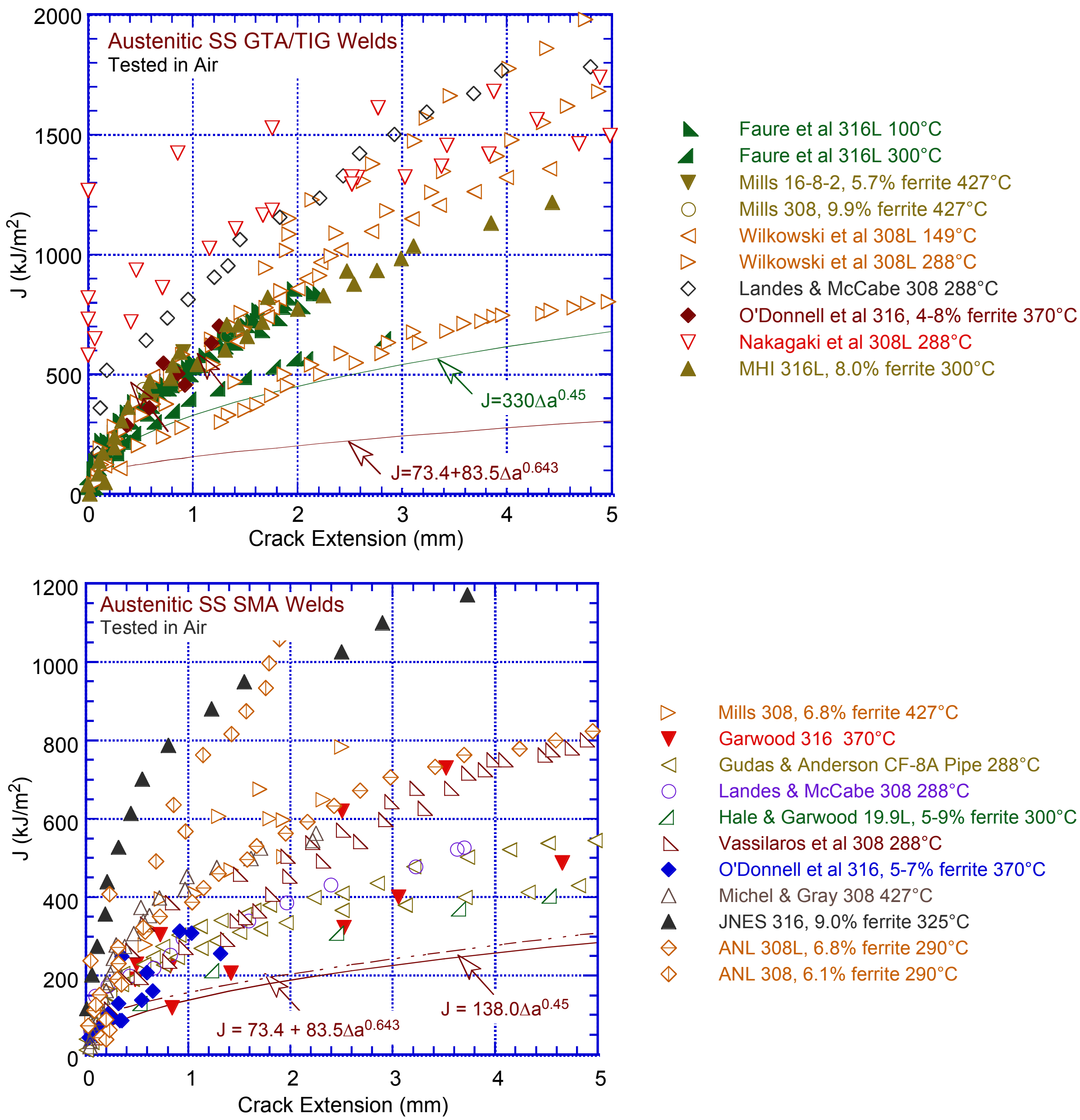

Figure 3-13 **Fracture toughness J-R curves for unaged SS welds at 100–427°C. Lines represent lower-bound curves (Ref. 12,13,27,39,62–68,75–77,78,79,80–85).**

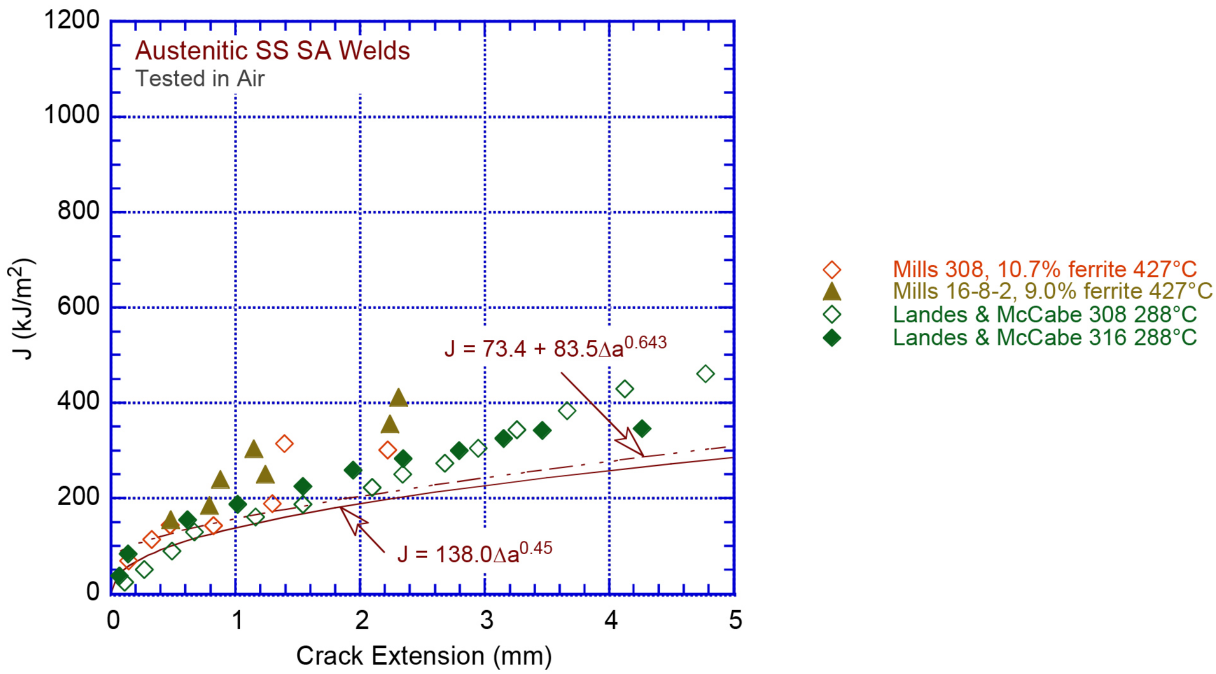

Figure 3-13 Fracture toughness J-R curves for unaged SS welds at 100–427°C. Lines represent lower-bound curves (Ref. 12,13,27,39,62–68,75–77,78,79,80–85) (Contd.)

The limited fracture toughness J-R data [12,13,27,62,85] at 288–427°C for thermally aged SMA/MMA and GTA/MIG/TIG welds are shown in Figure 3-14. In thermal aging studies, aging for about 7,000–10,000 h at 400°C is sufficient to achieve saturation toughness (i.e., the minimum value that could be achieved after long-term aging). The results indicate that the welds investigated at ANL [27] or by Mills [12,13] showed little or no effect of aging for 7,700 h or 10,000 h at 400°C. However, the SMA or GTA/TIG welds investigated by Mitsubishi Heavy Industries, Ltd. (MHI) show significant effects of aging for 10,000 h or higher at 400°C or for 40,000 h or higher at 300 and 350°C.[4] The difference, most likely, is because of differences in the amount and morphology of the ferrite in the welds. The welds studied at ANL or by Mills had relatively low ferrite content and discontinuous vermicular ferrite morphology, whereas the welds studied at MHI had higher ferrite and probably had continuous lacy ferrite morphology.

In the earlier study at ANL [27], the lower-bound fracture toughness J-R curve at 288°C for thermally aged austenitic SS welds was represented by the expression

$$J(kJ/m^2) = 40.0 + 83.5\ \Delta a(mm)^{0.643}, \qquad (21)$$

where 40 kJ/m^2 is the fracture toughness J_{Ic} of thermally aged SS welds. This lower bound J-R curve can be represented in terms of the power law J-R curve, expressed as

[4] K. Hojo, Japanese PWR Owner's Group's CASS Database prepared by Mitsubishi Heavy Industries, Ltd. presented at the ASME Code Meetings, Working Group Flaw Tolerance Evaluation, Washington DC, August 2014. However, the quality of the J-R curve plots was not good for Δa less then 1.0 mm and J less then 400 kJ/m^2.

$$J(kJ/m^2) = 117\ \Delta a(mm)^{0.45}. \tag{22}$$

Like the lower-bound J-R curve for unaged welds, Eq. 22 represents the lower-bound J-R curve for aged SA/SMA welds. Based on the fracture toughness data evaluated in this study, the lower-bound power-law J-R curve for aged GTA/MIG/TIG welds may be represented by

$$J(kJ/m^2) = 270\ \Delta a(mm)^{0.45}. \tag{23}$$

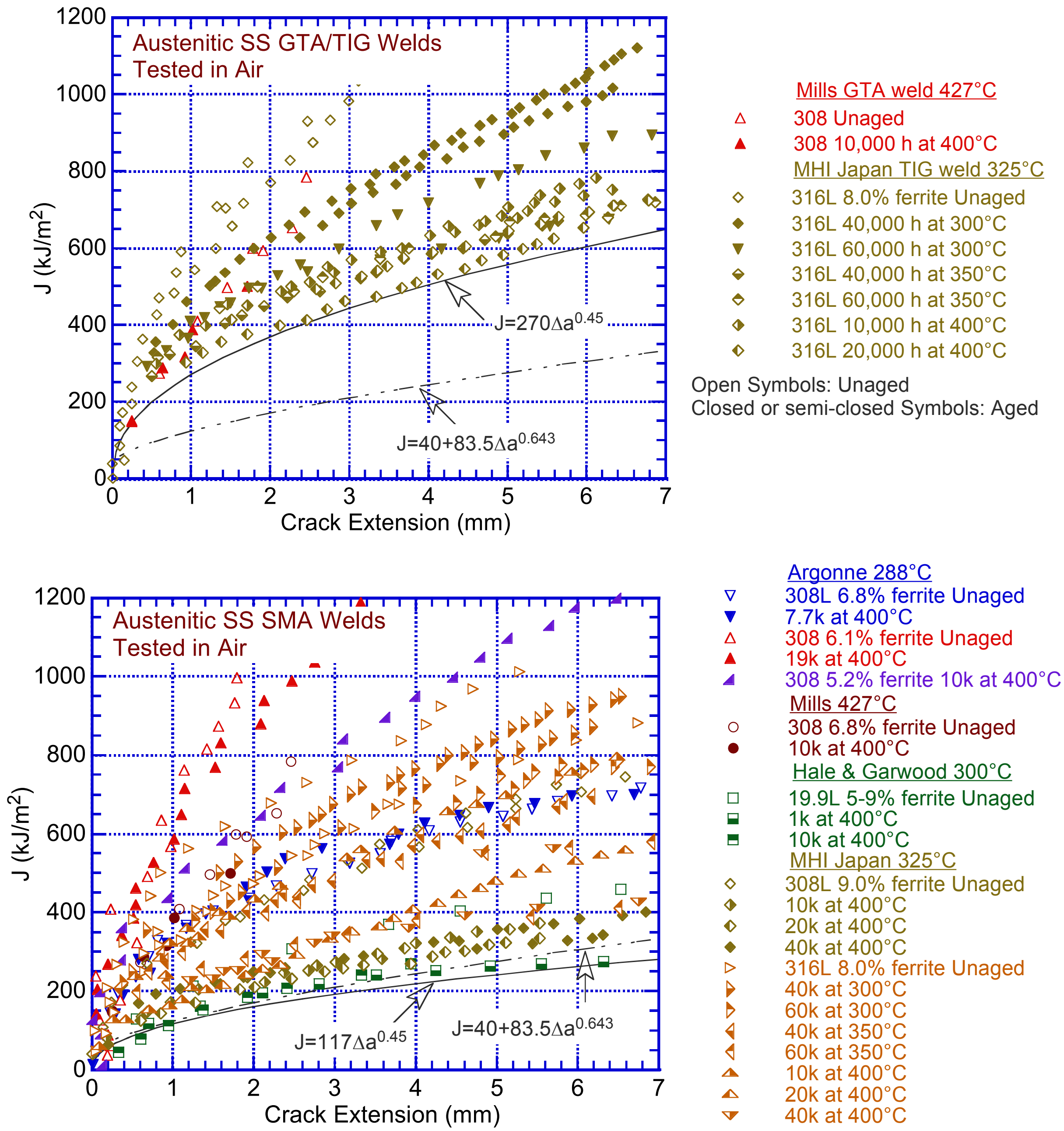

Figure 3-14 Fracture toughness J-R curves for aged austenitic stainless steel welds at 288–427°C. Chain dash and solid lines represent lower-bound curves (Ref. 12,13,27,39,62,85).

These lower bound curves for aged materials are shown in Figure 3-14. These proposed lower bound J-R curves for unaged SS welds are compared with the fracture toughness data used in the analysis performed for the technical basis document for American Society of Mechanical Engineers (ASME) Section XI, Article IWB-3640 (1989 edition), in Figure 3-15. The J-R curve reconstructed from the data for the ASME IWB-3640 SA weld is also shown in the figure. The lower bound curve for unaged welds (i.e., Eq. 19) bounds most of the experimental data obtained at 200 and 288°C (392 and 550°F) for Linde 80 weld metal [83].

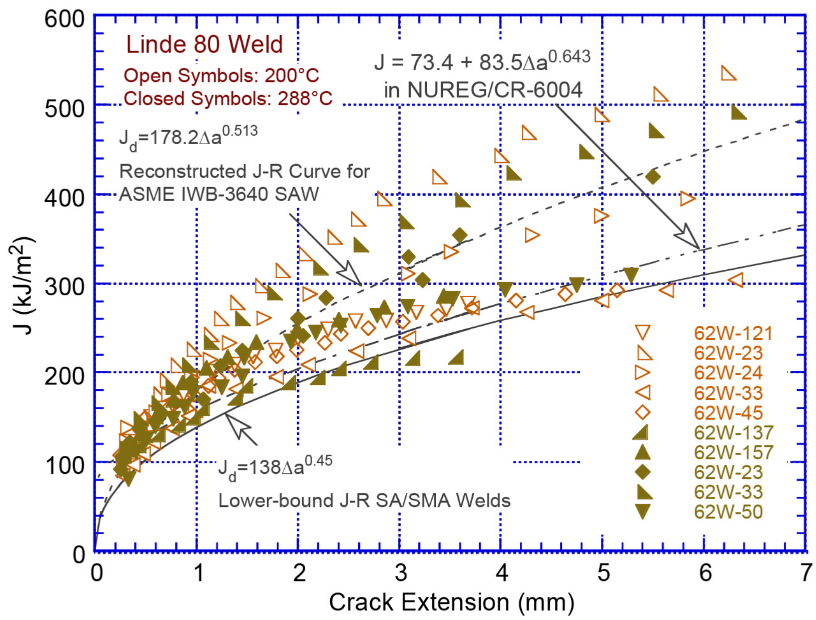

Figure 3-15 Fracture toughness J-R curves for Linde 80 welds at 200 and 288°C and the lower-bound J-R curve for unaged SS welds.

The J_{Ic} values for unaged and aged austenitic SS SA, SMA/MMA, and GTA/MIG/TIG welds are plotted as a function of test temperature in Figure 3-16. The results indicate that at reactor temperatures, the fracture toughness J_{Ic} of unaged and aged austenitic SS, SA and SMA welds can be as low as 40 kJ/m^2. At room temperature, the minimum J_{Ic} values of unaged and aged SA/SMA welds are slightly higher, 70 kJ/m^2.

However, the existing data are quite limited and the observed difference in the minimum fracture toughness of SS welds with temperature may be unique to the data set reviewed in this study. In the unaged condition, the 308/316 SA welds and 316 SMA welds have the lowest J_{Ic} values. The minimum J_{Ic} value of 308/316 GTA, MIG, or TIG welds is significantly higher than for SA or SMA welds. The available data in Figure 3-16 indicate that the fracture toughness J_{Ic} values of unaged and aged 308/316 GTA welds are above 170 kJ.m^2; however, the data for aged GTA welds is rather limited. As mentioned earlier, the data obtained by Lucas et al. on 316 GTA weld was excluded from this analysis; these data are considered outliers.

The fracture toughness J-R curves for unaged and aged austenitic SS welds (i.e., Eq. 19 for unaged welds and Eq. 22 for aged welds) are compared in Figure 3-17 with the data in the technical basis document for ASME Section XI, Article IWB-3640 (1989 edition) [62,67,74]. The results indicate that the proposed curves are consistent with the available fracture toughness data for unaged and aged austenitic SS, SMA and SA welds. Slightly higher lower-bound J-R curves (i.e., Eqs. 20 and 23) are proposed for unaged and aged GTA welds. However, the existing data for aged GTA welds are limited, and additional fracture data should be obtained to check the adequacy of the lower bound J-R curves for the GTA weld.

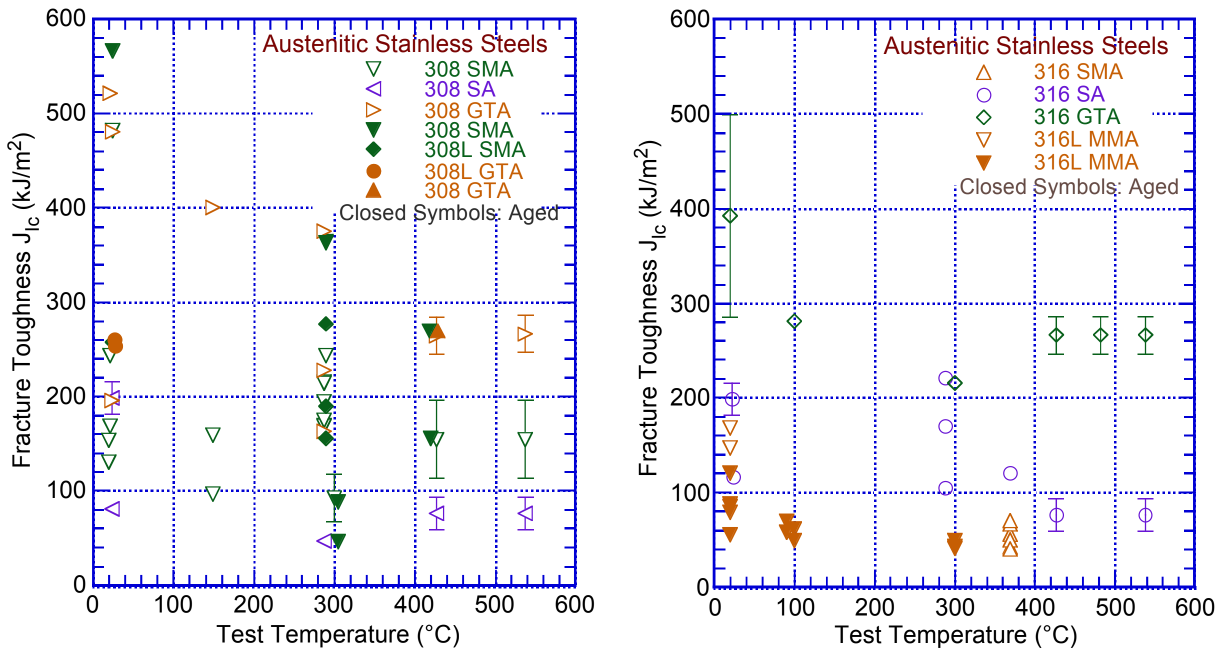

Figure 3-16 Fracture toughness J_{Ic} for unaged and aged SS welds, with or without Mo.

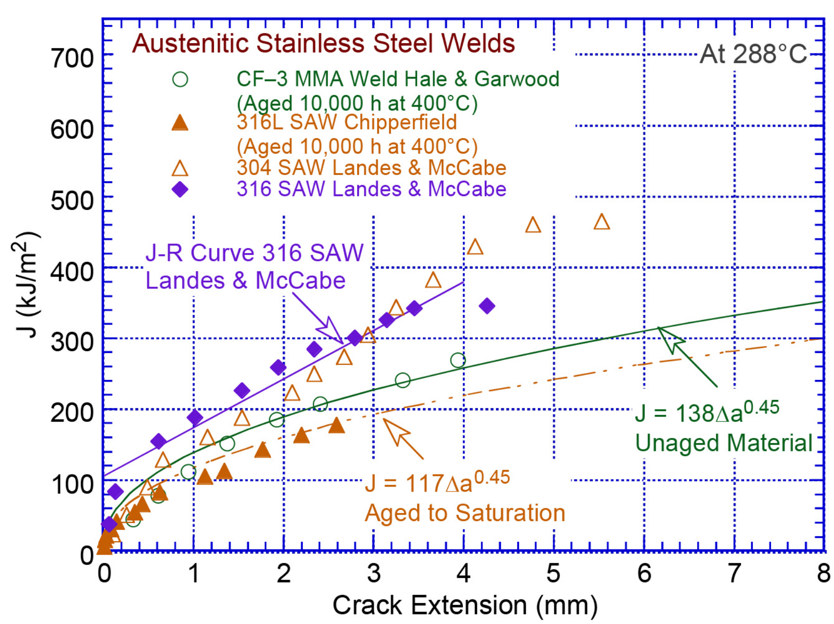

Figure 3-17 Fracture toughness lower-bound J-R curves and the data on Type 304, 316L, and CF-3 welds used to develop the ASME Code IWB-3640 analysis.

3.2.3.1 Potential Effects of Reactor Coolant Environment

A recent study on low-temperature crack propagation for thermally aged CF-8 material in PWR environments showed that at reactor operating temperatures, the fracture toughness J-R curve is generally lower in PWR water than it is in air, and in PWR shutdown water chemistry (SWC) at 54°C it is significantly lower than in air [126]. The CF-8 material was aged for about 15.8 y at 350°C. The large reduction in fracture toughness of the aged material was attributed to potential synergy between hydrogen embrittlement and thermal embrittlement associated with decomposition of the ferrite at reactor temperatures. The significant environmental effects in simulated PWR SWC were associated with hydrogen-induced intergranular cracking.

Similar effect of reactor coolant environment on fracture toughness J-R data has also been observed for Type 316L GTA welds containing 10% or 14% ferrite [78,79]. The fracture toughness J-R curves for these welds at 288°C in air and BWR environment with 300 ppb dissolved oxygen (DO) are shown in Figure 3-18. As mentioned earlier, these results indicate that the fracture toughness of the as-welded material is much lower than that of a typical GTA weld. It is comparable to that of a thermally aged SA/SMA weld. However, the results show that the in-situ fracture toughness of these welds in the reactor coolant environment is up to 40% lower than in air. The degradation was attributed to absorption of hydrogen in the material during exposure to the high-temperature aqueous environment [78,79].

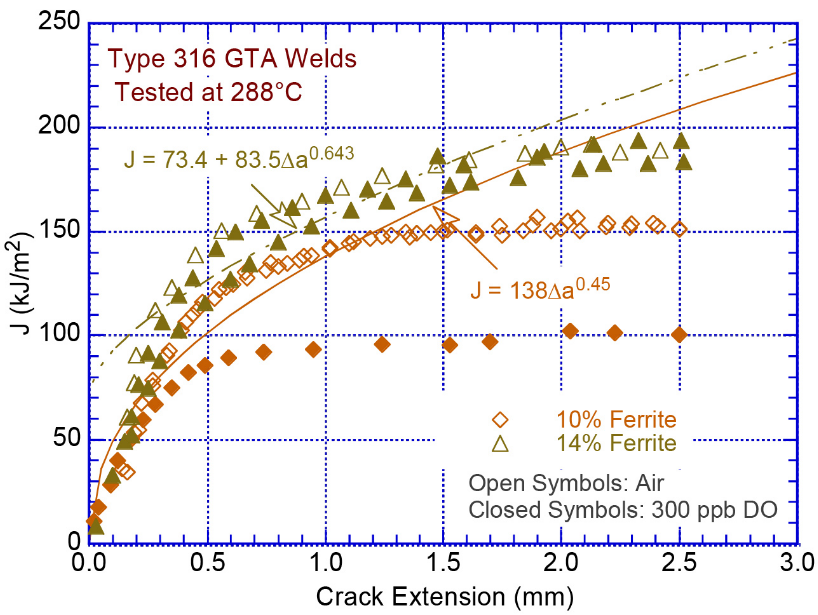

Figure 3-18 Fracture toughness J-R curve data for as-welded Type 316L GTA weld at 288°C in air and BWR environment with 300 ppb DO (Ref. 78,79).

In contrast, ANL studies on the effects of reactor coolant environment on fracture toughness of neutron-irradiated, wrought austenitic SSs, including HAZ material [47], indicated insignificant effect of environment. However, it was not clear why environmental effects were insignificant. It is possible that since the ANL study was conducted on irradiated SSs with very low fracture toughness (i.e., J_{Ic} <200 kJ/m^2), environmental effects are insignificant for such material. It is more likely that the difference was due to the differences in the material; the ANL study was conducted on single-phase wrought SS whereas the other two studies were on materials with duplex structure of ferrite and austenite phases. However, because the degradation in fracture toughness in BWR environment was attributed to absorption of hydrogen in the material, the results in Figure 3-18 do not necessarily over estimate environmental effects in BWR hydrogen water chemistry (HWC) environments. Additional fracture toughness data in LWR environments are needed to accurately establish the environmental effects on fracture toughness of SSs welds.

A low-fracture-toughness behavior has been observed for single-phase alloys such as Alloys 600 and 690 in hydrogenated water at 54°C and at low displacement rates (i.e., under quasi-static conditions) [127,128]. Nakajima et al. have also observed potential effects of a simulated BWR environment on the fracture toughness of sensitized Type 304 SS at 98 and 288°C and slow strain rates [129]. They observed no effect of displacement rate for the as-received Type 304 SS. However, the fracture toughness of the sensitized material decreased with a decreasing displacement rate and an increasing degree of sensitization. At 288°C, the effect of a water environment increased with increasing DO in the environment (i.e., the fracture toughness decreased with increasing DO).

These results indicate potential effects of the reactor coolant environment on the fracture toughness of thermally aged austenitic SS materials with duplex structures. The effects are particularly significant at low temperatures and under PWR SWC environments. However, the available data are inadequate to accurately establish the effects of environment on fracture toughness, particularly under low-temperature, BWR HWC conditions. Additional fracture toughness tests on thermally aged austenitic SS welds in air and LWR environments are needed to better understand the combined effects of hydrogen embrittlement and thermal embrittlement in LWR environments. In the interim, degradation of the fracture toughness of austenitic SS welds due to reactor coolant environment needs to be evaluated on a case-by-case basis.

3.3 Summary

Based on the above discussions and evaluation of the available fracture toughness J-R curve data, the recommended lower bound J-R curve for unaged and thermally aged austenitic SS welds are summarized below. Equation 19 represents the J-R curve for unaged SA and SMA welds:

$$J(kJ/m^2) = 138\ \Delta a(mm)^{0.45}.$$

Equation 20 represents the J-R curve for unaged GTA welds:

$$J(kJ/m^2) = 330\ \Delta a(mm)^{0.45}.$$

Equation 22 represents the J-R curve for thermally aged SA and SMA welds:

$$J(kJ/m^2) = 117\ \Delta a(mm)^{0.45}.$$

Equation 23 represents the J-R curve for thermally aged GTA welds:

$$J(kJ/m^2) = 270\ \Delta a(mm)^{0.45}.$$

In addition, potential degradation of the fracture toughness of austenitic SS welds due to reactor coolant environment also needs to be evaluated, particularly at low temperatures and under PWR SWC environments.

4 COMBINED EFFECTS OF THERMAL AND NEUTRON EMBRITTLEMENT

The potential combined effects of thermal and neutron embrittlement of austenitic SS welds was discussed briefly with those of CASS materials in a journal article entitled, “Methodology for Estimating Thermal and Neutron Embrittlement of Cast Austenitic Stainless Steels during Service in LWRs,” published earlier [97]. Although the actual values of maximum neutron dose for austenitic SS welds in reactor core internals after 60-y service are not available, they can be appreciable, particularly for PWRs. A neutron dose of 8–10 dpa is expected for BWR core shroud; it is likely also to bound welds in the PWR core barrel as well. The fracture toughness of these duplex materials decreases with increasing neutron irradiation dose. The extent of embrittlement (i.e., loss of fracture toughness) depends on the amount and morphology of the ferrite phase in the material. In addition, most of the existing fracture-toughness data on austenitic SS and associated welds have been obtained on materials irradiated in fast reactors, which may be non-conservative for LWR conditions.

4.1 Mechanism of Neutron Embrittlement

Neutron irradiation of materials can produce damage by displacing atoms from their lattice position. Each displaced atom creates a vacancy and self-interstitial atom pair. These defects are unstable, and most of them are annihilated by recombination. The surviving defects rearrange into more stable configurations such as dislocation loops, network dislocations, precipitates, and cavities (or voids), or migrate to sinks such as grain boundaries, dislocations, or surfaces of second phase particles. The production, annihilation, and migration of the point defects lead to changes in the microstructure and microchemistry of the material. These changes vary with the material composition and thermo-mechanical treatment and irradiation temperature and dose rate [32]. Irradiation damage is characterized by either the neutron fluence (n/m^2) or the average number of displacements per atom (dpa).[5]

Under LWR conditions, the microstructure produced by irradiation seems to change significantly for temperatures above 300°C. At 275–300°C, the defect structure primarily consists of small “black spot” defect clusters (<4 nm in diameter) and large dislocation loops (4-20 nm in diameter) that are primarily faulted interstitial Frank loops. At higher temperatures, the microstructure contains large faulted loops and network dislocations, and cavities/voids (clusters of vacancies and/or gas bubbles) and precipitates form at higher doses [32,49,130–132]. The size of the dislocation loops increases with increasing irradiation dose. The saturation size of the loops depends on the irradiation conditions and material characteristics. Under LWR conditions, the loop density saturates at a relatively low dose (about 1 dpa), and the average loop diameter saturates at about 5 dpa [32]. In addition, alloying elements can affect the material microstructure (e.g., P, Ti, and Nb increase the loop density and decrease loop size). The loop size increases and loop density decreases with irradiation temperature. At temperatures of 300–350°C, the microstructure primarily consists of large Frank loops and a network of tangled dislocations [32]. Also, cavities and voids form at high doses and high temperatures. Cavities or voids have not been observed in SSs irradiated below 300°C.

[5] Conversion to dpa is as follows: for LWRs, E>1 MeV and 10^{26} n/m^2 ~15 dpa; and for fast reactors, E>0.1 MeV and 10^{26} n/m^2 ~5 dpa.

Irradiation at temperatures above 350°C leads to the formation of second phase particles. The available data suggest that radiation-induced precipitation is not a concern at temperatures below 350°C. Metal carbides are the primary stable precipitates in 300-series SSs under LWR conditions, although RIS of Ni and Si to sinks may lead to the formation of γ' (Ni_3Si) and G phase ($M_6Ni_{16}Si_7$). Precipitation of Ni-Si clusters at LWR temperatures is quite commonly observed. Precipitates are primarily in the matrix and often attached to dislocations but are rarely observed at grain boundaries despite high levels of Ni and Si solute segregation [133].

4.2 Effect on Mechanical Properties

4.2.1 Tensile Properties

The point defect clusters and precipitates produced by irradiation act, to varying extent, as obstacles to dislocation motion, resulting in an increase in tensile strength and a reduction in ductility and fracture toughness of the material. In general, cavities (or voids) are strong barriers, large faulted Frank loops are intermediate barriers, and small loops and bubbles are weak barriers to dislocation motion [28]. The yield strength of irradiated SSs can increase up to five times that of the non-irradiated material after a neutron dose of about 5 dpa [30]. The extent of irradiation hardening and the increase in yield stress of austenitic SSs depend on the material composition and thermo-mechanical treatment, as well as the irradiation temperature. The greatest increase in yield strength for a given dose occurs at irradiation temperatures near 300°C (572°F).

Tensile properties data have been obtained on solution-annealed and cold worked (CW) Type 304, 304L, 316, 316L, and 347 SSs, including weld HAZ material, Type 308 and 309 weld metals, and CF-8 cast austenitic SSs, irradiated at 300–400°C (572–752°F) in fast reactors and LWRs [35–37,134–136]. The 0.2% yield strength, ultimate tensile strength, uniform elongation, and total elongation at elevated temperatures are plotted in Figure 4-1 as a function of neutron dose for the weld metals and CASS materials. However, most data in these figures were obtained on materials irradiated in the BOR-60 fast reactor. Data on LWR-irradiated materials are limited, in particular, for austenitic SS welds and at high neutron dose.

The curves in these figures represent the correlations [137] developed by the Materials Reliability Program (MRP) for estimating the tensile properties as a function of neutron dose. The 0.2% yield strength, ultimate tensile strength, uniform elongation, and total elongation data at 330°C were fitted to an exponential equation of the form:

$$\text{Property} = A_0 + A_1 (1-\exp(-d/d_0)), \tag{24}$$

where d is the neutron dose in dpa and the coefficients A_0, A_1, and d_0 for the irradiated material property equations are listed in Table 4-1 and Table 4-2. The baseline reference tensile properties of nonirradiated materials are represented by a fourth-order polynomial [137] of the form:

$$\text{Property} = C_0 + C_1T + C_2T^2 + C_3T^3 + C_4T^4, \tag{25}$$

where T is the temperature (°C) and the coefficients for the different tensile property equations are listed in Table 4-3.

At high neutron doses, as the irradiated yield strength approaches the ultimate strength of the material there is a change in the deformation mode. Deformation by a planar slip mechanism is

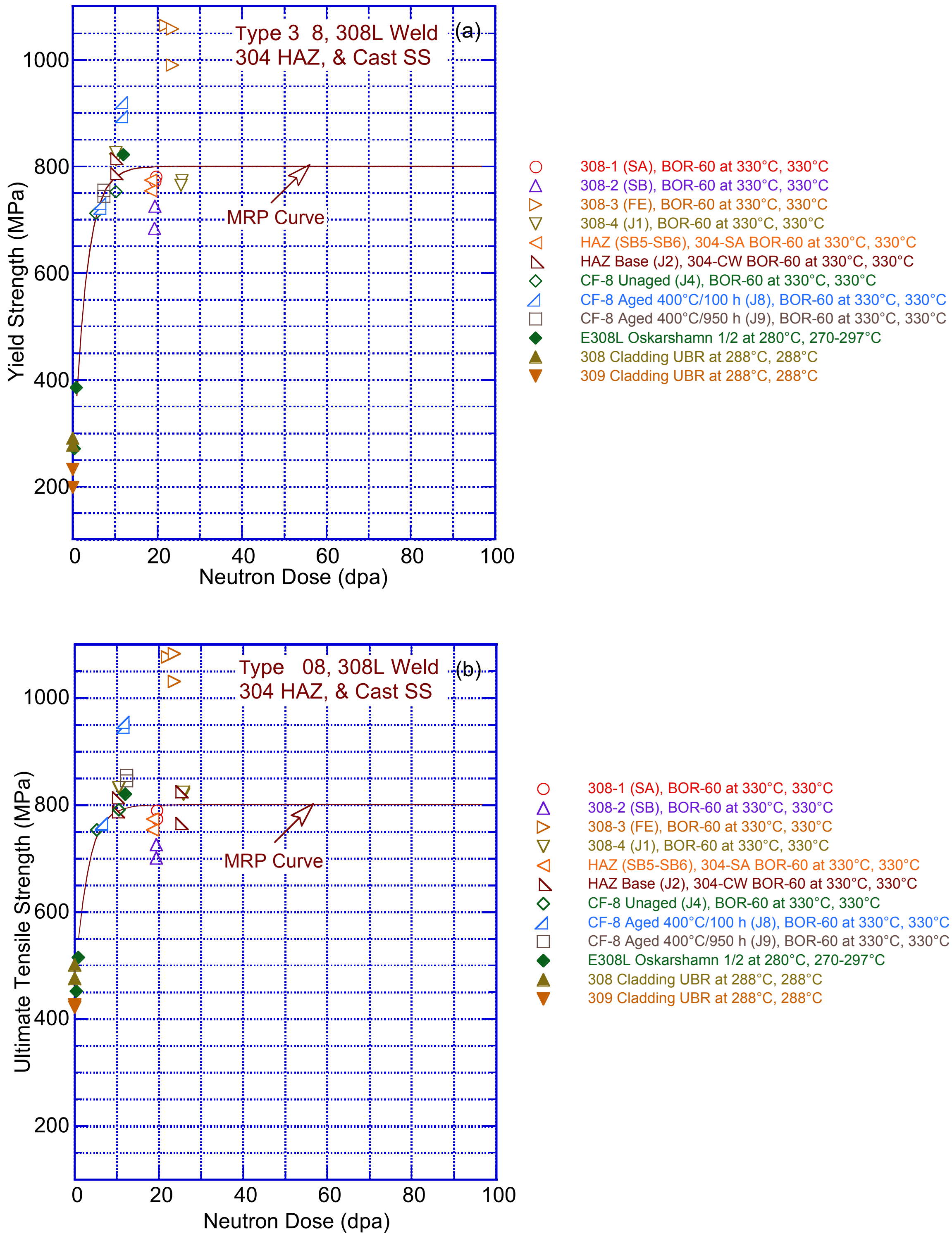

Figure 4-1 Change in (a) yield strength, (b) ultimate tensile strength, (c) uniform elongation, and (d) total elongation as a function of neutron dose for weld metals, Type 304 HAZ, and CF-8 CASS materials at elevated temperature (Ref. 47).

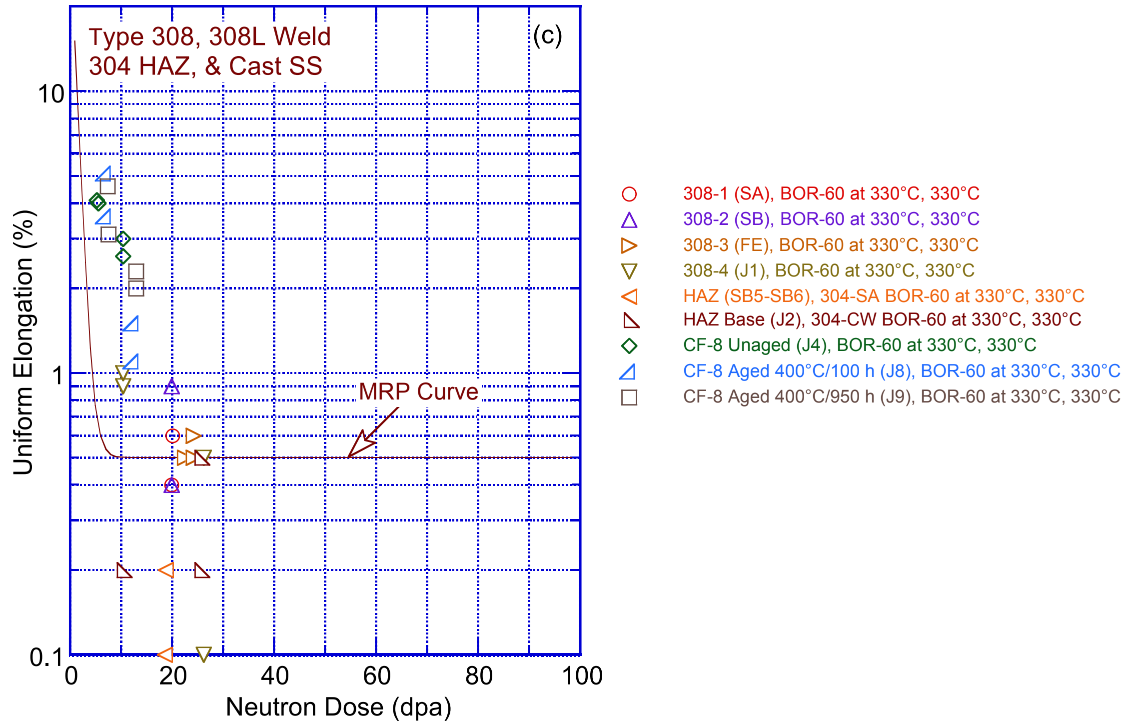

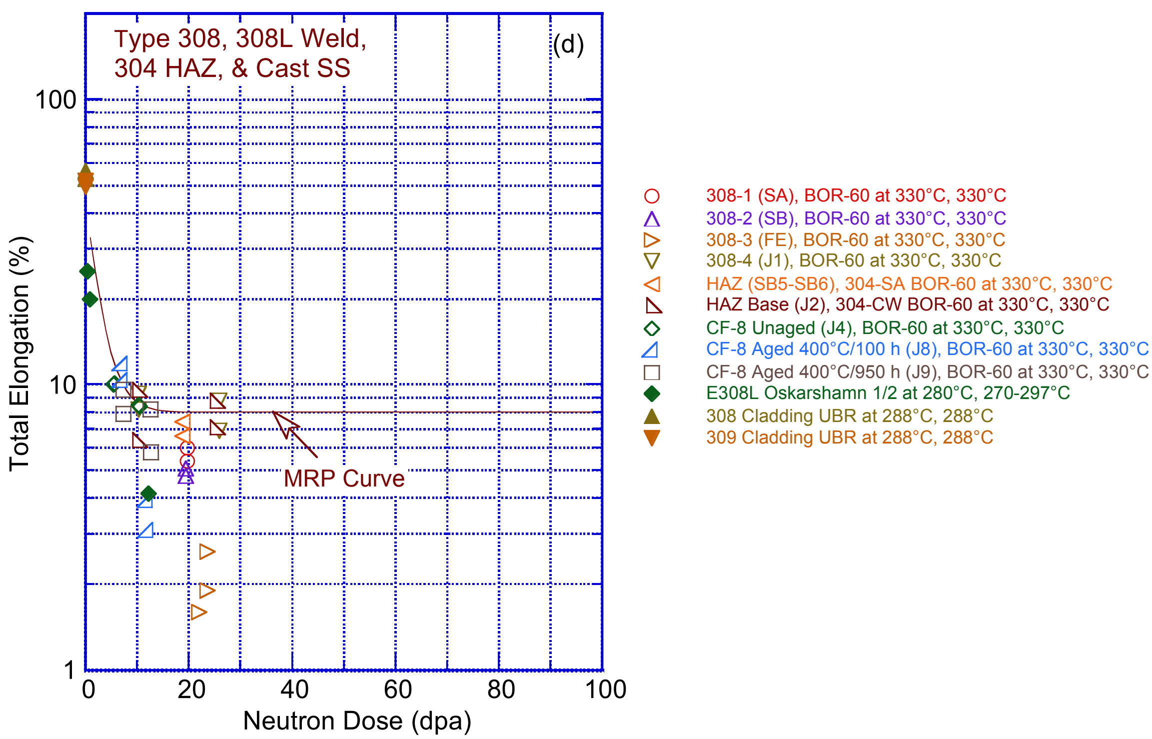

Figure 4-1 Change in (a) yield strength, (b) ultimate tensile strength, (c) uniform elongation, and (d) total elongation as a function of neutron dose for weld metals, Type 304 HAZ, and CF-8 CASS materials at elevated temperature (Ref. 47). (Contd.)

Table 4-1 Material property equations for irradiated CW Type 316 stainless steel.

Property	Units	Property = $A_0 + A_1 (1-\exp(-d/d_0))$		
		A_0	A_1	d_0
0.2% yield strength	MPa	500	470	3
Ultimate tensile strength	MPa	650	330	3
Uniform elongation	%	10	-9.7	2
Total elongation	%	18	-11	5

Table 4-2 Material property equations for irradiated solution-annealed Type 304 stainless steel.

Property	Units	Property = $A_0 + A_1 (1-\exp(-d/d_0))$		
		A_0	A_1	d_0
0.2% yield strength	MPa	200	600	3
Ultimate tensile strength	MPa	450	350	3
Uniform elongation	%	40	-39.5	1
Total elongation	%	45	-37	2.5

Table 4-3 Material property equations for solution-annealed and nonirradiated Type 304 stainless steel.

Property	Units	Property = $C_0 + C_1T + C_2T^2 + C_3T^3 + C_4T^4$				
		C_0	C_1	C_2	C_3	C_4
0.2% yield strength	MPa	270.09	-0.5702	9.1162E-4	-5.6198E-7	
Ultimate tensile strength	MPa	617.275	-1.7750	7.0659E-3	-1.0769E-5	4.8941E-9
Uniform elongation	%	55.8688	-0.1893	5.3656E-4	-4.5779E-7	
Total elongation	%	71.6321	-0.1956	5.7562E-4	-7.1266E-7	3.2172E-10

promoted, and the material exhibits strain softening [138]. This process can be explained by "dislocation channeling," whereby dislocation motion along a narrow band of slip planes clears the irradiation-induced defect structure, creating a defect-free channel that offers less resistance to subsequent dislocation motion or deformation. Nearly all SSs exhibit strain softening, and little or no uniform elongation, at irradiation dose above 3-5 dpa. The engineering stress vs. strain curves for Type 304 SS irradiated to 2 and 3 dpa showing strain softening is presented in Figure 4-2 [139,140]. The enhanced planar slip also leads to a pronounced degradation in the fracture toughness of austenitic SSs. An assessment of neutron embrittlement of irradiated austenitic SSs is presented in an Argonne topical report [47] as well as a journal article [55].

4.2.2 Charpy-Impact Energy

Figure 4-3a and b show the effects of thermal aging and neutron irradiation of austenitic SS welds as a function of test temperature [69,70]. The tests involving neutron irradiation at 371°C were conducted in the EBR-II reactor in Idaho. Similar to the results for the MMA weld, thermal aging decreases the C_V values for SA and SMA welds, the decrease at reactor temperature is greater than at room temperature. Neutron irradiation further decreases the Charpy-impact energy. For the irradiated welds, the effect of test temperature on C_V is insignificant. For the SA weld irradiated and tested at 371°C, C_V is decreased from 110 to 31 J/cm^2. However, although the C_V

values for the SA weld are lower then those for the SMA weld the SA welds contain 15% ferrite compared to 7.2% in the SMA welds.

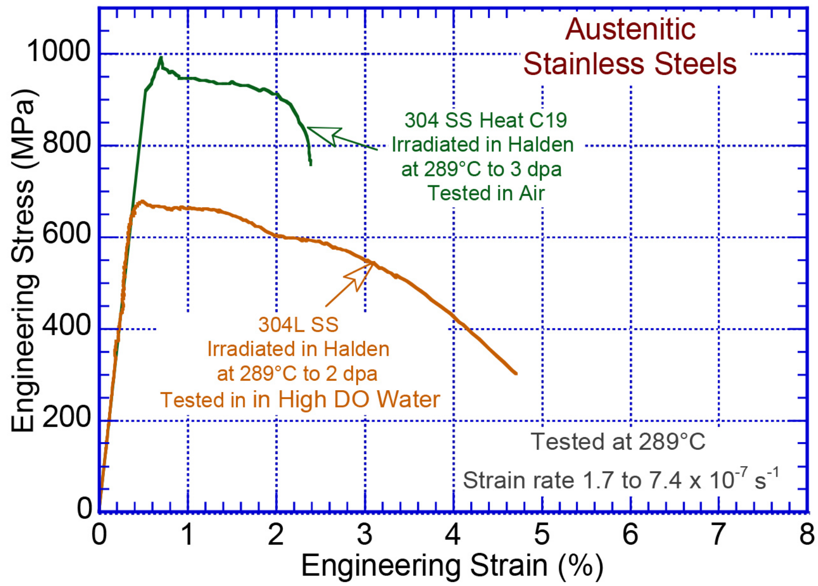

Figure 4-2 The engineering stress-strain plots at 289°C for irradiated Type 304 SS showing strain softening (Ref. 139,140).

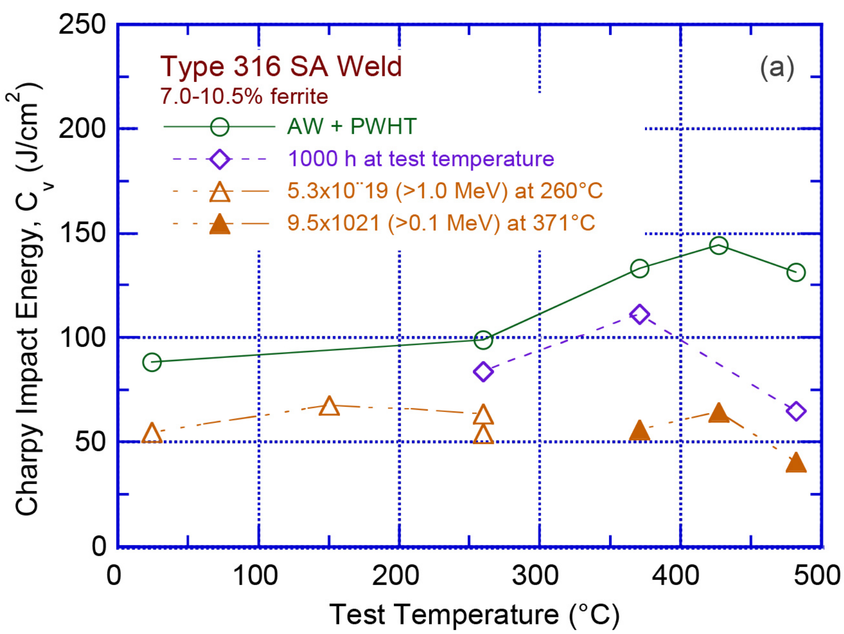

Figure 4-3 The change in Charpy-impact energy C_V with temperature for an unaged, aged, or neutron irradiated (a) Type 316 SA weld and (b) Type 308 SA and SMA welds (Ref. 69,70).

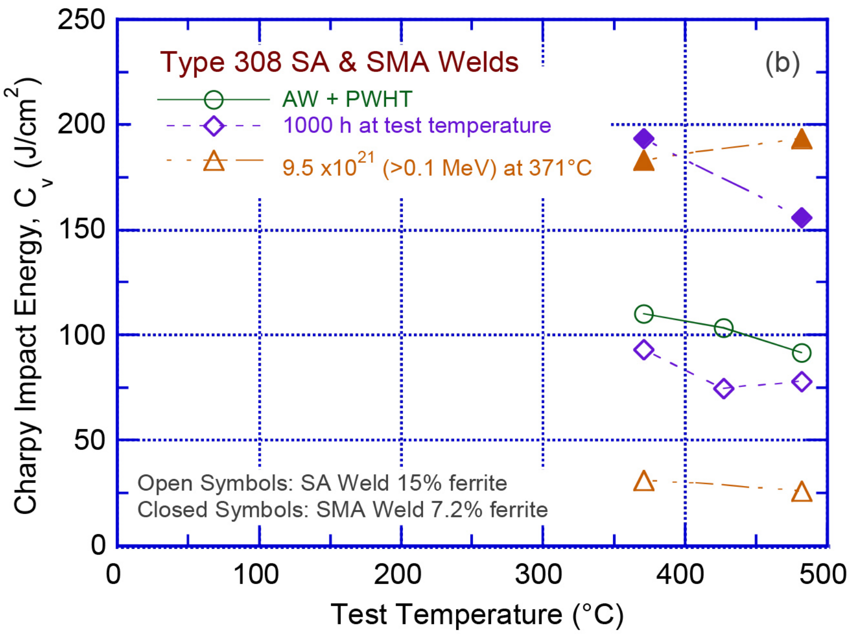

Figure 4-3 (Contd.)

4.2.3 Fracture Toughness

The existing data on neutron-irradiated wrought austenitic SSs, CASS materials, and their welds indicate (a) little or no loss of toughness below an exposure of about 0.3 dpa, (b) substantial decrease in toughness at 0.3–10 dpa, and (3) little or no further reduction in toughness beyond 10 dpa [45,47]. However, the extent and the rate of decrease in fracture toughness vary among the various grades of materials. The effects of material parameters (e.g., composition, thermo-mechanical treatment, microstructure, microchemistry, yield strength, stacking fault energy) and environmental parameters (e.g., water chemistry, irradiation temperature, dose, dose rate) on neutron embrittlement have been summarized in earlier ANL publications [45,47]. The results were used to (a) define a threshold fluence level above which irradiation effects on the fracture toughness of cast and wrought austenitic SSs are significant and (b) evaluate the potential of neutron embrittlement of these materials under LWR operating conditions.

Examples of fracture toughness J-R curves for unirradiated and irradiated Types 308 and 316 SS welds are presented in Figure 4-4. The Type 308 MMA weld was irradiated in a fast reactor, EBR-II, at 427°C [86] and the Type 316 weld was irradiated in Dido or Pluto materials test reactors at 370°C [39]. Prior to irradiation, the Type 316 weld was given a heat treatment at 650°C for 2 h for dimensional stability. The results indicate significant decrease in fracture toughness of these welds. However, the irradiation temperature for the Type 308 weld was much higher than in LWRs and the neutron spectrum was different. Existing fracture toughness data on neutron- irradiated, wrought austenitic SSs indicate that neutron embrittlement is maximum around 290°C and is greater for materials irradiated in LWRs than in fast reactors [45].

4.2.3.1 Effect of Test Temperature

The fracture toughness of nonirradiated austenitic SSs is known to decrease as the test temperature is increased. The change in the J_{Ic} of irradiated SSs as a function of test temperature is plotted in Figure 4-5 for several grades of SSs and welds irradiated in LWRs and

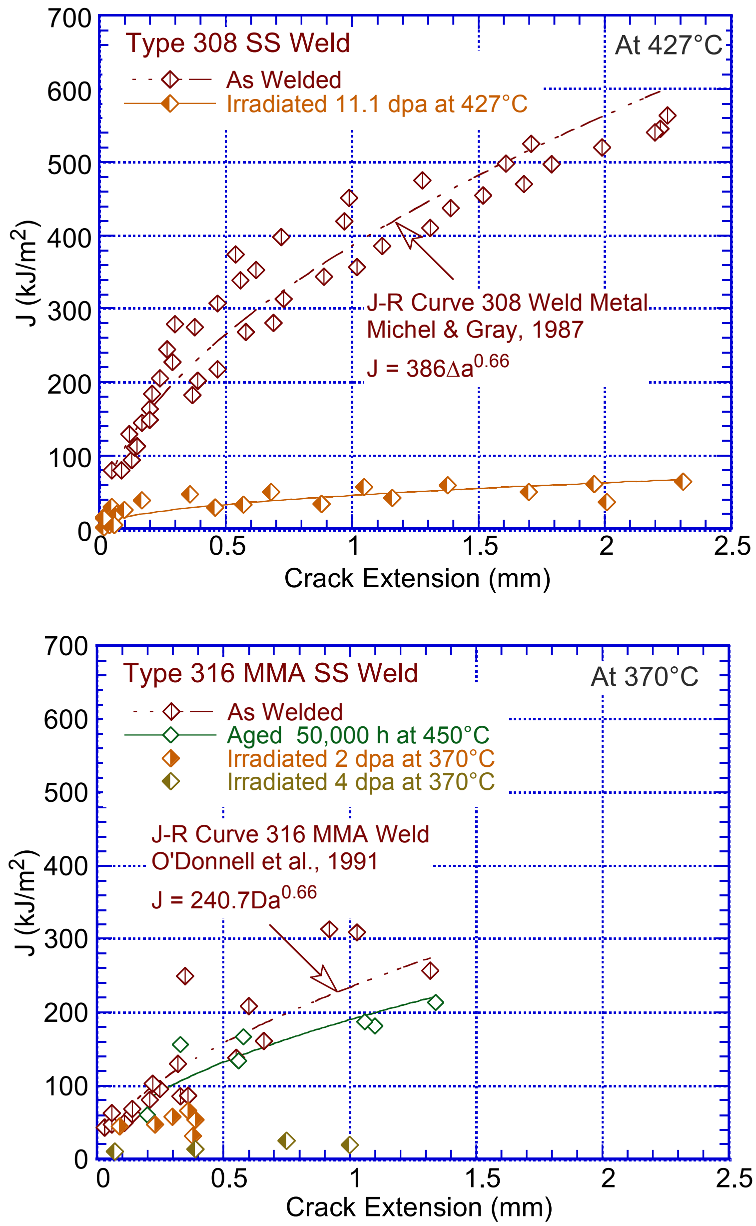

Figure 4-4 Fracture toughness J-R curves for unirradiated and irradiated Types 308 and 316 SS welds at 427 and 370°C, respectively (Refs. 39,86).

fast reactors. The fracture toughness of steels irradiated to relatively low doses (less than 5 dpa) decreases with increasing test temperature in most cases. However, for steels irradiated to more than 12 dpa, the test temperature has little effect on fracture toughness. The data on materials irradiated in LWRs or fast reactors exhibit similar trends. It should be noted that at 12-dpa-fluence level, the toughness value is already low, which makes it difficult to discern definitive trends. The effect of test temperature is also reflected in the fracture morphology of highly irradiated materials.

At temperatures above 230°C (446°F) the failure mode is predominantly channel fracture characterized by a faceted fracture surface. It is associated with highly localized deformation along a narrow band of slip planes whereby the initial dislocation motion along the narrow band clears away the irradiation-induced defect structure, creating a defect-free channel that offers less resistance to subsequent dislocation motion. The localization of the deformation ultimately leads to channel failure.

4.2.3.2 Effect of Irradiation Temperature

The available data are inadequate to establish accurately the effects of the irradiation temperature on the fracture toughness of austenitic SSs. However, tensile data indicate that irradiation hardening is highest, and ductility loss is maximum, at an irradiation temperature of ≈300°C (≈572°F) [138]. Thus, the J_{Ic} values for all materials irradiated above 350°C (662°F) (e.g., fast reactor irradiations), particularly for neutron exposures greater than 20 dpa, would be greater than for materials irradiated at temperatures of 290–320°C (554–608°F).

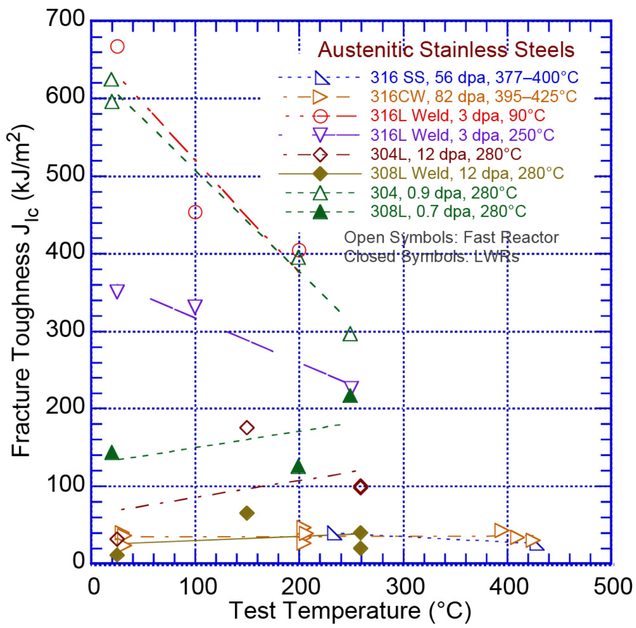

Figure 4-5 Fracture toughness J_{Ic} of irradiated austenitic stainless steels and welds as a function of test temperature (Ref. 46).

4.2.3.3 Fracture Toughness Lower-bound J-R Curves

A fracture toughness J-R curve may be used to analyze material deformation behavior for loading beyond J_{IC}. The J-R curve is expressed in terms of the J integral and crack extension (Δa) by the power law $J = C(\Delta a)^n$. At dose levels below the threshold dose for saturation (~7 dpa), the neutron embrittlement of austenitic SSs can be represented by a decrease in the coefficient C with neutron dose. The variation of fracture toughness coefficient C of austenitic SS welds as a function of neutron dose is plotted in Figure 4-6. The two curves in the figure represent the disposition curve proposed by EPRI for BWRs [38], and a modified version of the trend curve proposed for coefficient C that bounds the existing fracture toughness data for austenitic SSs, CASS materials, and their welds, in earlier ANL studies [45,47]. All fracture toughness tests were conducted in air, except the test conducted by Dr. Chen at ANL on a SA weld from the Grand Gulf Type 304L core shroud (shown as closed inverted triangle), which was performed in low-DO, high-purity water. The solid curve represents a modified version of the trend curve proposed in

NUREG/CR-7027 for coefficient C that bounds the existing data. The experimental data shown in Figure 4-6 are bounded by the following expression for C:

$$C = 25 + 92 \exp[-0.35(\text{dpa})^{1.4}]. \quad (26)$$

The value of the coefficient C for welds irradiated to neutron dose less than 0.1 dpa represents the lower-bound value for the unirradiated SA, SMA, or MMA welds. The existing data indicate that the lower-bound fracture toughness curve for unaged and aged GTA welds is likely to be higher, it is not clear whether this trend would also be observed for irradiated welds. The existing data are inadequate to accurately establish the lower-bound J-R curve for GTA, MIG, or TIG welds as a function of neutron dose. The results plotted in Figure 4-6 also indicate that the lower bound curve proposed by EPRI between coefficient C and neutron dose, overestimates the value of coefficient C, particularly at neutron dose <0.5 dpa. A large fraction of the existing experimental data is below the proposed EPRI lower-bound curve.

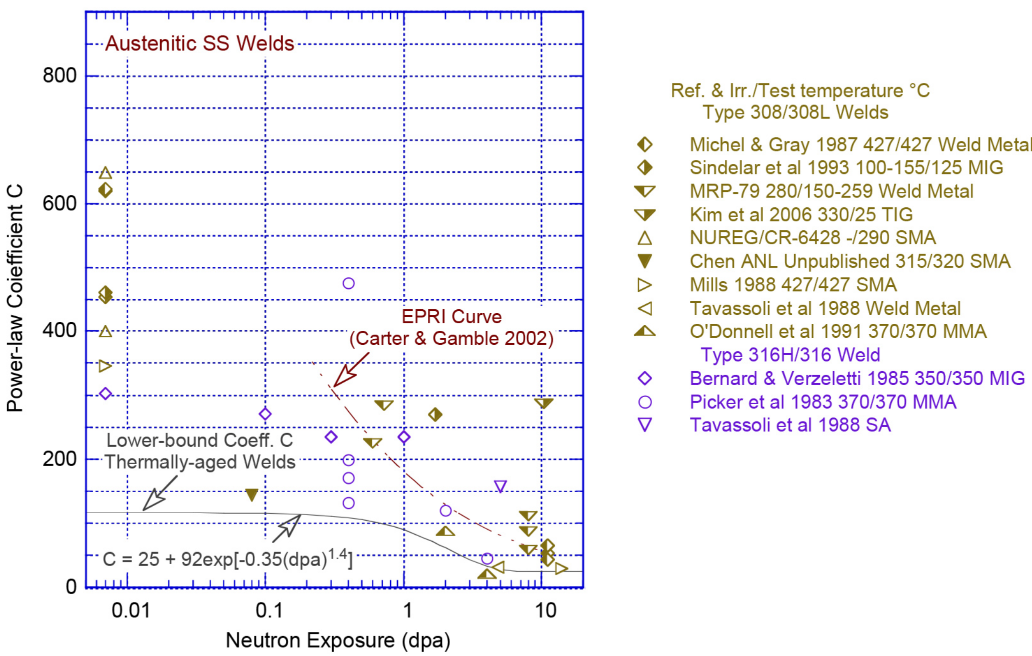

Figure 4-6 Coefficient C of the J-R curve as a function of neutron dose for SS welds. The data points plotted at 0.007 dpa are for nonirradiated materials.

The variation of fracture toughness power-law exponent n for the irradiated austenitic SS weld data shown in Figure 4-6 is plotted as a function of neutron dose in Figure 4-7. A value of 0.45 is assumed as the minimum value for unirradiated, but thermally aged, welds. In addition, the value of the exponent decreases with increasing neutron dose, and is assumed to reach a saturation value of 0.20 at a dose of 5 dpa. Fracture toughness data for neutron does >10 dpa are very limited. Most of the experimental data shown in Figure 4-7 are bounded by the expression for exponent n given by:

$$n = 0.45 - 0.0926\,[2 + \log(\text{dpa})]. \quad (27)$$

Note that the fracture mechanics methodology proposed by EPRI for irradiated SSs [36], and adopted by MRP [42], assumes a value of exponent n that increases with neutron dose; n increases from about 0.40 at 0.2 dpa to 0.64 at 4.5 dpa. The n values for fracture toughness

J-R curves for SS welds are typically lower then these values, and n generally decreases with increasing neutron dose [45,47]. The estimated value of J at 2.5-mm crack extension, $J_{2.5}$, determined from Eqs. 26 and 27, is plotted as a function of neutron dose in Figure 4-8.

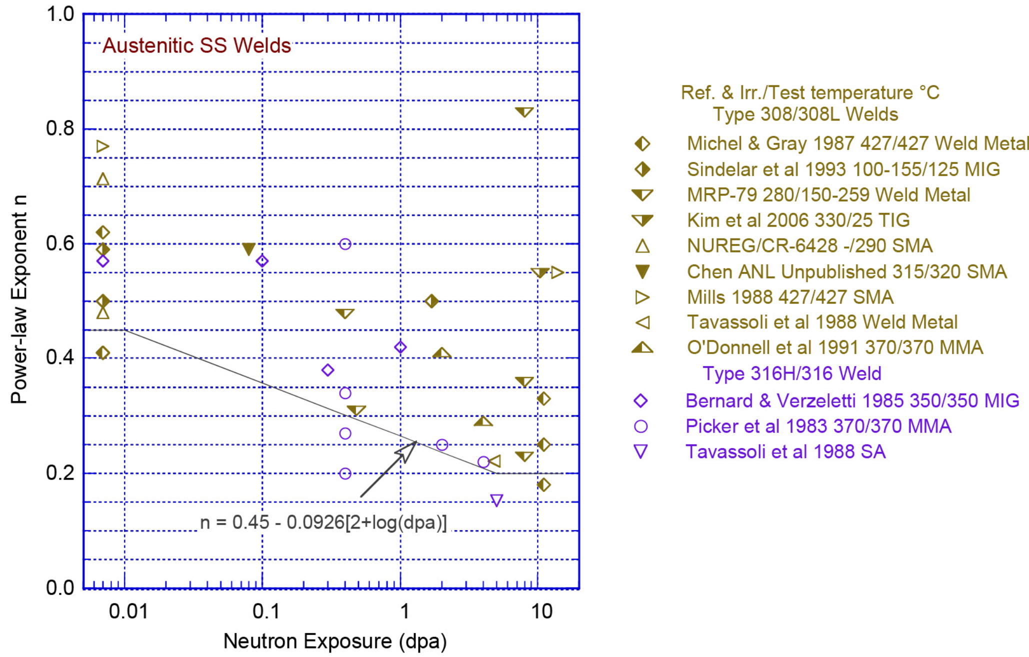

Figure 4-7 Exponent n of the J-R curve as a function of neutron dose for SS welds. The data points plotted at 0.007 dpa are for nonirradiated materials.

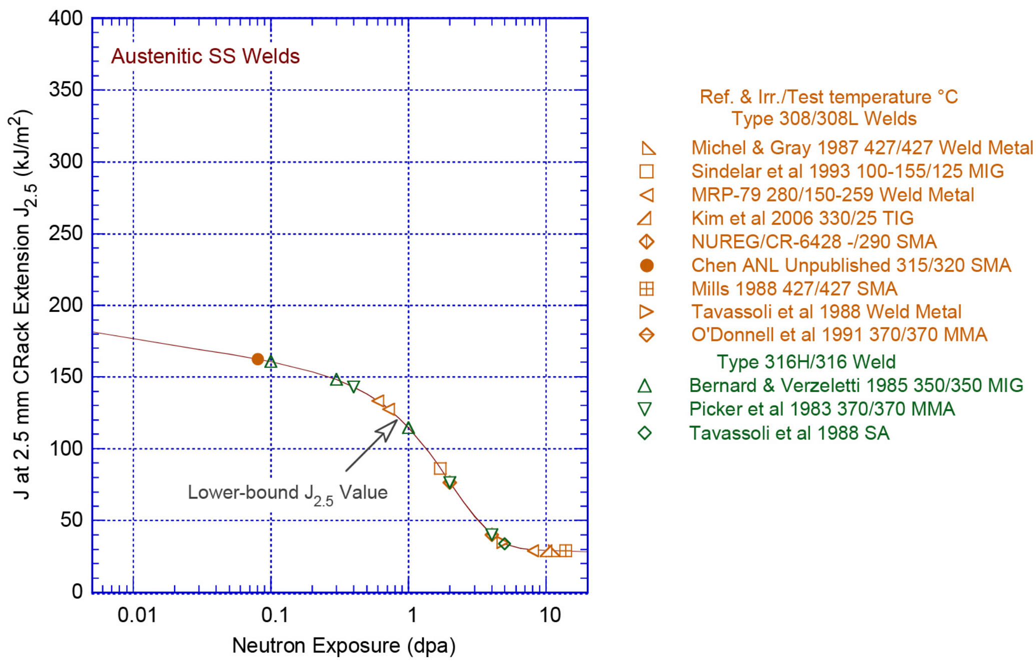

Figure 4-8 $J_{2.5}$ as a function of neutron dose for austenitic SS welds.

The results indicate that the $J_{2.5}$ values are below 150 kJ/m^2 for welds irradiated above about 0.3 dpa. The saturation $J_{2.5}$ for welds irradiated above 7 dpa is about 30 kJ/m^2. The existing fracture toughness J_{Ic} data at 290–320°C for austenitic SS welds irradiated in fast reactors[6] and LWRs are plotted as a function of neutron dose in Figure 4-9 [27,35,36,78,86–91]. The change in lower-bound J_{Ic} value as a function of neutron dose is given by

$$J_{Ic} = 7.5 + 67 \exp[-0.23(\text{dpa})^{1.4}]. \quad (28)$$

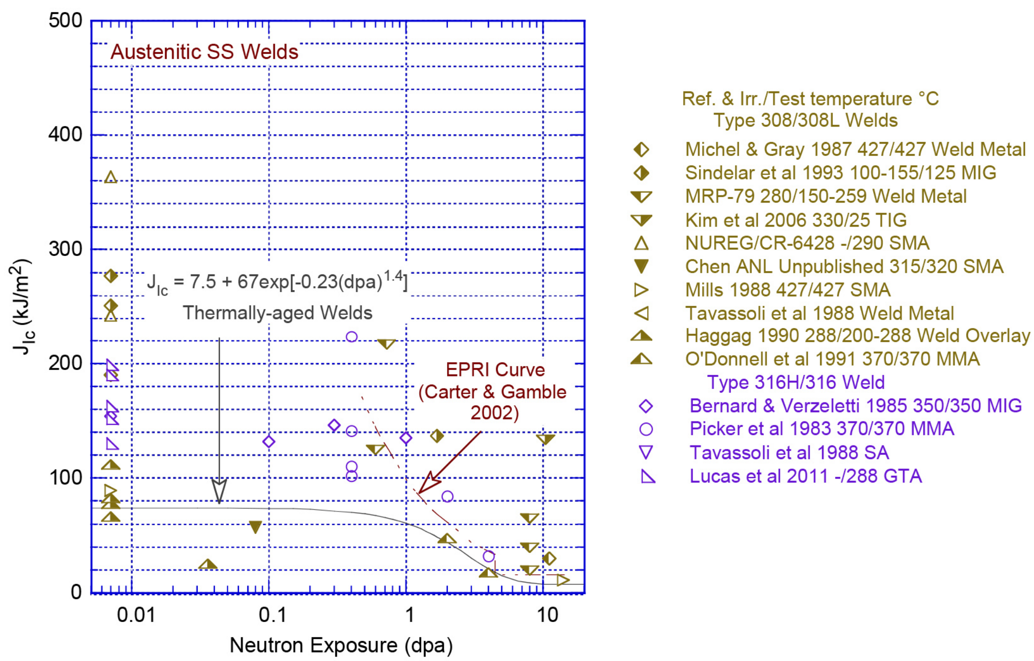

Figure 4-9 Fracture toughness J_{Ic} values as a function of neutron dose for SS welds. The data points plotted at 0.007 dpa are for nonirradiated materials.

The lower-bound curve represents (a) a threshold dose of about 0.3 dpa for neutron embrittlement; (b) a minimum fracture toughness J_{Ic} of about 74.5 kJ/m^2 for neutron doses below 0.15 dpa; (c) a saturation threshold of about 6–8 dpa beyond which the fracture toughness of these materials appears to saturate; (d) a saturation fracture toughness J_{Ic} of 7.5 kJ/m^2; and (e) a description of the change in toughness between 0.1 and 10 dpa. The J_{Ic} value of ~74 kJ/m^2 for neutron doses below the threshold dose is appropriate for austenitic SS unaged SMA and SA welds. A value higher than 74 kJ/m^2 may be considered (and justified) for SS GTA/MIG/TIG welds. At typical temperatures for LWR core internals (i.e., 290–370°C), the saturation J_{Ic} of 7.5 kJ/m^2 corresponds to K_{Jc} of ~38 MPa m$^{1/2}$, and the minimum J_{Ic} of 74.5 kJ/m^2 for welds with neutron doses below 0.15 dpa corresponds to a K_{Jc} of 118–120 MPa m$^{1/2}$.

The experimental data shown in Figure 4-6 and Figure 4-9 also indicate that the existing fracture toughness data for irradiated austenitic SSs and their welds are not bounded by the disposition curve proposed by EPRI for BWRs [38]. Furthermore, saturation K_{Jc} of 55 MPa m$^{1/2}$ at 4.5 dpa, proposed by the EPRI curve, is also higher than the value of 38 MPa m$^{1/2}$ predicted

[6] The data obtained by Sindelar et al., Kim et al., and Mills are for materials irradiated in fast reactors.

by the lower-bound curve shown in Figure 4-9, and proposed by MRP for PWRs [42]. The saturation K_{Jc} for the EPRI curve was based on data for which the specimen orientation was unknown. Studies about the effect of specimen orientation on fracture toughness indicate that fracture toughness in the transverse orientation is nearly half of that in the longitudinal orientation [36]. Therefore, the saturation K_{Jc} proposed by EPRI may not represent the actual lower-bound value.

5 SUMMARY

The existing mechanical property data on thermal and neutron embrittlement of austenitic SS welds has been compiled and evaluated to (a) update the results presented earlier in NUREG/CR-6428 (1996) on Charpy impact energy, tensile properties, and fracture toughness J-R curves, (b) establish the effects of thermal embrittlement on the degradation of fracture properties, and (c) evaluate the potential combined effects of thermal and neutron embrittlement. The lower-bound fracture-toughness J-R curves for austenitic SS welds during extended service in LWRs have been revised to incorporate the effects of thermal and neutron embrittlement using a much larger database. The potential effects of reactor coolant environment on fracture-toughness J-R curves were also discussed.

Austenitic SS welds have a duplex structure, with ferrite being the minor phase distributed in various forms in the austenite matrix. Typically, the commercial AISI 300 series austenitic SSs welds contain up to 20% ferrite depending on the weld composition and weld cooling-rate. Based on these material and weld process conditions, four different ferrite morphologies are observed in the weld. These morphologies are vermicular, lacy, acicular, and globular ferrite. Vermicular ferrite is most common.

Thermal Embrittlement

The degradation of fracture properties of austenitic SS welds due to thermal embrittlement occurs due to a combination of the strengthening of the ferrite matrix by spinodal decomposition and the weakening of grain/phase boundaries because of the presence of second phase particles. Thermal aging increases the hardness and tensile strength, and decreases ductility, impact strength, and fracture toughness. Fracture occurs along the delta ferrite regions where the second phase particles initiate voids/cracks either by decohesion of the ferrite/austenite interphase or particle cracking. The kinetics of thermal embrittlement were discussed.

Thermal aging of welds decreases the Charpy upper-shelf energy and increases the Charpy energy transition temperature. The effect of thermal aging is greater in welds with more than 10% ferrite. Charpy impact energy at reactor temperatures is greater then at room temperature, but the difference decreases with thermal aging. The effect of thermal aging on tensile properties is to increase the yield and ultimate tensile stress and decrease the ductility. The effect on ultimate tensile stress is greater then on the yield stress. However, the effect is insignificant on welds with <10% ferrite.

Thermal aging also degrades the fracture toughness of austenitic SS welds. The welding process has a significant effect on the extent of degradation. The effect on SA and SMA welds is greater than on the GTA weld. However, since the composition and microstructure of welds varies with the welding process and conditions, it is difficult to estimate the change in fracture toughness as a function of time and temperature of aging. Therefore, the approach adopted in this report is to establish the effect of thermal embrittlement on the fracture toughness of SS welds and define the lower bound values of fracture toughness parameters, such as, J_{Ic} and coefficient C and exponent n of the power-law J-R curve. Separate lower bound values are presented for SA/SMA and GTA welds for unaged and aged SS welds.

Combined Effects of Thermal and Neutron Embrittlement

The fracture toughness of austenitic SS welds decreases with increasing neutron irradiation dose. The extent of embrittlement depends on the amount and morphology of the ferrite phase in the weld. The mechanism of neutron embrittlement was briefly discussed. The point defects produced by neutron irradiation strengthen the material, resulting in an increase in tensile strength and a reduction in ductility and fracture toughness. The yield strength of austenitic SSs and welds can increase significantly. The extent of irradiation hardening and the increase in yield stress depend on the material composition, heat treatment and irradiation temperature. The MRP has developed correlations for estimating the tensile properties as a function of neutron dose.

The fracture toughness of nonirradiated austenitic SSs is known to decrease as the test temperature is increased. The J_{Ic} values of austenitic SS and welds either nonirradiated or irradiated to relatively low doses, decrease with increasing test temperature. However, for SSs irradiated to 12 dpa or more, test temperature has no effect on fracture toughness. Available data are inadequate to accurately establish the effect of irradiation temperature on fracture toughness of SS welds. Similar to the effect of thermal embrittlement, lower bound values of J_{Ic} and coefficient "C" and exponent "n" of the fracture toughness J-R curve are defined as a function of neutron dose.

6 REFERENCES

1. Mills, W.J., "Fracture Toughness of Type 304 and 316 Stainless Steels and Their Welds," *Intl. Mater. Rev*. 42, 45–82, 1997.

2. Trautwein, A., and W. Gysel, "Influence of Long Time Aging of CF-8 and CF-8M Cast Steel at Temperatures Between 300 and 500°C on the Impact Toughness and the Structure Properties," in *Spectrum, Technische Mitteilungen aus dem+GF+Konzern, No. 5* (May 1981); also in *Stainless Steel Castings*, V.G. Behal and A.S. Melilli, eds., STP 756, ASTM, Philadelphia, PA, pp. 165–189, 1982.

3. Landerman, E.I., and W.H. Bamford, "Fracture Toughness and Fatigue Characteristics of Centrifugally Cast Type 316 Stainless Steel Pipe after Simulated Thermal Service Conditions," in *Ductility and Toughness Considerations in Elevated-Temperature Service*, MPC 8, ASME, New York, pp. 99–127, 1978.

4. Solomon, H.D., and T.M. Devine, "Influence of Microstructure on the Mechanical Properties and Localized Corrosion of a Duplex Stainless Steel," in *Micon 78: Optimization of Processing, Properties, and Service Performance through Microstructural Control*, H. Abrams, G.N. Maniar, D.A. Nail, and H.D. Solomon, eds., ASTM STP 672, p. 430, 1979.

5. Solomon, H.D., and T.M. Devine, Jr., "Duplex Stainless Steels - A Tale of Two Phases," in *Duplex Stainless Steels*, R.A. Lula, ed., ASM, Metals Park, pp. 693–756, 1983.

6. Slama, G., P. Petrequin, and T. Mager, "Effect of Aging on Mechanical Properties of Austenitic Stainless Steel Castings and Welds," presented at SMIRT Post-Conference Seminar 6, *Assuring Structural Integrity of Steel Reactor Pressure Boundary Components*, Aug. 29–30, Monterey, CA, 1983.

7. McConnell, P., and J.W. Sheckherd, "Fracture Toughness Characterization of Thermally Embrittled Cast Duplex Stainless Steel," Report NP-5439, Electric Power Research Institute, Palo Alto, CA, September 1987.

8. Meyzaud, Y., P. Ould, P. Balladon, M. Bethmont, and P. Soulat, "Tearing Resistance of Aged Cast Austenitic Stainless Steel," *Int. Conf. on Thermal Reactor Safety (NUCSAFE 88)*, Avignon, France, October 1988.

9. Bethmont, M., Y. Mezaud, and P. Soulat, "Properties of Cast Austenitic Materials for Light Water Reactors," *Int. J. Pres. Ves. & Piping* 66, 221–229, 1996.

10. Jayet-Gendrot, S., P. Ould, and T. Meylogan, "Fracture Toughness Assessment of In-Service Aged Primary Circuit Elbows Using Mini-CT Specimens Taken from Outer Skin," *Nucl. Eng. and Design* 184, 3–11, 1998.

11. Mills, W.J., "Heat-to-Heat Variations in the Fracture Toughness of Austenitic Stainless Steels," *Eng. Fract. Mech.*, 30(4), 469–492, 1988.

12. Mills, W.J., "Fracture Toughness of Stainless Steel Welds," in *Fracture Mechanics: Nineteenth Symposium*, STP 969, ASTM, Philadelphia, PA, 330–355, 1988.

13. Mills, W.J., “Fracture Toughness of Aged Stainless Steel Primary Piping and Reactor Vessel Materials,” *J. Pres. Ves. Technol. (Trans ASME)* 109, 440–448, 1987.

14. Chung, H.M., and O.K. Chopra, “Kinetics and Mechanism of Thermal Aging Embrittlement of Duplex Stainless Steels,” in *Environmental Degradation of Materials in Nuclear Power Systems - Water Reactors*, G.J. Theus and J.R. Weeks, eds., Metallurgical Society, Warrendale, PA, pp. 359–370, 1988.

15. Bonnet, S., J. Bourgoin, J. Champredonde, D. Guttmann, and M. Guttmann, “Relationship between Evolution of Mechanical Properties of Various Cast Duplex Stainless Steels and Metallurgical and Aging Parameters: An Outline of Current EDF Programmes,” *Mater. Sci. Technol.*, 6, 221–229, 1990.

16. Pumphrey, P.H., and K.N. Akhurst, “Aging Kinetics of CF3 Cast Stainless Steel in Temperature Range 300–400°C,” *Mater. Sci. Technol.*, 6, 211–219, 1990.

17. Grimes, C.I., U.S. Nuclear Regulatory Commission, License Renewal and Standardization Branch, letter to D.J. Walters, Nuclear Energy Institute, License Renewal Issue No. 98-0030, “Thermal Aging Embrittlement of Cast Stainless Steel Components,” May 19, 2000.

18. Nickell, R.E., and M.A. Rinckel, “Evaluation of Thermal Aging Embrittlement for Cast Austenitic Stainless Steels Components in LWR Reactor Coolant Systems,” EPRI TR-106092, Electric Power Research Institute, Palo Alto, CA, 1997.

19. Rinckel, M.A., “Evaluation of Thermal Aging Embrittlement for Cast Austenitic Stainless Steels Components,” EPRI 1000976, Electric Power Research Institute, Palo Alto, CA, January 2001.

20. Yukawa, S., "Review of Evaluation of the Toughness of Austenitic Steels and Nickel Alloys after Long-Term Elevated Temperature Exposures," *WRC Bulletin 378*, Pressure Vessel and Research Council of the Welding Research Council, 1993.

21. Sasikala, G., and S.K. Ray, "Influence of Aging on the Quasistatic Fracture Toughness of an SS 316(N) Weld at Ambient and Elevated Temperatures," *J. Nucl. Mater*. 408, 45–53, 2011.

22. Chopra, O.K., and A. Sather, “Initial Assessment of the Mechanisms and Significance of Low-Temperature Embrittlement of Cast Stainless Steels in LWR Systems,” NUREG/CR-5385, ANL-89/17, August 1990.

23. Chopra, O.K., and H.M. Chung, “Effect of Low-Temperature Aging on the Mechanical Properties of Cast Stainless Steels,” in *Properties of Stainless Steels in Elevated Temperature Service*, M. Prager, ed., MPC-Vol. 26 / PVP-Vol. 132, ASME, New York, pp. 79–105,1988.

24. Chopra, O.K., “Estimation of Fracture Toughness of Cast Stainless Steels during Thermal Aging in LWR Systems,” NUREG/CR-4513, Rev. 1, ANL-93/22, August 1994.

25. Chopra, O.K. and W.J. Shack, “Mechanical Properties of Thermally Aged Cast Stainless Steels from Shippingport Reactor Components,” NUREG/CR-6275, ANL-94/37, April 1995.

26. Michaud, W.F., P.T. Toben, W.K. Soppet, and O.K. Chopra, "Tensile-Property Characterization of Thermally Aged Cast Stainless Steels," NUREG/CR-6142, ANL-93/35, February 1994.

27. Gavenda, D.J., W.F. Michaud, T.M. Galvin, W.F. Burke, and O.K. Chopra, "Effects of Thermal Aging on Fracture Toughness and Charpy-Impact Strength of Stainless Steel Pipe Welds," NUREG/CR-6428, ANL-95/47, 1996.

28. Bruemmer, S.M., et al., "Critical Issue Reviews for the Understanding and Evaluation of Irradiation-Assisted Stress Corrosion Cracking," EPRI TR-107159, Electric Power Research Institute, Palo Alto, CA, 1996.

29. Scott, P., "A Review of Irradiation Assisted Stress Corrosion Cracking," *J. Nucl. Mater*. 211, 101–122, 1994.

30. Was, G.S., and P.L. Andresen, "Stress Corrosion Cracking Behavior of Alloys in Aggressive Nuclear Reactor Core Environments," *Corrosion* 63, 19–45, 2007.

31. Andresen, P.L., F.P. Ford, S.M. Murphy, and J.M. Perks, "State of Knowledge of Radiation Effects on Environmental Cracking in Light Water Reactor Core Materials," in *Proc. 4th Intl. Symp. on Environmental Degradation of Materials in Nuclear Power Systems - Water Reactors*, NACE, Houston, TX, pp. 1.83–1.121, 1990.

32. Bruemmer, S.M., E.P. Simonen, P.M. Scott, P.L. Andresen, G.S. Was, and J.L. Nelson, "Radiation-Induced Material Changes and Susceptibility to Intergranular Failure of Light-Water-Reactor Core Internals," *J. Nucl. Mater*. 274, 299–314, 1999.

33. Herrera, M.L., et al., "Evaluation of the Effects of Irradiation on the Fracture Toughness of BWR Internal Components," *Proc. ASME/JSME 4th Intl. Conf. on Nucl. Eng. (ICONE-4)*, Vol. 5, A.S. Rao, R.M. Duffey, and D. Elias, eds., American Society of Mechanical Engineers, New York, pp. 245–251, 1996.

34. Mills, W.J., "Fracture Toughness of Irradiated Stainless Steels Alloys," *Nucl. Technol.* 82, 290–303, 1988.

35. Xu., H., and S. Fyfitch, "Materials Reliability Program: A Review of Radiation Embrittlement for Stainless Steels (MRP-79)," Rev. 1, EPRI Report 1008204, Electric Power Research Institute, Palo Alto, CA, September 2004.

36. Demma, A., R. Carter, A. Jenssen, T. Torimaru, and R. Gamble, "Fracture Toughness of Highly Irradiated Stainless Steels in Boiling Water Reactors," in *Proc. 13th Intl. Conf. on Environmental Degradation of Materials in Nuclear Power Systems – Water Reactors*, T.R. Allen. P.J. King, and L. Nelson, eds., Canadian Nuclear Society, Toronto, Canada, Paper No. 114, 2007.

37. Ehrnsten, U., K. Wallin, P. Karjalainen-Roikonen, S. van Dyck, and P. Ould, "Fracture Toughness of Stainless Steels Irradiated to ≈9 dpa in Commercial BWRs," in *Proc. 6th Intl. Symp. on Contribution of Materials Investigations to Improve the Safety and Performance of LWRs*, Vol. 1, Fontevraud 6, French Nuclear Energy Society, SFEN, Fontevraud Royal Abbey, France, pp. 661–670, September 18–22, 2006.

38. Carter, R.G., and R.M. Gamble, “Assessment of the Fracture Toughness of Irradiated Stainless Steel for BWR Core Shrouds,” in *Fontevraud 5 Intl. Symp., Contribution of Materials Investigation to the Resolution of Problems Encountered in Pressurized Water Reactors*, Avignon, France, September 25, 2002.

39. O’Donnell, I.J., H. Huthmann, and A.A. Tavassoli, “The Fracture Toughness Behaviour of Austenitic Steels and Weld Metal Including the Effects of Thermal Aging and Irradiation,” *Intl. J. Pres. Ves. and Piping* 65 (3), 209–220, 1996.

40. Tavassoli, A-A.F., “16-8-2 Weld Metal Design Data for 316L(N) Steel,” *Proc. of The 8th Inter. Symp. on Fusion Nuclear Technology*, Paper #20, Heidelberg, Germany, 2007.

41. Kim C., R. Lott, S. Byrne, M. Burke, and G. Gerzen, “Embrittlement of Cast Austenitic Stainless Steel Reactor Internals Components,” in *Proc. 6th Intl. Symp. on Contribution of Materials Investigations to Improve the Safety and Performance of LWRs*, Vol. 1, Fontevraud 6, French Nuclear Energy Society, SFEN, Fontevraud Royal Abbey, France, September 18–22, 2006.

42. Fyfitch, S., H. Xu, A. Demma, R. Carter, R. Gamble, and P. Scott, “Fracture Toughness of Irradiated Stainless Steel in Nuclear Power Systems,” in *Proc. 14th Intl. Conf. on Environmental Degradation of Materials in Nuclear Power Systems - Water Reactors*, American Nuclear Society, Lagrange Park, IL, 2009.

43. Fyfitch, S., H. Xu, K. Moore, and R. Gurdal, “Materials Reliability Program: PWR Internals Material Aging Degradation Mechanism Screening and Threshold Values (MRP-175),” EPRI Report 1012081, Dec. 2005.

44. Electric Power Research Institute, Materials Reliability Program, “Fracture Toughness Testing of Decommissioned PWR Core Internals Material Samples (MRP-160),” EPRI Report 1012079, September 2005.

45. Chopra, O.K., and A.S. Rao, "A Review of Irradiation Effects on LWR Core Internal Materials - Neutron Embrittlement," *J. Nucl. Mater*. 412, 195–208, 2011.

46. Chopra, O.K., and W.J. Shack, “Crack Growth Rates and Fracture Toughness of Irradiated Austenitic Stainless Steels in BWR Environments,” NUREG/CR-6960, ANL-06/58, March 2008.

47. Chopra, O.K., “Degradation of LWR Core Internal Materials Due to Neutron Irradiation,” NUREG/CR-7027, December 2010.

48. Andresen, P.L. “Emerging Issues and Fundamental Processes in Environmental Cracking in Hot Water,” in *Proc. Research Topical Symposium on Environmental Cracking, Corrosion/07*, NACE, 2007.

49. Bruemmer, S.M., “New Issues Concerning Radiation-Induced Material Changes and Irradiation-Assisted Stress Corrosion Cracking in Light-Water Reactors,” in *Proc. Tenth Intl. Symp. on Environmental Degradation of Materials in Nuclear Power Systems - Water Reactor*, Paper No. 0008V, NACE, Houston, TX, 2001.

50. Edwards, D., E. Simonen, and S. Bruemmer, “Radiation-Induced Segregation Behavior in Austenitic Stainless Steels: Fast Reactor versus Light Water Reactor Irradiations,” in *Proc. 13th Intl. Conf. on Environmental Degradation of Materials in Nuclear Power Systems - Water Reactors*, T.R. Allen, P.J. King, and L. Nelson, eds., Canadian Nuclear Society, Toronto, Canada, Paper No. P0139, 2007.

51. Fyfitch, S., H. Xu, P. Scott, L. Fournier, and A. Demma, “Criteria for Initiation of Irradiation-Assisted Stress Corrosion Cracking in Stainless Steels in PWR Systems,” in *Proc. 14th Intl. Conf. on Environmental Degradation of Materials in Nuclear Power Systems - Water Reactors*, American Nuclear Society, Lagrange Park, IL, 2009.

52. Jenssen, Anders, Johan Stjarnsater, and Raj Pathania, "Crack Growth Rates of Irradiated Commercial Stainless Steels in BWR and PWR Environments," in *Proc. 15th Intl. Conf. on Environmental Degradation of Materials in Nuclear Power Systems - Water Reactors*, Jeremy T. Busby, Gabriel Ilevbare, and Peter L. Andresen, eds., The Minerals, Metals & Materials Society, Warrendale, PA, pp. 1229–1240, 2011.

53. Jenssen, A., and L.G. Ljungberg, “Irradiation Assisted Stress Corrosion Cracking: Post Irradiation CERT Tests of Stainless Steels in a BWR Test Loop,” in *Proc. Seventh Intl. Symp. on Environmental Degradation of Materials in Nuclear Power Systems - Water Reactor*, G. Airey et al., eds., NACE, Houston, TX, pp. 1043–1052, 1995.

54. Jenssen, A., and L.G. Ljungberg, “Irradiation Assisted Stress Corrosion Cracking of Stainless Alloys in BWR Normal Water Chemistry and Hydrogen Water Chemistry,” in *Proc. Sixth Intl. Symp. on Environmental Degradation of Materials in Nuclear Power Systems - Water Reactor*, R.E. Gold and E.P. Simonen, eds., Minerals, Metals & Materials Society, Warrendale, PA, pp. 547–553, 1993.

55. Chopra, O.K., and A.S. Rao, "A Review of Irradiation Effects on LWR Core Internal Materials - IASCC Susceptibility and Crack Growth Rates of Austenitic Stainless Steels," *J. Nucl. Mater*. 409, 235–256, 2011.

56. Chen, Y., B. Alexandreanu, and K. Natesan, “Crack Growth Rate and Fracture Toughness Tests on Irradiated Cast Stainless Steels,” NUREG/CR-7184, ANL-12/56, July 2015.

57. Chopra, O.K., “Effect of Thermal Aging and Neutron Irradiation on Crack Growth Rate and Fracture Toughness of Cast Stainless Steels and Austenitic Stainless Steel Welds,” NUREG/CR-7185, ANL-14/10, July 2015.

58. Chopra, O.K., “Estimation of Fracture Toughness of Cast Stainless Steels during Thermal Aging in LWR Systems,” NUREG/CR-4513, Rev. 2, ANL-15/08, May 2016.

59. Vitek, J.M., S.A. David, D.J. Alexander, J.R, Keiser, and R.K. Nanstad, “Low Temperature Aging Behavior of Type 308 Stainless Steel Weld Metal,” *Acta Metall.*, 39, 503–516, 1991.

60. Alexander D.J., K.B. Alexander, M.K. Miller, and R.K. Nanstad, “The Effect of Aging at 343°C on Type 308 Stainless Steel Weldments,” in *Fatigue, Degradation, and Fracture–1990*, W.H. Bamford, C. Becht, S. Bandari, J.D. Gilman, L.A. James, and M. Prager, eds., MPV Vol. 30, PVP Vol. 195, ASME New York, NY, pp. 187–192, 1990.

61. Alexander D.J., K.B. Alexander, M.K. Miller, R.K. Nanstad, and Y.A. Davidov, "The Effect of Aging at 343°C on the Microstructure and Mechanical Properties of Type 308 Stainless Steel Weldments," NUREG/CR-6628, ORNL/TM-13767, November 2000.

62. Hale, G.E., and S.J. Garwood, "Effect of Aging on Fracture Behaviour of Cast Stainless Steel and Weldments," *Mater. Sci. Technol.*, 6, 230–236, 1990.

63. Garwood, S.J., "Fracture Toughness of Stainless Steel Weldments at Elevated Temperatures," in *Fracture Mechanics: 15th Symposium*, R.J. Sanford, ed., ASTM STP 833, American Society for Testing and Materials, Philadelphia, PA, pp. 333–359, 1984.

64. Vassilaros, M. G., R.A. Hays, and J.P. Gudas, "Investigation of the Ductile Fracture Properties of Type 304 Stainless Steel Plate, Welds, and 4-inch Pipe," in *Proc. 12th Water Reactor Safety Research Information Meeting*, NUREG/CP-0058, Vol. 4, U.S. Nuclear Regulatory Commission, pp. 176–189, 1985.

65. Faure, F., B. Houssin, and P. Balladon, "Mechanical Properties of Automatic TIG/GTA Welds of Stainless Steel Piping in Nuclear Reactors," in *Trends in Welding Research*, ASM Conf., Gatlinburg, May 14–18, 1989.

66. Horn, R.M., H.S. Mehta, W.R. Andrews, and S. Ranganath, "Evaluation of the Toughness of Austenitic Stainless Steel Pipe Weldments," EPRI NP-4668, Electric Power Research Institute, Palo Alto, CA, June 1986.

67. Landes, J.D., and D.E. McCabe, "Toughness of Austenitic Stainless Steel Pipe Welds," EPRI NP-4768, Electric Power Research Institute, Palo Alto, CA, October 1986.

68. Gudas, J.P., and D.R. Anderson, "J-R Curve Characteristics of Piping Material and Welds," in *Proc. 9th Water Reactor Safety Research Information Meeting*, U.S. Nuclear Regulatory Commission, October 1981.

69. Hawthorne, J.R., and B.H. Menke, "Influence of Delta Ferrite Content and Welding Variables on Notch Toughness of Austenitic Stainless Steel Weldments," in *Structural Materials for Service at Elevated Temperatures in Nuclear Power Generation*, G.V. Smith, ed., MPC–1, ASME, New York, pp. 351–364, 1975.

70. Hawthorne, J.R., and H.E. Watson, "Notch Toughness of Austenitic Stainless Steel Weldments with Nuclear Irradiation," in *Welding Research Supplement*, American Welding Society and Welding Research Council, pp256-s to 260-s, June 1973.

71. Commission of the European Communities, *Mechanical Testing of Austenitic Steel Welded Joints*, Joint Final Report–Vol. 2, Ispra, Italy (1990).

72. Mills, W.J., L.A. James, and L.D. Blackburn, "Results of Fracture Mechanics Tests on PNC SU 304 Plate," Westinghouse Hanford Report HEDL-7544, Hanford Engineering Development Laboratory, Richland, WA, 1985.

73. Ould, P., P. Balladon, and Y. Meyzaud, "Fracture Toughness Properties of Austenitic Stainless Steel Welds," Bull. Cercle Etud. Metaux 15, 31.1–31.12, 1988.

74. Chipperfield, C.G., “A Toughness and Defect Size Assessment of Welded Stainless Steel Components,” *Tolerance of Flaws in Pressurized Components*, Inst. Mech. Eng. pp. 125–137, 1978.

75. Strangwood, M., and S.G. Druce, “Aging Effects in Welded Cast CF–3 Stainless Steel,” *Mater. Sci. Technol.*, 6, 237–248, 1990.

76. Wilkowski, G., et al., "Analysis of Experiments on Stainless Steel Flux Welds," NUREG/CR-4878, BMI-2151, April 1987.

77. Nakagaki, M., C. Marshall, and F. Brust, "Analysis of Cracks in Stainless Steel TIG Welds," NUREG/CR-4806, BMI-2144, December 1986.

78. Lucas, T., R.G. Ballinger, H. Hanninen, and T. Saukkonen, "Effect of Thermal Aging on SCC, Material Properties and Fracture Toughness of Stainless Steel Weld Metals," *15th Intl. Conf. on Environmental Degradation of Materials in Nuclear Power Systems - Water Reactors*, Jeremy T. Busby, Gabriel Ilevbare, and Peter L. Andresen, eds., The Minerals, Metals & Materials Society, Warrendale, PA, pp. 883–900, 2011.

79. Lucas, Timothy R., "The Effect of Thermal Aging and Boiling Water reactor Environment on Type 316L Stainless Steel Welds," Doctoral Thesis, Massachusetts Institute of Technology, Cambridge, MA, May 2011.

80. Hiser, A.L., and G.M. Callahan, "A User's Guide to the NRC's Piping Fracture Mechanics Database (PIFRAC)," NUREG/CR-4894, May 1987.

81. Wilkowski, G.M., et al., "Short Cracks in Piping and Piping Welds," NUREG/CR-4599, Vols. 1–3, Nos. 1 and 2, May 1991 to March 1994.

82. Wilkowski, G.M., et al., "Probabilistic Pipe Fracture Evaluations for Leak-Rate-Detection Applications," NUREG/CR-6004, April 1995.

83. Hiser, A.L., F.J. Loss, and B.H. Menke, "J-R Curve Characterization of Irradiated Low Upper Shelf Welds," Report No. NUREG/CR-3506, April 1984.

84. Hojo, K., I. Muroya, S. Kawaguchi, K. Koyama, and K. Sakai, “Application of the Two-Criteria Approach to the Austenitic Cast Stainless Steel Pipe,” *5th International Conference on Nuclear Engineering (ICONE-5)*, ICONE5-2379, May 26–30, American Society of Mechanical Engineers, New York, 1997.

85. JNES-SS Report, “Investigation Report on the Integrity of Thermally-Embrittled Cast Stainless Steel Pipe,” Nuclear Energy System Safety Division, Japan Nuclear Energy Safety

86. Michel, D.J., and R.A. Gray, “Effects of Irradiation on the Fracture Toughness of FBR Structural Materials,” *J. Nucl. Mater.* 148, 194–203, 1987.

87. Haggag, F.M., W.R. Corwin, and R.K. Nanstad, “Effects of Irradiation on the Fracture Properties of Stainless Steel Weld Overlay Cladding,” *Nucl. Eng. and Design* 124, 129–141, 1990.

88. Sindelar, R.L., G.R. Caskey, Jr., J.K. Thomas, J.R. Hawthorne, A.L. Hiser, R.A. Lott, J.A. Begley, and R.P. Shogan, “Mechanical Properties of 1950s Vintage Type 304 Stainless Steel Weldment Components after Low Temperature Neutron Irradiation,” *16th Intl. Symp. on Effects of Radiation on Materials*, ASTM STP 1175, American Society of Testing and Materials, Philadelphia, PA, pp. 714–746, 1993.

89. Sindelar, R.L., P. Lam, A.J. Duncan, B.J. Wiersma, K.H. Subramanian, and J.B. Edler, “Development and Application of Materials Properties for Flaw Stability Analysis in Extreme Environment Service,” *Proc. of PVP2007 ASME Pressure Vessel and Piping Conf.*, July 22–26, 2007, San Antonio, TX, PVP2007-26660, 2007.

90. Chen, Yiren, private communications, Nuclear Engineering Division, Argonne National Laboratory, January 2014

91. Picker, C., A.L. Stott, and H. Cocks, “Effects of Low-Dose Fast Neutron Irradiation on the Fracture Toughness of Type 316 Stainless Steel and Weld Metal,” *Proc. Specialists Meeting on Mechanical Properties of Fast Reactor Structural Materials*, Chester, UK, Paper IWGFR 49/440-4, 1983.

92. Bernard, J., and G. Verzeletti, “Elasto-Plastic Fracture Mechanics Characterization of Type 316H Irradiated Stainless Steel up to 1 dpa,” *Effects of Radiation on Materials: 12th Intl. Symp.*, ASTM STP 870, F.A. Garner and J.S. Perrin, eds., American Society for Testing and Materials, Philadelphia, PA, pp. 619–641, 1985.

93. Alexander, D.J., J.E. Pawel, L.M. Grossbeck, A.F. Rowcliffe, and K. Shiba, “Fracture Toughness of Irradiated Candidate Materials for ITER First Wall/Blanket Structures,” *Effect of Radiation on Materials: 17th Intl. Symp.*, ASTM STP 1270, American Society of Testing and Materials, Philadelphia, PA, pp. 945–970, 1996.

94. Valo, M. “Fracture toughness and Tensile Properties of Irradiated Austenitic Stainless Steel Components removed from Service (BWRVIP-35),” EPRI Report TR-108279, EPRI, Palo Alto, CA, June 1997.

95. Tavassoli, A.A., “The Influence of Radiation on the Properties of Welds and Joints,” *J. Nucl. Mater*. 155–157, 105–112, 1988.

96. Tavassoli, A.A., J.L. Bertin, and P. Nicolino, “Effect of Low to Medium Dose Neutron Irradiation on Toughness of Austenitic Stainless Steel Welded Joints,” Technical Note, FR/MWG/P(91)777, AGT9A-9A0207 & PSM 2/7.

97. Chopra, O.K., and A.S. Rao, “Methodology for Estimating Thermal and Neutron Embrittlement of Austenitic Stainless Steel Welds during Service in Light Water Reactors,” *J. Press. Vessel Technol.* Vol. 138(4), 040802, 1–16, 2016.

98. DeLong, W.T., G. Ostrom, and E. Szumachowski, “Measurement and Calculation of Ferrite in Stainless Steel Weld Metals,” *Welding Journal*, Vol. 35 (11), Research Supplement, pp. 526s–533s, November 1956.

99. Tsuk, T., M. Hubert, and C. Messager, Influence of Welding Heat on Residual Ferrite of Deposits of Austenitic Nickel-Chrome Steels," *Rev. de Metall*, 68, 829-837, December 1971.

100. Goodwin, G.M., N.C. Cole, and G.M. Slaughter, " A Study of Ferrite Morphology in Austenitic Stainless Steel Weld Metals," *Welding Journal*, Vol. 51 (9), Research Supplement, pp. 425s–429s, September 1972.

101. Hull, F.C., "Delta Ferrite and Martensite Formation in Stainless Steels," *Welding Journal*, Vol. 52 (5), Research Supplement, pp. 193s–203s, May 1973.

102. Suutala, N., T. Takalo, and T. Moisio, "Relationship between Solidification and Microstructure in Austenitic and Austenitic-Ferritic Stainless Steel Welds," *Metall. Trans.*, 10 A, 512–514, 1979.

103. Lippold, J.C., and W.F. Savage, "Solidification of Austenitic Stainless Steel Weldments: Part I-A Proposed Mechanism," *Welding Journal*, Vol. 59 (12), Research Supplement, pp. 362s–374s, December 1979.

104. David, S.A., "Ferrite Morphology and Variations in Ferrite Content in Austenitic Stainless Steel Welds," Welding Research Supplement, American Welding Society and Welding Research Council, pp73-s to 71-s, April 1981.

105. Brooks, J.A., J.C. Williams, and A.W. Thompson, "Microstructural Origin of the Skeletal Ferrite Morphology of Austenite Stainless Steel Welds," *Metall. Trans.*, 14A, 1271–1281, 1983.

106. Olson, D.L., "Prediction of Austenitic Weld Metal Microstructure and Properties," *Welding Journal*, Vol. 59 (12), Research Supplement, pp. 281s-295s, October 1985.

107. Siewert, T.A., C.N. McCowan, and D.L. Olson, "Prediction of Austenitic Weld Metal Microstructure and Properties," *Welding Journal*, Vol. 59 (12), Research Supplement, pp. s289s–298s, December 1988.

108. Inoue, H., and T. Koseki, "Clarification of Solidification Behaviors in Austenitic Stainless Steels Based on Welding Process," Nippon Steel Technical Report No. 95, Steel Research Laboratories, Nippon Steel Corporation, January 2007.

109. Abe, H., and Y. Watanabe, "Low-Temperature Aging Characteristics of Type 316L Stainless Steel Welds: Dependence on Solidification Mode," *Metall. & Metal. Trans*. 39A, 1392–1398, 2008.

110. ASTM A 800/A 800M, "Standard Practice for Steel Casting, Austenitic Alloy, Estimating Ferrite Content thereof," American Society of Testing and Materials, West Conshohocken, PA, 2001.

111. Schoefer, E.A., "A diagram for estimation of Ferrite Content in Stainless Steel Castings," in Appendix to Mossbauer-Effect Examination of Ferrite in Stainless Steel Welds and Castings, by L.J. Schwartzgruber et al., *Welding Journal*, Vol. 53, Research Supplement, pp. 10s–12s, 1974.

112. Davies, G.J., *Solidification and Casting*, App. Sc. Pub. Ltd., 1973.

113. AWS A4.2-74, Standard Procedures for Calibrating Magnetic Instruments to Measure Delta Ferrite Content of Austenitic Stainless Steel Weld Metal," American Welding Society, Miami, FL, 1974.

114. Schaeffler, A.L., “Selection of Austenitic Electrodes for Welding Dissimilar Metals,” *Welding Journal*, Vol. 26, No. 10, pp. 601–620, 1947.

115. DeLong, W.T., “Ferrite in Austenitic Stainless Steel Weld Metal,” *Welding Journal*, Vol. 53, No. 7, Research Supplement, pp. 273s–286s, 1974.

116. Fredricksson, H., "The Solidification Sequence in an 18-8 Stainless Steel, Investigated by Directional Solidification," *Met. Trans*. 3 (11), 2898–2997, 1972.

117. NRC, Generic Aging Lessons Learned (GALL) Report, NUREG-1801, Rev. 2, Washington, DC, December 2010.

118. Heger, J.J., “885°F Embrittlement of the Ferritic Chromium-Iron Alloys,” *Met. Progress*, p. 55, 1951.

119. Lagneborg, R., “Metallography of the 475°C Embrittlement in an Iron-30% Chromium Alloy,” *Trans. ASM 60*, 67, 1967.

120. Grobner, P.J. “The 885°F (475°C) Embrittlement of Ferritic Stainless Steels,” *Metall. Trans*. 4, 251, 1973.

121. Nichol, T J., A. Datta, and G. Aggen, “Embrittlement of Ferritic Stainless Steels,” *Metall. Trans.* 11A, 573, 1980.

122. Chandra, K., V. Kain, V. Bhutani, V.S. Raja, R. Tewari, G.K. Dey, and J.K. Chakravartty, “Low Temperature Thermal Aging of Austenitic Stainless Steel Welds: Kinetics and Effects on Mechanical Properties,” *Mater. Sci. and Eng*. A 534, 163–175, 2012.

123. Server, W.L., “Impact Three-Point Bend Testing for Notched and Precracked Specimens,” *J. Test. Eval.*, 6, 29, 1978.

124. Ould, P., and P. Balladon, “Influence of Metallurgical Parameters on the Fracture Toughness of Stainless Steel Welds,” Fracture from Defects Vol. 2/3, *Elastic-Plastic Fracture Mechanics*, edited by Brown, de los Rios, and Miller, Proc. Twelfth Biennial European Conference on Fracture, June 2015.

125. Balladon, P., J. Heritier, and P. Rabbe, “Influence of Microstructure on the Ductile Rupture Mechanisms of a 316L Steel at Room and Elevated Temperatures,” *Fracture Mechanics: 14th Symp., Vol. II: Testing and Applications*, ASTM STP 791, American Society for Testing and Materials, Philadelphia, PA, pp. 496–516, 1983.

126. Morra, M., "Program on Technology Innovation: Scoping Study of Low Temperature Crack Propagation for 182 Weld Metal in BWR Environments and for Cast Austenitic Stainless Steel in PWR Environments (Revision 1)," EPRI 1020957, Electric Power Research Institute, Palo Alto, CA, May 2010.

127. Mills, W.J., and C.M. Brown, “Fracture Toughness of Alloy 600 and an EN82H Weld in Air and Water,” *Metall. and Mater. Trans. A*, 32A, 1161–1174, 2001.

128. Brown, C.M. and W.J. Mills, "Fracture Toughness of Alloy 690 and EN52 Welds in Air and Water," *Metall. and Mater. Trans. A*, 33A, 1725–1735, 2002.

129. Nakajima, N., S. Shima, H. Nakajima, and T. Kondo, "The Fracture Toughness of Sensitized 304 Stainless Steel in Simulated Reactor Water," *Nucl. Eng. Des.*, 93, 95–106, 1986.

130. Maziasz, P.J., “Overview of Microstructural Evolution in Neutron-Irradiated Austenitic Stainless Steels,” *J. Nucl. Mater*. 205, 118–145, 1993.

131. Zinkle, S.J., P.J. Maziasz, and R.E. Stoller, “Dose Dependence of the Microstructural Evolution in Neutron-Irradiated Austenitic Stainless Steels,” *J. Nucl. Mater*. 206, 266–286, 1993.

132. Edwards, D.J., E.P. Simonen, and S.M. Bruemmer, “Evolution of Fine-Scale Defects in Stainless Steels Neutron-Irradiated at 275°C,” *J. Nucl. Mater*. 317, 13–31, 2003.

133. Lee, E.H., P.J. Maziasz, and A.F. Rowcliffe, “The Structure and Composition of Phases Occurring in Austenitic Stainless Steels in Thermal and Irradiation Environments,” in *Conf. Proc. of Phase Stability During Irradiation*, J.R. Holland, D.I. Potter, and L.K. Mansur, eds.,TMS-AIME, Warrendale, PA, pp. 191-218, 1981.

134. Karlsen, T. M., M. Espeland, and A. Horvath, “Summary Report on the PWR Crack Growth Rate Investigation, IFA-657,” HWR-773, OECD Halden Reactor Project, May 2005.

135. Conermann, J., R. Shogan, K. Fujimoto, T. Yonezawa, and T. Yamaguchi, “Irradiation Effects in a Highly Irradiated Cold Worked Stainless Steel Removed from a Commercial PWR,” *Proc. 12th Intl. Conf. on Environmental Degradation of Materials in Nuclear Power Systems - Water Reactors*, T. R. Allen, P. J. King, and L. Nelson, eds., Minerals, Metals & Materials Society, Warrendale, PA, pp. 277-284, 2005.

136. Takakura, K., K. Nakata, M. Ando, K. Fujimoto, and E. Wachi, “Lifetime Evaluation for IASCC Initiation of Cold Worked 316 Stainless Steel’s BFB in PWR Primary Water,” *Proc. 13th Intl. Conf. on Environmental Degradation of Materials in Nuclear Power Systems - Water Reactors*, T. R. Allen, P. J. King, and L. Nelson, eds., Canadian Nuclear Society, Toronto, Canada, Paper No. P0009, 2007.

137. Electric Power Research Institute, Materials Reliability Program, “Development of Material Constitutive Model for Irradiated Austenitic Stainless Steels (MRP-135),” EPRI Report 1011127, Dec. 2004.

138. Lucas, G.E., “The Evolution of Mechanical Property Change in Irradiated Austenitic Stainless Steels,” *J. Nucl. Mater*. 206, 287–305, 1993.

139. Chen, Y., O.K. Chopra, W.K. Soppet, N.L. Dietz Rago, and W.J. Shack, “IASCC Susceptibility of Austenitic Stainless Steel and Alloy 690 in High Dissolved Oxygen Water Environment,” *Proc. 13th Intl. Conf. on Environmental Degradation of Materials in Nuclear Power Systems - Water Reactors*, T. R. Allen, P. J. King, and L. Nelson, eds., Canadian Nuclear Society, Toronto, Canada, Paper No. P0026, 2007.

140. Chung, H.M., and W.J. Shack, “Irradiation-Assisted Stress Corrosion Cracking Behavior of Austenitic Stainless Steels Applicable to LWR Core Internals,” NUREG/CR-6892, ANL-04/10, 2006.

APPENDIX A MATERIAL INFORMATION

The various grades of CASS materials and their product form, heat designation, chemical composition, and mechanical properties such as Charpy-impact energy, tensile properties, and fracture toughness J-R curves of materials in the as-cast condition or after thermal aging in the laboratory at temperatures between 290 and 400°C up to 60,000 h are presented in the following tables.

Table A1. The grade, weld type, chemical composition, and ferrite content of the various austenitic stainless steel welds.

ID	Grade	Weld	Source	C	Mn	Si	P	S	Ni	Cr	Mo	N	Other	Ferrite	Ref.
V41	308	MMA	Hawthorne & Menke 1975	0.056	1.88	0.32	0.024	0.011	10.35	19.71	0.05	0.068	-	5.2	A.1
V42	308	MMA	Hawthorne & Menke 1975	0.060	1.54	0.31	0.029	0.009	9.25	19.90	0.05	0.074	-	10.4	A.1
V43	308	MMA	Hawthorne & Menke 1975	0.060	1.65	0.32	0.029	0.011	9.11	20.89	0.06	0.079	-	15.7	A.1
V44	308	MMA	Hawthorne & Menke 1975	0.060	1.38	0.43	0.028	0.010	8.93	21.08	0.08	0.084	-	19.0	A.1
V23	316	SA	Hawthorne & Menke 1975	-	-	-	-	-	-	-	-	-	-	7-10.5	A.1
-	316	SA	Hawthorne & Watson 1973	-	-	-	-	-	-	-	-	-	-	-	A.1
CGC1	17-8-2	MMA	Chipperfield 1978	0.073	1.90	0.43	-	<0.01	9.80	18.10	1.70	-	-	7-9 (9)	A.2
OU6	17-8-2	MMA	Chipperfield 1978	0.058	2.00	0.41	-	-	9.60	18.30	1.70	-	-	5.0	A.2
PH21	17-8-2	MIG	Chipperfield 1978	0.080	1.50	0.30	-	-	10.80	17.80	2.30	-	-	2-4	A.2
PH22	17-8-2	MMA	Chipperfield 1978	0.064	2.00	0.26	-	-	9.00	17.90	1.40	-	-	1-4	A.2
PH19	17-8-2	MIG	Chipperfield 1978	0.083	1.50	0.30	-	-	8.50	17.50	2.30	-	-	2-4	A.2
PH/8	17-8-2	MMA	Chipperfield 1978	0.054	2.00	0.37	-	-	9.60	18.40	1.60	-	-	5	A.2
-	CF-8A	Weld	Gudas & Anderson 1981	-	-	-	-	-	-	-	-	-	-	-	A.3
-	316	MMA	Picker 1983	0.068	1.73	0.35	0.023	0.014	9.50	18.00	2.09	-	0.005 B	-	A.4
B	308L	Weld	Slama et al. 1983	0.014	1.40	0.62	0.017	0.007	10.65	19.02	0.02	0.043	-	6.0	A.5
D	308L	Weld	Slama et al. 1983	0.018	1.15	0.74	0.022	0.013	10.62	18.59	0.19	0.027	-	7.3	A.5
-	316	SA	Garwood 1984	-	-	-	-	-	-	-	-	-	-	-	A.6
-	316	MMA	Garwood 1984	-	-	-	-	-	-	-	-	-	-	-	A.6
62W	Linde 80	SA	Hiser et al. 1984	0.088	1.61	0.63	0.020	0.008	0.583	0.173	0.39	-	0.26 Cu	-	A.7
-	308	SMA	Vassilaros et al. 1985	-	-	-	-	-	-	-	-	-	-	-	A.8
-	316H	Weld	Bernard & Verzetetti 1985	-	-	-	-	-	-	-	-	-	-	-	A.9
A46-1	308	GTA	Nakagaki et al. 1986	-	-	-	-	-	-	-	-	-	-	-	A.11
A46-2	308	GTA	Nakagaki et al. 1986	-	-	-	-	-	-	-	-	-	-	-	A.11
A46-WM1	308	GTA	Nakagaki et al. 1986	-	-	-	-	-	-	-	-	-	-	-	A.11
A-46-WM2	308	GTA	Nakagaki et al. 1986	-	-	-	-	-	-	-	-	-	-	-	A.11
5G1	308	SMA	Horn et al. 1986	-	-	-	-	-	-	-	-	-	-	-	A.12
5G3	308	SMA	Horn et al. 1986	-	-	-	-	-	-	-	-	-	-	-	A.12
5G4	308	SMA	Horn et al. 1986	-	-	-	-	-	-	-	-	-	-	-	A.12
3RE	316L	SA	Horn et al. 1986	-	-	-	-	-	-	-	-	-	-	-	A.12

ID	Grade	Weld	Source	C	Mn	Si	P	S	Ni	Cr	Mo	N	Other	Ferrite	Ref.
2-1RE	316L	SA	Horn et al. 1986	-	-	-	-	-	-	-	-	-	-	-	A.12
2-2RE	316L	SA	Horn et al. 1986	-	-	-	-	-	-	-	-	-	-	-	A.12
-	-	-	Landes & McCabe 1986	-	-	-	-	-	-	-	-	-	-	-	A.13
-	-	-	Landes & McCabe 1986	-	-	-	-	-	-	-	-	-	-	-	A.13
-	-	-	Wilkowski 1987	-	-	-	-	-	-	-	-	-	-	-	A.24
-	-	-	Wilkowski 1987	-	-	-	-	-	-	-	-	-	-	-	A.24
-	308	Weld	Michel & Gray 1987	-	-	-	-	-	-	-	-	-		-	A.15
Y2412U308	308	GTA	Mills 1987	0.040	1.77	0.40	0.023	0.014	9.60	20.21	-	-	-	9.9	A.16
D/H	308	SMA	Mills 1987	0.070	1.92	0.62	0.010	0.010	9.58	20.26	0.16	-	-	7.0	A.16
-	308	MA	Mills 1988	0.060	1.90	0.37	0.040	-	9.77	19.80	0.12	0.05	0.15 Cu, 0.17 Co	-	A.17
Y2367R16.8.2	16-8-2	GTA	Mills 1988	0.045	1.25	0.29	0.024	0.013	8.62	16.36	1.67	-	-	5.7	A.18
D3418R304L	308	SA	Mills 1988	0.030	2.30	1.03	0.010	0.009	9.51	19.41	0.21	-	0.01 Nb+Ta	10.7	A.18
	16-18-2	SA	Mills 1988	0.047	1.95	1.00	0.020	0.006	6.98	16.10	1.91	-	0.017 Ti, 0.05 Nb+Ta	9.0	A.18
	308	SMA	Mills 1988	0.070	1.96	0.67	0.010	0.012	9.67	20.28	0.20	-	-	-	A.18
131	316L	SA	Ould et al. 1988	0.015	1.11	0.94	0.021	0.008	12.50	17.80	2.60	0.086	0.122 O	-	A.19
2047	316L	SA	Ould et al. 1988	0.015	1.12	0.84	0.012	0.004	12.30	17.80	2.70	0.076	0.136 O	-	A.19
-	ERNiCr3	GTA	Faure et al. 1989	0.010	3.09	0.05	0.003	0.011	72.10	19.73	0.01	-	2.7 Nb	-	A.20
-	316L	GTA[d]	Faure et al. 1989	0.008	1.49	0.51	0.018	0.011	12.70	19.20	2.60	0.051	0.012 Al	-	A.20
-	19.9L	MMA	Hale & Garwood 1990	0.030	0.84	0.21	0.017	0.005	9.80	19.20	0.07	0.064	=	5-9	A.21
-	316	GTA	ISPRA1990	-	-	-	-	-	-	-	-	-	-	-	A.22
	316	MMA	ISPRA1990	-	-	-	-	-	-	-	-	-	-	-	A.22
	316	SA	ISPRA1990	-	-	-	-	-	-	-	-	-	-	-	A.22
CF-3 Pipe	-	MMA	Strangewood & Druce 1990	0.020	0.71	0.85	0.015	0.013	9.81	19.20	0.01	-	0.080 O	-	A.23
304L	308	GTA	Vitek et al 1991	0.049	1.92	0.37	0.016	0.002	9.62	20.35	-	-	-	11.0	A.24
-	308	MIG	Sindelar STP 1175 1993	-	-	-	-	-	-	-	-	-	-	-	A.25
Riser Pipe	E308L	-	M. Valo, VTT, 1993	-	-	-	-	-	-	-	-	-	-	-	A.26
CR handle	E308L	-	M. Valo, VTT, 1993	-	-	-	-	-	-	-	-	-	-	-	A.26
PWWO	308L	SMA	Gavenda et al. 1996	0.030	2.12	0.44	0.018	0.018	10.72	20.35	0.27	0.072	0.20 Cu	6.8	A.27
PWER	308L	SMA	Gavenda et al. 1996	0.020	1.78	0.36	0.018	0.009	10.29	20.12	0.19	0.074	0.12 Cu	5.2	A.27
PWCE	308	SMA	Gavenda et al. 1996	0.050	1.79	0.44	0.003	0.002	9.54	20.22	0.05	0.060	0.04 Cu	6.1	A.27
-	316	MMA	O'Donnell et al. 1996	0.068	1.86	0.15	0.019	0.013	8.72	18.00	1.70	-	-	5-7	A.28
-	316	TIG	O'Donnell et al. 1996	0.042	2.60	0.42	0.018	0.011	8.80	17.30	1.80	-	-	4-8	A.28
-	316L	-	Alexander et al. 1996	-	-	-	-	-	-	-	-	-	-	-	A.29
-	308L	SMA	Hojo et al. 1997	-	-	-	-	-	-	-	-	-	-	-	A.30
-	316L	SMA	Hojo et al. 1997	-	-	-	-	-	-	-	-	-	-	-	A. 30

ID	Grade	Weld	Source	C	Mn	Si	P	S	Ni	Cr	Mo	N	Other	Ferrite	Ref.
-	316L	TIG	Hojo et al. 1997	-	-	-	-	-	-	-	-	-	-	-	A.30
304L	308	SMA	Alexander et al. 2000	0.055	1.98	0.46	0.025	0.017	9.30	18.95	0.23	-	-	4.0	A.85
304L	308	SMA	Alexander et al. 2000	0.054	0.22	0.47	0.027	0.015	8.75	20.15	0.22	-	-	8.0	A.85
304L	308	SMA	Alexander et al. 2000	0.052	1.34	0.68	0.027	0.018	8.05	20.70	0.21	-	-	12.0	A.85
-	308	GTA	Kim et al. 2006	-	-	-	-	-	-	-	-	-	-	-	A.32
CF-8M	Weld	SMA	JNES-SS-0602, 2006	0.040	1.26	0.37	0.014	0.006	11.60	19.60	2.27	0.030	0.06 O	9.0	A.32
-	308	Weld	Tavassoli 1988	-	-	-	-	-	-	-	-	-	-	-	A.33
-	308L	SAW	Tavassoli xxxx	-	-	-	-	-	-	-	-	-	-	-	A.34
	316LN	SAW	Tavassoli xxxx	-	-	-	-	-	-	-	-	-	-	-	A.34
-	316L	GTA	Lucas et al. 2011	0.022	1.85	0.44	0.001	0.021	12.68	19.34	2.51	-	0.26 Cu	14.0	A.36
-	316L	GTA	Lucas et al. 2011	0.15	1.75	0.35	0.014	0.017	12.30	19.20	2.61	-	0.05 Cu	10.0	A.36
304L	308	SA	Chen et al. 2014	-	-	-	-	-	-	-	-	-	-	-	A.37

APPENDIX B J-R CURVE CHARACTERIZATION

The fracture toughness J-R curve data were fitted to the power-law curve (of the form $J = C\Delta a^n$), and the fracture toughness J_{Ic} values were determined in accordance with ASTM Specifications E 813-81 and E 813-85. For the former, J_{Ic} is defined as the intersection of the blunting line given by $J = 2\sigma_f\,\Delta a$, and the linear fit of the J-vs.-Δa test data between the 0.15-mm and 1.5-mm exclusion lines. The flow stress, σ_f, is the average of the 0.2% yield strength and the ultimate strength. The ASTM Specification E 813-85 procedure defines J_{Ic} as the intersection of the 0.2-mm offset line with the power-law fit of the test data between the exclusion lines.

However, fracture toughness J-R curve tests on materials with relatively high toughness, ductility, and significant strain hardening ability, such as austenitic stainless steel, indicate that a slope of four times the flow stress ($4\sigma_f$) for the blunting line expresses the J-vs.-Δa data better than the slope of $2\sigma_f$ that is defined in E 813-81 or E 813-85. Therefore, in this study, the fracture toughness J_{Ic} values were determined from the reported values of flow stress and coefficient C and exponent n of the power-law curve, using a slope of $4\sigma_f$ for the blunting line and the 0.2-mm offset line. The reported values of J_{Ic} are listed in Table B2, only when any of these values was not available.

The various validity criteria specified in ASTM Specification E 813-85 for J_{Ic} and in ASTM Specification E 1152-87 for the J-R curve have been used to qualify the results from test data. The various criteria include maximum values of crack extension and J-integral as well as the limit for initial uncracked ligament. Hutchinson and Paris [A.37] have suggested a crack extension limit defined in terms of a ω value expressed as

$$\omega = (b/J)\,(dJ/da) >> 1, \qquad \text{(B-1)}$$

where b is the unbroken ligament given by (W-a), the difference between specimen width W and crack length a. Typically, a critical ω-value of 5 is used as a minimum value. The tentative J-R curve procedure proposed by Albrecht et al. [A.37], limits crack extension to 10% of the original unbroken ligament (i.e., $0.1b_0$). However, Ernst [A.37] had suggested that the crack length limit could be increased to $0.3b_0$ [i.e., ~3.8 mm crack extension for a 0.5T compact tension (CT) specimen].

The J vs. Δa values as well as the associated values of coefficient C, exponent n, and J_{Ic}, for austenitic SS welds in the unaged or aged and with or without neutron irradiation, are listed in Table B3. Note that for a few tests, the modified-J values are listed instead of deformation-J. These J-R curves are identified as J_m vs. Δa in Table B2, and the rest as deformation-J vs. Δa. For the modified-J tests, the J_{Ic}, coefficient C, and exponent n, correspond to the modified-J vs. Δa curves. In these earlier J-R tests, modified-J values were reported because Ernst [A.41] had shown that J_m was independent of the test specimen size. In general, J_m vs. Δa curve is higher than the J_d vs. Δa curve; the difference between the two increases with crack extension. An example of the deformation and modified J-R curves for thermally aged cast SS material is shown in Fig. B.1. Typically, the values of the coefficient C of the J-R curve are not increased significantly, but the J_m values at 2.5 mm crack extension are about 12% higher than the J_d values.

The tensile property and Charpy V-notch impact test data for unaged and thermally aged austenitic SS welds from the Argonne study, are presented in NUREG/CR-6428 [A.27].

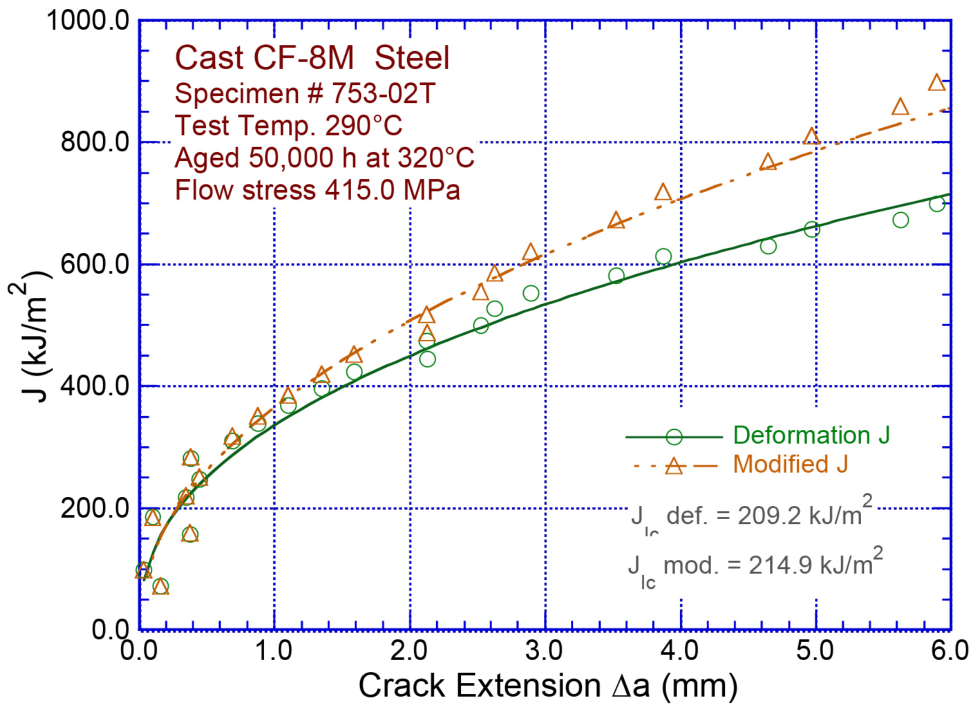

Figure B.1 Comparison of the deformation-J and modified-J vs. crack extension curves at 290°C for a thermally aged cast stainless steel material.

Table B1. The tensile property, Charpy-impact energy, and fracture toughness J-R curve data for austenitic stainless steel welds.

Grade	Type	Condition	ID	Ferrite (%)	Aging Temp (°C)	Aging Time (h)	Irrad-iation Temp. (°C)	Irrad-iation Dose. (dpa)	Test Temp (°C)	Coeff. C	Expo-nent n	Jic (kJ/m^2)	Test Temp (°C	Yield Stress (MPa)	Ultimate Stress (MPa)	Flow Stress (MPa)	Elong-ation (%)	Red. in Area (%)	Charpy Impact Energy (J/cm^2)	Ref.
308	MMA	-	V41	5.2	-	-	-	-	-	-	-	-	24	484.0	636.3	560.2	-	-	108.5	A.1
308	MMA	-	V41	5.2	-	-	-	-	-	-	-	-	260	387.0	479.9	433.5	-	-	137.3	A.1
308	MMA	-	V41	5.2	-	-	-	-	-	-	-	-	482	329.0	435.2	382.1	-	-	135.6	A.1
308	MMA	-	V42	10.4	-	-	-	-	-	-	-	-	24	541.3	702.0	621.6	-	-	96.6	A.1
308	MMA	-	V42	10.4	-	-	-	-	-	-	-	-	260	425.4	528.0	476.7	-	-	125.4	A.1
308	MMA	-	V42	10.4	-	-	-	-	-	-	-	-	482	362.5	484.0	423.3	-	-	-	A.1
308	MMA	-	V43	15.7	-	-	-	-	-	-	-	-	24	524.6	691.5	608.0	-	-	83.0	A.1
308	MMA	-	V43	15.7	-	-	-	-	-	-	-	-	260	420.5	527.3	473.9	-	-	120.3	A.1
308	MMA	-	V43	15.7	-	-	-	-	-	-	-	-	482	366.7	488.2	427.5	-	-	115.2	A.1
308	MMA	-	V44	19.0	-	-	-	-	-	-	-	-	24	564.4	727.8	646.1	-	-	100.0	A.1
308	MMA	-	V44	19.0	-	-	-	-	-	-	-	-	260	452.6	570.7	511.6	-	-	133.9	A.1
308	MMA	-	V44	19.0	-	-	-	-	-	-	-	-	482	380.7	523.9	452.3	-	-	127.1	A.1
316	SA	-	V23	7.0-10.5	-	-	-	-	-	-	-	-	24	456.1	616.8	536.4	-	-	114.7	A.1
316	SA	-	V23	7.0-10.5	-	-	-	-	-	-	-	-	260	354.8	505.0	429.9	-	-	139.8	A.1
316	SA	-	V24	7.0-10.5	-	-	-	-	-	-	-	-	24	459.6	629.3	544.5	-	-	94.9	A.1
316	SA	-	V24	7.0-10.5	-	-	-	-	-	-	-	-	260	-	-	-	-	-	118.6	A.1
316	SA	-	V25	7.0-10.5	-	-	-	-	-	-	-	-	24	459.6	611.2	535.4	-	-	92.4	A.1
316	SA	-	V25	7.0-10.5	-	-	-	-	-	-	-	-	260	353.4	494.5	424.0	-	-	112.4	A.1
17-8-2	MMA	AW	CGC1	7.0-9.0	-	-	-	-	370	-	-	56.3	370	401.0	486.0	443.5	12	31	88.8	A.2
17-8-2	MMA	2h @ 650°C	CGC1	3.5-6.5	-	-	-	-	370	-	-	42.0	370	286.0	431.0	358.5	16	35	86.3	A.2
17-8-2	MMA	2h @ 650°C	CGC1	3.5-6.5	-	-	-	-	370	-	-	49.5	370	286.0	431.0	358.5	16	35	86.3	A.2
17-8-2	MMA	2h @ 850°C	CGC1	1.0-3.0	-	-	-	-	370	-	-	39.2	370	261.0	423.0	342.0	16	37	108.8	A.2
17-8-2	MMA	2h @ 850°C	CGC1	0-0.5	-	-	-	-	370	-	-	65.1	370	184.0	449.0	316.5	24	47	156.3	A.2
17-8-2	MMA	-	OU6	5.0	-	-	-	-	370	-	-	40-60	370	-	-	-	-	-	-	A.2
17-8-2	MIG	-	PH21	2.0-4.0	-	-	-	-	370	-	-	40-60	370	-	-	-	-	-	-	A.2
17-8-2	MMA	-	PH22	1.0-4.0	-	-	-	-	370	-	-	40-60	370	-	-	-	-	-	-	A.2
17-8-2	MIG	-	PH19	2.0-4.0	-	-	-	-	370	-	-	40-60	370	-	-	-	-	-	-	A.2
17-8-2	MMA	-	PH/8	5.0	-	-	-	-	370	-	-	40-60	370	-	-	-	-	-	-	A.2
-	Weld	CF-8A base	FUC-6	-	-	-	-	-	24	367.0	0.482			-	-	489.0[a]	-	-	-	A.3
-	Weld	CF-8A base	FUC-7	-	-	-	-	-	24	297.6	0.518	153.5	-	-	-	489.0[a]	-	-	-	A.3
-	Weld	CF-8A base	FUC-5	-	-	-	-	-	149	236.0	0.395	141.2	-	-	-	489.0[a]	-	-	-	A.3
-	Weld	CF-8A base	FUC-9	-	-	-	-	-	149	154.8	0.373	91.9	-	-	-	489.0[a]	-	-	-	A.3
-	Weld	CF-8A base	FUC-10	-	-	-	-	-	288	292.5	0.406	186.1	-	-	-	362.6[a]	-	-	-	A.3
-	Weld	CF-8A base	FUC-12	-	-	-	-	-	288	252.4	0.370	164.3	-	-	-	362.6[a]	-	-	-	A.3

[a] Tensile data for 308L MMA weld from Ould et al., 1986. Used room temperature flow stress for 149°C data.

Table B1. The tensile property, Charpy-impact energy, and fracture toughness J-R curve data for austenitic stainless steel welds. (Contd.)

Grade	Type	Condition	ID	Ferrite (%)	Aging Temp (°C)	Aging Time (h)	Irrad-iation Temp. (°C)	Irrad-iation Dose. (dpa)	Test Temp (°C)	Coeff. C	Expo-nent n	Jic (kJ/m^2)	Test Temp (°C	Yield Stress (MPa)	Ultimate Stress (MPa)	Flow Stress (MPa)	Elong-ation (%)	Red. in Area (%)	Charpy Impact Energy (J/cm^2)	Ref.
316	MMA	As welded	-	-	-	-	370	0.50	370	160.1	0.250	-	-	-	-	-	-	-	-	A.4
316	MMA	Ht treat 650°C	-	-	-	-	370	0.35	370	160.1	0.330	-	-	-	-	-	-	-	-	A.4
316	MMA	Ht treat 650°C	-	-	-	-	370	0.35	370	120.0	0.250	-	-	-	-	-	-	-	-	A.4
316	MMA	Ht treat 650°C	-	-	-	-	370	0.35	370	73.4	0.960	-	-	-	-	-	-	-	-	A.4
316	MMA	As welded	-	-	-	-	420	0.54	370	257.7	0.610	-	-	-	-	-	-	-	-	A.4
316	MMA	Ht treat 1050°C	-	-	-	-	370	0.48	370	469.6	0.580	-	-	-	-	-	-	-	-	A.4
308L	Weld	-	B	6.0	-	-	-	-	20	380.7	0.600	176.2	20	500.0	645.0	572.5[b]	-	-	-	A.5
308L	Weld	-	D	7.3	-	-	-	-	20	343.6	0.614	152.6	20	500.0	645.0	572.5[b]	-	-	-	A.5
316	SA	-	-	-	-	-	-	-	370	342.7	0.610	165.7	370	325.0	473.0	399.0	22.0	-	-	A.6
316	MMA	-	-	-	-	-	-	-	370	146.8	0.951	35.1	370	386.0	471.0	428.5	38.0	-	-	A.6
Linde 80	SA	A508 Cl3 0.5T	62W-135[c]	-	-	-	-	-	200	166.58	0.555	73.5	200	409.4	522.0	465.7	-	-	-	A.7
Linde 80	SA	A508 Cl3 0.5T	62W-160	-	-	-	-	-	200	218.85	0.456	119.2	200	409.4	522.0	465.7	-	-	-	A.7
Linde 80	SA	A508 Cl3 0.8T	62W-47	-	-	-	-	-	200	248.29	0.494	130.0	200	409.4	522.0	465.7	-	-	-	A.7
Linde 80	SA	A508 Cl3 1.6T	62W-30	-	-	-	-	-	200	251.09	0.465	137.5	200	409.4	522.0	465.7	-	-	-	A.7
Linde 80	SA	A508 Cl3 1.6T	62W-32	-	-	-	-	-	200	263.13	0.538	130.0	200	409.4	522.0	465.7	-	-	-	A.7
Linde 80	SA	A508 Cl3 4.0T	62W-21	-	-	-	-	-	200	279.23	0.512	144.9	200	409.4	522.0	465.7	-	-	-	A.7
Linde 80	SA	A508 Cl3 0.5T	62W-118	-	-	-	260-293	d	200	116.70	0.455	59.2	200	545.5	647.6	596.6	-	-	-	A.7
Linde 80	SA	A508 Cl3 0.8T	62W-42	-	-	-	260-293	d	200	237.23	0.501	118.4	200	545.5	647.6	596.6	-	-	-	A.7
Linde 80	SA	A508 Cl3 1.6T	62W-34	-	-	-	260-293	d	200	171.62	0.400	97.1	200	545.5	647.6	596.6	-	-	-	A.7
Linde 80	SA	A508 Cl3 4.0T	62W-20	-	-	-	260-293	d	200	210.41	0.412	118.8	200	545.5	647.6	596.6	-	-	-	A.7
Linde 80	SA	A508 Cl3 0.5T	62W-137	-	-	-	-	-	288	147.16	0.422	81.4	288	385.0	509.9	447.5	-	-	-	A.7
Linde 80	SA	A508 Cl3 0.5T	62W-157	-	-	-	-	-	288	167.41	0.512	81.6	288	385.0	509.9	447.5	-	-	-	A.7
Linde 80	SA	A508 Cl3 0.8Td	62W-50	-	-	-	-	-	288	152.98	0.441	82.4	288	385.0	509.9	447.5	-	-	-	A.7
Linde 80	SA	A508 Cl3 1.6T	62W-33	-	-	-	-	-	288	211.90	0.526	103.9	288	385.0	509.9	447.5	-	-	-	A.7
Linde 80	SA	A508 Cl3 4.0T	62W-23	-	-	-	-	-	288	195.76	0.523	95.5	288	385.0	509.9	447.5	-	-	-	A.7
Linde 80	SA	A508 Cl3 0.5T	62W-116	-	-	-	260-293	d	288	107.31	0.340	64.9	288	519.9	629.9	574.9	-	-	-	A.7
Linde 80	SA	A508 Cl3 0.8T	62W-44	-	-	-	260-293	d	288	104.15	0.397	57.6	288	519.9	629.9	574.9	-	-	-	A.7
-	SMA	Type 304 weld	-	-	-	-	-	-	24	627.3	0.585	-	-	-	-	-	-	-	-	A.8
-	SMA	Type 304 weld	-	-	-	-	-	-	150	554.0	0.587	-	-	-	-	-	-	-	-	A.8
-	SMA	Type 304 weld	-	-	-	-	-	-	288	379.8	0.469	-	-	-	-	-	-	-	-	A.8
-	SMA	Type 304 weld	-	-	-	-	-	-	288	281.0	0.648	-	-	-	-	-	-	-	-	A.8
316H	Weld	-	-	-	-	-	-	0.007	350	303.3	0.570	154.0	350	300.0	445.0	372.5	16.0	-	-	A.9
316H	Weld	-	-	-	-	-	350	0.10	350	270.9	0.570	-	-	-	-	-	-	-	-	A.9

[b] Tensile data for 308L Weld A with FN=11.
[c] The fracture toughness data represents modified-J vs. crack extension curves, and not deformation-J vs. crack extension curves.
[d] Samples irradiated to a fast neutron fluence of 1.0 – 1.8 x 10^{19} n/cm^2 (E > 1 MeV) at 260 – 293°C in Bulk Shielded Reactor (BSR) at Oak Ridge..

Table B1. (Contd.)

Grade	Type	Condition	ID	Ferrite (%)	Aging Temp (°C)	Aging Time (h)	Irrad-iation Temp. (°C)	Irrad-iation Dose. (dpa)	Test Temp (°C)	Coeff. C	Expo-nent n	Jic (kJ/m^2)	Test Temp (°C	Yield Stress (MPa)	Ultimate Stress (MPa)	Flow Stress (MPa)	Elong-ation (%)	Red. in Area (%)	Charpy Impact Energy (J/cm^2)	Ref.
316H	Weld	-	-	-	-	-	350	0.30	350	234.9	0.380	-	-	-	-	-	-	-	-	A.9
316H	Weld	-	-	-	-	-	350	1.00	350	234.3	0.420	-	-	-	-	-	-	-	-	A.9
308L	TIG	-	A46-1	-	-	-	-	-	288	1,001.0	0.277	954	288	298.0	447.0	372.5	31.6	73.6	-	A.11
308L	TIG	-	A46-2	-	-	-	-	-	288	1,493.2	0.085	1519	288	298.0	447.0	372.5	31.6	73.6	-	A.11
308L	TIG	-	A46-WM1	-	-	-	-	-	288	960.3	0.345	887	288	298.0	447.0	372.5	31.6	73.6	-	A.11
308L	TIG	-	A46-WM2	-	-	-	-	-	288	1,232.4	0.112	1236	288	298.0	447.0	372.5	31.6	73.6	-	A.11
308	SMA	As deposited	5G1	-	-	-	-	-	288	272.3	0.381	192.6	288	319.2	454.7	387.0	26.0	58.1	133.9	A.12
308	SMA	As deposited	5G3	-	-	-	-	-	288	298.2	0.406	213.8	288	319.2	454.7	387.0	26.0	58.1	133.9	A.12
308	SMA	Solution Anneal	5G4	-	-	-	-	-	288	238.5	0.415	167.6	288	194.2	430.3	312.3	33.0	62.6	279.6	A.12
316L	SA	As deposited	3RE	-	-	-	-	-	288	227.7	0.312	169.3	288	312.9	439.3	376.1	22.0	45.8	123.7	A.12
316L	SA	As deposited	2-1RE	-	-	-	-	-	288	-	-	208.8	288	312.9	439.3	376.1	22.0	45.8	123.7	A.12
316L	SA	Solution Anneal	2-2RE	-	-	-	-	-	288	264.0	0.266	219.2	288	194.9	406.5	300.7	34.0	57.8	135.6	A.12
308	SA	-	-	-	-	-	-	-	24	268.7	0.792	-	-	-	-	-	-	-	-	A.13
308	SA	-	-	-	-	-	-	-	288	138.9	0.752	-	-	-	-	-	-	-	-	A.13
308	SMA	-	-	-	-	-	-	-	24	505.8	0.449	-	-	-	-	-	-	-	-	A.13
308	SMA	-	-	-	-	-	-	-	288	292.6	0.430	-	-	-	-	-	-	-	-	A.13
308	TIG	-	-	-	-	-	-	-	24	934.2	0.823	-	-	-	-	-	-	-	-	A.13
308	TIG	-	-	-	-	-	-	-	288	864.0	0.495	-	-	-	-	-	-	-	-	A.13
316	SA	-	-	-	-	-	-	-	24	289.7	0.530	-	-	-	-	-	-	-	-	A.13
316	SA	-	-	-	-	-	-	-	288	181.4	0.510	-	-	-	-	-	-	-	-	A.13
308L	GTA	Weld	1-T CT	-	-	-	-	-	25	662.1	0.572	378.4	25	464.7	611.6	538.2	38.0	65.0	-	A.24
308L	GTA	Weld	1-T CT	-	-	-	-	-	149	583.6	0.570	351.8	149	355.8	476.4	416.1	29.0	59.0	-	A.24
308L	GTA	Weld	1-T CT	-	-	-	-	-	288	398.8	0.436	256.0	288	337.8	452.3	395.1	25.0	55.0	-	A.24
308L	GTA	Weld	1-T CT	-	-	-	-	-	288	303.8	0.596	146.0	288	337.8	452.3	395.1	25.0	55.0	-	A.24
308L	GTA	Weld	2-T CT	-	-	-	-	-	288	674.6	0.670	394.9	288	337.8	452.3	395.1	25.0	55.0	-	A.24
308L	GTA	Weld	2-T CT	-	-	-	-	-	288	538.3	0.702	267.5	288	337.8	452.3	395.1	25.0	55.0	-	A.24
308L	GTA	Fusion line	1-T CT	-	-	-	-	-	288	610.9	0.516	-	-	-	-	-	-	-	-	A.24
308	Weld	-	W10-10	-	-	-	-	0.007	427	410.8	0.470	190	-	-	-	-	-	-	-	A.15
308	Weld	-	W10-12	-	-	-	-	0.007	427	349.4	0.594	190	-	-	-	-	-	-	-	A.15
308	Weld	EBRII Irradiated	W10-9	-	-	-	-	11.1	427	53.2	0.250	30	-	-	-	-	-	-	-	A.15
308	Weld	EBRII Irradiated	W10-6	-	-	-	-	11.1	427	30.6	0.298	30	-	-	-	-	-	-	-	A.15
308	Weld	EBRII Irradiated	W10-3	-	-	-	-	11.1	427	39.2	0.354	30	-	-	-	-	-	-	-	A.15
308	GTA	-	Y2412U308	9.9	-	-	-	-	427	618.8	0.578	269	-	-	-	-	-	-	-	A.16
308	GTA	-	Y2412U308	-	427	10000	-	-	427	539.0	0.486	269	-	-	-	-	-	-	-	A.16

Table B1. (Contd.)

Grade	Type	Condition	ID	Ferrite (%)	Aging Temp (°C)	Aging Time (h)	Irrad-iation Temp. (°C)	Irrad-iation Dose. (dpa)	Test Temp (°C)	Coeff. C	Expo-nent n	Jic (kJ/m^2)	Test Temp (°C	Yield Stress (MPa)	Ultimate Stress (MPa)	Flow Stress (MPa)	Elong-ation (%)	Red. in Area (%)	Charpy Impact Energy (J/cm^2)	Ref.
308	SMA	-	D/H	-	-	-	-	-	427	389.9	0.694	155	-	-	-	-	-	-	-	A.16
308	SMA	-	D/H	-	427	10000	-	-	427	362.1	0.586	155	-	-	-	-	-	-	-	A.16
308	SMA	-	-	-	-	-	-	-	427	345.9	0.770	89	-	-	-	-	-	-	-	A.17
308	SMA	-	-	-	-	-	400-427	14.0	427	29.1	0.550	11	-	-	-	-	-	-	-	A.17
308	GTA	-	Y2412U308	9.9	-	-	-	-	427	573.5	0.605	342.7	427	278.0	477.0	377.5	23.0	54	-	A.18
308	SA	-	D3418R304L	10.7	-	-	-	-	24	331.2	0.475	183.6	24	408.0	627.0	517.5	41.0	58	-	A.18
308	SA	-	D3418R304L	10.7	-	-	-	-	427	197.0	0.584	88.5	427	344.0	474.0	409.0	24.0	59	-	A.18
308	SMA	-	-	7.0	-	-	-	-	427	423.1	0.565	232.3	427	323.0	472.0	397.5	24.0	58	-	A.18
16-8-2	GTA	-	Y2367R16-8-2	5.7	-	-	-	-	24	682.8	0.845	267.7	24	360.0	668.0	514.0	54.0	74	-	A.18
16-8-2	GTA	-	Y2367R16-8-2	5.7	-	-	-	-	427	350.4	0.438	218.8	427	265.0	510.0	387.5	29.0	51	-	A.18
16-8-2	SA	-	D4494T16-8-2	9.0	-	-	-	-	24	554.2	0.585	298.1	24	391.0	627.0	509.0	45.0	40	-	A.18
16-8-2	SA	-	D4494T16-8-2	9.0	-	-	-	-	427	238.8	0.591	110.5	427	297.0	476.0	386.5	25.0	49	-	A.18
316L	SA	-	131	-	-	-	-	-	300	223.0	-	129	320	333.0	448.0	390.5	18.0	41	-	A.19
316L	SA	-	131	-	550 & 610	10 16	-	-	300	176.0	-	94	320	302.0	450.0	376.0	19.0	48	-	A.19
316L	SA	-	131	-	750	25	-	-	300	146.0	-	67	320	235.0	440.0	337.5	23	51	-	A.19
316L	SA	-	2047	-	-	-	-	-	300	187.0	-	78	320	385.0	464.0	424.5	14	35	-	A.19
316L	SA	-	2047	-	550 & 610	10 16	-	-	300	160.0	-	78	320	345.0	486.0	415.5	20	43	-	A.19
ER NiCr3	GTA	A508 Cl3 weld	-	-	-	-	-	-	20	-	-	-	20	376.7	670.9	523.8	43.2	57.8	-	A.20
ER NiCr3	GTA	A508 Cl3 weld	-	-	-	-	-	-	100	563.6	0.564	318.0	100	353.1	629.8	491.5	43.4	57.6	-	A.20
ER NiCr3	GTA	A508 Cl3 weld	-	-	-	-	-	-	300	454.4	0.575	241.0	300	327.3	585.5	456.4	43.4	58.2	-	A.20
316L	GTA	CF-3 weld	-	10.0	-	-	-	-	20	-	-	-	20	512.5	614.8	563.6	26.5	52.9	-	A.20
316L	GTA	CF-3 weld	-	10.0	-	-	-	-	100	531.8	0.555	295.0	100	471.3	543.0	507.1	18.2	64.1	-	A.20
316L	GTA	CF-3 weld	-	10.0	-	-	-	-	300	384.3	0.527	210.0	300	413.7	475.7	444.7	15.7	52.8	-	A.20
19.9L	MMA	-	-	5.0-9.0	-	-	-	-	300	184.2	0.504	90.0	24	483.8	606.0	544.9	30.5	-	-	A.21
19.9L	MMA	-	-	5.0-9.0	375	1000	-	-	-	-	-	-	24	495.9	626.6	561.3	29.7	-	-	A.21
19.9L	MMA	-	-	5.0-9.0	375	5000	-	-	-	-	-	-	24	499.3	633.0	566.1	31.0	-	-	A.21
19.9L	MMA	-	-	5.0-9.0	375	10000	-	-	-	-	-	-	24	501.1	614.2	557.6	32.4	-	-	A.21
19.9L	MMA	-	-	5.0-9.0	375	20000	-	-	-	-	-	-	24	486.8	632.6	559.7	29.8	-	-	A.21
19.9L	MMA	-	-	5.0-9.0	400	1000	-	-	300	142.1	0.387	81.3	24	495.8	626.6	561.2	28.6	-	-	A.21
19.9L	MMA	-	-	5.0-9.0	400	5000	-	-	-	-	-	-	24	499.7	649.2	574.4	24.4	-	-	A.21
19.9L	MMA	-	-	5.0-9.0	400	10000	-	-	300	121.0	0.593	49.6	24	501.0	614.2	557.6	21.6	-	-	A.21
19.9L	MMA	-	-	5.0-9.0	400	20000	-	-	-	-	-	-	24	484.2	643.5	563.9	33.4	-	-	A.21
316	GTA	-	-	-	-	-	-	-	-	-	-	-	20	439.5	625.5	-	-	156.5	-	A.22
316	MMA	-	-	-	-	-	-	-	-	-	-	-	20	450.8	596.8	-	-	75.0	-	A.22

Table B1. (Contd.)

Grade	Type	Condition	ID	Ferrite (%)	Aging Temp (°C)	Aging Time (h)	Irrad-iation Temp. (°C)	Irrad-iation Dose. (dpa)	Test Temp (°C)	Coeff. C	Expo-nent n	Jic (kJ/m^2)	Test Temp (°C	Yield Stress (MPa)	Ultimate Stress (MPa)	Flow Stress (MPa)	Elong-ation (%)	Red. in Area (%)	Charpy Impact Energy (J/cm^2)	Ref.
316	GTA	-	-	-	-	-	-	-	-	-	-	-	20	378.8	578.5	-	-	85.3	-	A.22
-	MMA	CF-3 pipe	repair weld	4.0-5.0	-	-	-	-	-	-	-	-	22	-	-	-	-	-	57.4	A.23
-	MMA	CF-3 pipe	repair weld	4.0-5.0	300	5,000	-	-	-	-	-	-	22	-	-	-	-	-	63.6	A.23
-	MMA	CF-3 pipe	repair weld	4.0-5.0	350	5,000	-	-	-	-	-	-	22	-	-	-	-	-	57.3	A.23
-	MMA	CF-3 pipe	repair weld	4.0-5.0	400	1,500	-	-	-	-	-	-	22	-	-	-	-	-	51.1	A.23
-	MMA	CF-3 pipe	repair weld	4.0-5.0	-	-	-	-	-	-	-	-	50	-	-	-	-	-	56.0	A.23
-	MMA	CF-3 pipe	repair weld	4.0-5.0	300	5,000	-	-	-	-	-	-	50	-	-	-	-	-	61.3	A.23
-	MMA	CF-3 pipe	repair weld	4.0-5.0	350	5,000	-	-	-	-	-	-	50	-	-	-	-	-	58.4	A.23
-	MMA	CF-3 pipe	repair weld	4.0-5.0	400	1,500	-	-	-	-	-	-	50	-	-	-	-	-	52.4	A.23
-	MMA	CF-3 pipe	repair weld	4.0-5.0	300	500	-	-	-	-	-	-	60	-	-	-	-	-	59.7	A.23
-	MMA	CF-3 pipe	repair weld	4.0-5.0	300	3,000	-	-	-	-	-	-	60	-	-	-	-	-	70.1	A.23
-	MMA	CF-3 pipe	repair weld	4.0-5.0	300	10,000	-	-	-	-	-	-	60	-	-	-	-	-	54.5	A.23
-	MMA	CF-3 pipe	repair weld	4.0-5.0	350	100	-	-	-	-	-	-	60	-	-	-	-	-	61.3	A.23
-	MMA	CF-3 pipe	repair weld	4.0-5.0	350	500	-	-	-	-	-	-	60	-	-	-	-	-	64.3	A.23
-	MMA	CF-3 pipe	repair weld	4.0-5.0	350	1,000	-	-	-	-	-	-	60	-	-	-	-	-	63.6	A.23
-	MMA	CF-3 pipe	repair weld	4.0-5.0	350	2,000	-	-	-	-	-	-	60	-	-	-	-	-	66.3	A.23
-	MMA	CF-3 pipe	repair weld	4.0-5.0	350	3,000	-	-	-	-	-	-	60	-	-	-	-	-	60.0	A.23
-	MMA	CF-3 pipe	repair weld	4.0-5.0	350	5,000	-	-	-	-	-	-	60	-	-	-	-	-	56.6	A.23
-	MMA	CF-3 pipe	repair weld	4.0-5.0	350	10,000	-	-	-	-	-	-	60	-	-	-	-	-	60.6	A.23
-	MMA	CF-3 pipe	repair weld	4.0-5.0	400	100	-	-	-	-	-	-	60	-	-	-	-	-	63.5	A.23
-	MMA	CF-3 pipe	repair weld	4.0-5.0	400	500	-	-	-	-	-	-	60	-	-	-	-	-	63.8	A.23
-	MMA	CF-3 pipe	repair weld	4.0-5.0	400	1,000	-	-	-	-	-	-	60	-	-	-	-	-	59.9	A.23
-	MMA	CF-3 pipe	repair weld	4.0-5.0	400	3,000	-	-	-	-	-	-	60	-	-	-	-	-	60.0	A.23
-	MMA	CF-3 pipe	repair weld	4.0-5.0	400	10,000	-	-	-	-	-	-	60	-	-	-	-	-	60.3	A.23
-	MMA	CF-3 pipe	repair weld	4.0-5.0	400	1,500	-	-	-	-	-	-	200	-	-	-	-	-	55.8	A.23
-	MMA	CF-3 pipe	repair weld	4.0-5.0	350	5,000	-	-	-	-	-	-	200	-	-	-	-	-	55.8	A.23
-	MMA	CF-3 pipe	repair weld	4.0-5.0	300	5,000	-	-	-	-	-	-	200	-	-	-	-	-	68.6	A.23
-	MMA	CF-3 pipe	repair weld	4.0-5.0	-	-	-	-	-	-	-	-	300	-	-	-	-	-	74.8	A.23
-	MMA	CF-3 pipe	repair weld	4.0-5.0	400	1,500	-	-	-	-	-	-	300	-	-	-	-	-	63.3	A.23
-	MMA	CF-3 pipe	repair weld	4.0-5.0	350	5,000	-	-	-	-	-	-	300	-	-	-	-	-	63.3	A.23
-	MMA	CF-3 pipe	repair weld	4.0-5.0	300	5,000	-	-	-	-	-	-	300	-	-	-	-	-	72.4	A.23
308	GTA	304L plate	Top of weld	11.0	-	-	-	-	-	-	-	774.4	24	329.5	615.0	472.3	42.6	75.0	69.2[d]	A.24
308	GTA	304L plate	Top of weld	11.0	475	100	-	-	-	-	-	747.3	24	313.2	572.1	442.6	42.2	70.1	73.9[d]	A.24
308	GTA	304L plate	Top of weld	11.0	475	1,000	-	-	-	-	-	420.1	24	424.8	664.3	544.5	28.0	59.9	39.3[d]	A.24
308	GTA	304L plate	Top of weld	11.0	475	5,000	-	-	-	-	-	258.7	24	379.9	644.5	512.2	38.7	50.2	22.6[d]	A.24

Table B1. (Contd.)

Grade	Type	Condition	ID	Ferrite (%)	Aging Temp (°C)	Aging Time (h)	Irrad-iation Temp. (°C)	Irrad-iation Dose. (dpa)	Test Temp (°C)	Coeff. C	Expo-nent n	Jic (kJ/m^2)	Test Temp (°C	Yield Stress (MPa)	Ultimate Stress (MPa)	Flow Stress (MPa)	Elong-ation (%)	Red. in Area (%)	Charpy Impact Energy (J/cm^2)	Ref.
308	GTA	304L plate	Middle of weld	11.0	-	-	-	-	-	-	-	-	24	395.0	648.0	521.5	31.1	59.7	-	A.24
308	GTA	304L plate	Middle of weld	11.0	475	100	-	-	-	-	-	-	24	444.2	634.2	539.2	39.6	65.8	-	A.24
308	GTA	304L plate	Middle of weld	11.0	475	1,000	-	-	-	-	-	-	24	393.4	645.8	519.6	31.1	51.0	-	A.24
308	GTA	304L plate	Middle of weld	11.0	475	5,000	-	-	-	-	-	-	24	412.5	652.4	532.4	31.8	59.0	-	A.24
308	GTA	304L plate	Bottom of weld	11.0	-	-	-	-	-	-	-	479.4	24	391.5	599.7	495.6	34.6	59.6	56.0[e]	A.24
308	GTA	304L plate	Bottom of weld	11.0	475	100	-	-	-	-	-	357.9	24	427.9	665.9	546.9	28.7	66.3	16.1[e]	A.24
308	GTA	304L plate	Bottom of weld	11.0	475	1,000	-	-	-	-	-	273.8	24	408.2	641.7	524.9	35.1	59.6	17.4[e]	A.24
308	GTA	304L plate	Bottom of weld	11.0	475	5,000	-	-	-	-	-	263.4	24	458.9	703.8	581.4	26.7	41.6	22.3[e]	A.24
308	MIG	304 plate	2W164	-	-	-	100-155	0.007	125	454.0	0.500	277.0	-	-	-	-	-	-	-	A.25
308	MIG	304 plate	2W132	-	-	-	100-155	0.007	125	461.0	0.590	251.0	-	-	-	-	-	-	-	A.25
308	MIG	304 plate	2W2	-	-	-	100-155	1.7	125	270.0	0.500	137.0	-	-	-	-	-	-	-	A.25
E308L	-	weld	Riser pipe	-	-	-	280	0.8	24	296.0	0.533	145.6	22	416.0	643.0	529.5	42.0	-	-	A.26
E308L	-	weld	Riser pipe	-	-	-	280	0.6	199	223.6	0.466	124.9	270	270.0	452.0	361.0	25.0	-	-	A.26
E308L	-	weld	Riser pipe	-	-	-	280	0.7	249	280.8	0.358	183.8	270	385.0	515.0	450.0	20.0	-	-	A.26
E308L	-	weld	Control rod handle	-	-	-	280	12	24	29.1	0.659	10.2	24	1,005.0	1013.0	1,009	25.5	-	-	A.26
E308L	-	weld	Control rod handle	-	-	-	280	12	150	107.8	0.574	44.1	24	1,005.0	1013.0	1,009	25.5	-	-	A.26
E308L	-	weld	Control rod handle	-	-	-	280	12	259	84.1	0.665	29.7	297	821.0	819.0	820.0	4.0	-	-	A.26
E308L	-	weld	Control rod handle	-	-	-	280	12	259	58.6	0.222	41.6	297	821.0	819.0	820.0	4.0	-	-	A.26
308	SMA	304 pipe	-	-	-	-	-	-	24	-	-	-	-	-	-	-	-	-	268.8	A.27
308	SMA	304 pipe	PWCE-01	-	-	-	-	-	290	648.8	0.713	357.6	290	315.0	450.0	382.5	-	-	353.3	A.27
308	SMA	304 pipe	-	-	400	10,000	-	-	24	-	-	-	-	-	-	-	-	-	168.3	A.27
308	SMA	304 pipe	PWCE-03	-	400	10,000	-	-	290	614.2	0.611	363.7	290	321.0	490.0	405.5	-	-	271.3	A.27
308L	SMA	304 pipe	-	-	-	-	-	-	24	-	-	-	-	-	-	-	-	-	169.0	A.27
308L	SMA	304 pipe	PWWO-01	-	-	-	-	-	290	400.9	0.481	242.8	290	349.0	446.0	397.5	-	-	186.6	A.27
308L	SMA	304 pipe	-	-	400	7,700	-	-	24	-	-	-	-	-	-	-	-	-	128.6	A.27
308L	SMA	304 pipe	PWWO-02	-	400	7,700	-	-	290	330.2	0.621	154.5	290	346.0	472.0	409.0	-	-	136.9	A.27
308L	SMA	304 pipe	-	-	400	7,700	-	-	24	-	-	-	-	-	-	-	-	-	128.6	A.27
308L	SMA	304 pipe	PWWO-04	-	400	7,700	-	-	290	338.8	0.505	189.3	290	346.0	472.0	409.0	-	-	136.9	A.27
308L	SMA	304 pipe	PWER	-	-	-	-	-	290	-	-	-	-	-	-	-	-	-	-	A.27
308L	SMA	304 pipe	PWER-01	-	400	10,000	-	-	290	459.4	0.509	-	-	-	-	-	-	-	-	A.27
316	TIG	As welded	-	4.0-8.0	-	-	-	-	370	565.0	0.687	-	-	-	-	-	-	-	-	A.28

[e] Notch in the TL orientation, i.e., axial crack propagating along the length of the crack. Value in TS orientation is 35% lower (i.e., circumferential crack propagation through wall). .

Table B1. (Contd.)

Grade	Type	Condition	ID	Ferrite (%)	Aging Temp (°C)	Aging Time (h)	Irrad-iation Temp. (°C)	Irrad-iation Dose. (dpa)	Test Temp (°C)	Coeff. C	Expo-nent n	Jic (kJ/m^2)	Test Temp (°C	Yield Stress (MPa)	Ultimate Stress (MPa)	Flow Stress (MPa)	Elong-ation (%)	Red. in Area (%)	Charpy Impact Energy (J/cm^2)	Ref.
316	MMA	AW' + AW[f]	-	5.0-7.0	-	-	-	-	370	245.5	0.579	-	-	-	-	-	-	-	-	A.28
316	MMA	AW	-	5.0-7.0	-	-	370	2.0	370	138.3	0.750	-	-	-	-	-	-	-	-	A.28
316	MMA	AW'	-	5.0-7.0	-	-	370	4.0	370	21.1	0.510	-	-	-	-	-	-	-	-	A.28
316	MMA	AW'	-	5.0-7.0	400	50,000	-	-	370	226.9	0.782	-	-	-	-	-	-	-	-	A.28
316	MMA	AW'	-	5.0-7.0	450	50,000	-	-	370	193.8	0.549	-	-	-	-	-	-	-	-	A.28
316L	-	weld	-	-	-	-	90	3	25	854.0	0.310	-	-	-	-	-	-	-	-	A.29
316L	-	weld	-	-	-	-	90	3	100	664.0	0.390	-	-	-	-	-	-	-	-	A.29
316L	-	weld	-	-	-	-	90	3	200	669.0	0.520	-	-	-	-	-	-	-	-	A.29
316L	-	weld	-	-	-	-	250	3	25	519.0	0.330	-	-	-	-	-	-	-	-	A.29
316L	-	weld	-	-	-	-	250	3	100	479.0	0.310	-	-	-	-	-	-	-	-	A.29
316L	-	weld	-	-	-	-	250	3	200	368.0	0.380	-	-	-	-	-	-	-	-	A.29
308L	SMA	-	K	9.0	-	-	-	-	325	304.9	0.475	-	-	-	-	-	-	-	-	A.30
308L	SMA	-	K	9.0	400	10,000	-	-	325	171.3	0.434	-	-	-	-	-	-	-	-	A.30
308L	SMA	-	K	9.0	400	20,000	-	-	325	153.9	0.466	-	-	-	-	-	-	-	-	A.30
308L	SMA	-	K	9.0	400	40,000	-	-	325	176.0	0.413	-	-	-	-	-	-	-	-	A.30
308L	SMA	-	J	8.0	-	-	-	-	325[g]	335.6	0.528	-	-	-	-	-	-	-	-	A.30
308L	SMA	-	J	8.0	300	40,000	-	-	325[g]	340.1	0.522	-	-	-	-	-	-	-	-	A.30
308L	SMA	-	J	8.0	300	60,000	-	-	325	356.6	0.410	-	-	-	-	-	-	-	-	A.30
308L	SMA	-	J	8.0	-	-	-	-	325[g]	318.3	0.545	-	-	-	-	-	-	-	-	A.30
308L	SMA	-	J	8.0	350	40,000	-	-	325	308.2	0.436	-	-	-	-	-	-	-	-	A.30
308L	SMA	-	J	8.0	350	60,000	-	-	325[g]	236.2	0.294	-	-	-	-	-	-	-	-	A.30
308L	SMA	-	J	8.0	400	10,000	-	-	325	254.4	0.621	-	-	-	-	-	-	-	-	A.30
308L	SMA	-	J	8.0	400	20,000	-	-	325	153.2	0.699	-	-	-	-	-	-	-	-	A.30
308L	SMA	-	J	8.0	400	40,000	-	-	325	214.8	0.357	-	-	-	-	-	-	-	-	A.30
308L	SMA	-	H	8.0	-	-	-	-	325	562.5	0.514	-	-	-	-	-	-	-	-	A.30
308L	SMA	-	H	8.0	300	40,000	-	-	325[g]	448.4	0.434	-	-	-	-	-	-	-	-	A.30
308L	SMA	-	H	8.0	300	60,000	-	-	325[g]	399.3	0.409	-	-	-	-	-	-	-	-	A.30
308L	SMA	-	H	8.0	350	40,000	-	-	325	347.4	0.377	-	-	-	-	-	-	-	-	A.30
308L	SMA	-	H	8.0	350	60,000	-	-	325	389.7	0.315	-	-	-	-	-	-	-	-	A.30
308L	SMA	-	H	8.0	400	10,000	-	-	325	374.6	0.382	-	-	-	-	-	-	-	-	A.30
308L	SMA	-	H	8.0	400	20,000	-	-	325[g]	341.8	0.391	-	-	-	-	-	-	-	-	A.30
308	SMA	on 304L plate	-	4.0	-	-	-	-	-	-	-	-	20	408.9	601.3	505.1	-	-	132.5	A.31
308	SMA	on 304L plate	-	4.0	-	-	-	-	-	-	-	-	>150	-	-	-	-	-	134.3	A.31

[f] AW is as welded, and AW' is as welded plus 2 hr at 650°C.
[g] Lower bound J-R curve.

Table B1. (Contd.)

Grade	Type	Condition	ID	Ferrite (%)	Aging Temp (°C)	Aging Time (h)	Irrad-iation Temp. (°C)	Irrad-iation Dose. (dpa)	Test Temp (°C)	Coeff. C	Expo-nent n	Jic (kJ/m^2)	Test Temp (°C	Yield Stress (MPa)	Ultimate Stress (MPa)	Flow Stress (MPa)	Elong-ation (%)	Red. in Area (%)	Charpy Impact Energy (J/cm^2)	Ref.
308	SMA	on 304L plate	-	4.0	343	3,000	-	-	-	-	-	-	20	359.1	599.1	479.1	-	-	122.8	A.31
308	SMA	on 304L plate	-	4.0	343	10,000	-	-	-	-	-	-	20	362.1	604.7	483.4	-	-	120.1	A.31
308	SMA	on 304L plate	-	4.0	343	20,000	-	-	-	-	-	-	20	379.1	612.3	495.7	-	-	124.7	A.31
308	SMA	on 304L plate	-	4.0	343	50,000	-	-	-	-	-	-	20	377.4	631.9	504.6	-	-	114.2	A.31
308	SMA	on 304L plate	-	4.0	343	50,000	-	-	-	-	-	-	>150	-	-	-	-	-	122.1	A.31
308	SMA	on 304L plate	-	8.0	-	-	-	-	-	-	-	-	20	385.6	601.3	493.4	-	-	112.2	A.31
308	SMA	on 304L plate	-	8.0	-	-	-	-	-	-	-	-	>150	-	-	-	-	-	129.7	A.31
308	SMA	on 304L plate	-	8.0	343	3,000	-	-	-	-	-	-	20	389.6	619.8	504.7	-	-	114.1	A.31
308	SMA	on 304L plate	-	8.0	343	10,000	-	-	-	-	-	-	20	425.7	665.2	545.4	-	-	95.9	A.31
308	SMA	on 304L plate	-	8.0	343	20,000	-	-	-	-	-	-	20	403.4	658.4	530.9	-	-	84.3	A.31
308	SMA	on 304L plate	-	8.0	343	50,000	-	-	-	-	-	-	20	423.4	668.6	546.0	-	-	71.0	A.31
308	SMA	on 304L plate	-	8.0	343	50,000	-	-	-	-	-	-	>150	-	-	-	-	-	88.1	A.31
308	SMA	on 304L plate	-	12.0	-	-	-	-	-	-	-	-	20	368.0	619.9	494.0	-	-	109.4	A.31
308	SMA	on 304L plate	-	12.0	-	-	-	-	-	-	-	-	>150	-	-	-	-	-	142.5	A.31
308	SMA	on 304L plate	-	12.0	343	3,000	-	-	-	-	-	-	20	423.2	637.4	530.3	-	-	79.1	A.31
308	SMA	on 304L plate	-	12.0	343	10,000	-	-	-	-	-	-	20	426.2	665.2	545.7	-	-	82.7	A.31
308	SMA	on 304L plate	-	12.0	343	20,000	-	-	-	-	-	-	20	421.5	676.7	549.1	-	-	66.7	A.31
308	SMA	on 304L plate	-	12.0	343	50,000	-	-	-	-	-	-	20	422.4	695.0	558.7	-	-	45.4	A.31
308	SMA	on 304L plate	-	12.0	343	50,000	-	-	-	-	-	-	>150	-	-	-	-	-	93.3	A.31
308	SMA	on 304L plate	-	4.0	-	-	-	-	290	279.0	0.340	-	-	-	-	-	-	-	-	A.31
308	SMA	on 304L plate	-	4.0	343	50,000	-	-	290	308.7	0.445	-	-	-	-	-	-	-	-	A.31
308	SMA	on 304L plate	-	8.0	-	-	-	-	290	253.2	0.279	-	-	-	-	-	-	-	-	A.31
308	SMA	on 304L plate	-	8.0	343	50,000	-	-	290	179.1	0.513	-	-	-	-	-	-	-	-	A.31
308	SMA	on 304L plate	-	12.0	-	-	-	-	290	248.8	0.407	-	-	-	-	-	-	-	-	A.31
308	SMA	on 304L plate	-	12.0	343	50,000	-	-	290	164.4	0.317	-	-	-	-	-	-	-	-	A.31
308	GTA	-	J1-5	5.0-10	-	-	325	10.4	25	287.4	0.550	-	-	-	-	-	-	-	-	A.32
CF-8M	SMA	Weld	LWA01	9.0	450	13,300	-	-	325	750.1	0.363	-	-	-	-	-	-	-	-	A.32
308	Weld	-	-	-	-	-	-	-	400	75.8	0.457	-	-	-	-	-	-	-	-	A.33
308	Weld	-	-	-	-	-	400-427	1.0	400	103.5	0.544	-	-	-	-	-	-	-	-	A.33
308L	SAW	-	-	-	-	-	-	4.8	-	30.7	0.221	-	-	-	-	-	-	-	-	A.34
316LN	SAW	-	-	-	-	-	-	5.0	-	157.2	0.152	-	-	-	-	-	-	-	-	A.34
316L	GTA	-	-	10.0	-	-	-	-	25	153.9	0.300	101.0	25	417.0	619.0	518.0	26.0	54.0	220.0	A.36
316L	GTA	-	-	10.0	300	5,000	-	-	25	-	-	-	25	494.0	620.0	557.0	30.5	65.0	176.3	A.36
316L	GTA	-	-	10.0	300	20,000	-	-	25	-	-	-	25	460.0	601.0	530.5	25.0	57.0	163.8	A.36

Table B1. (Contd.)

Grade	Type	Condition	ID	Ferrite (%)	Aging Temp (°C)	Aging Time (h)	Irradiation Temp. (°C)	Irradiation Dose. (dpa)	Test Temp (°C)	Coeff. C	Exponent n	Jic (kJ/m^2)	Test Temp (°C	Yield Stress (MPa)	Ultimate Stress (MPa)	Flow Stress (MPa)	Elongation (%)	Red. in Area (%)	Charpy Impact Energy (J/cm^2)	Ref.
316L	GTA	-	-	10.0	400	1,000	-	-	25	-	-	-	25	506.0	652.0	579.0	34.5	61.5	145.0	A.36
316L	GTA	-	-	10.0	400	5,000	-	-	25	-	-	-	25	517.0	671.0	594.0	-	-	100.0	A.36
316L	GTA	-	-	10.0	400	10,000	-	-	25	-	-	-	25	424.0	659.0	541.5	-	-	101.3	A.36
316L	GTA	-	-	10.0	-	-	-	-	288	132.3	0.220	98.2	288	372.0	472.0	422.0	-	-	267.5	A.36
316L	GTA	-	-	10.0	-	-	-	-	288	134.6	0.220	100.0	288	372.0	472.0	422.0	-	-	267.5	A.36
316L	GTA	-	-	10.0	-	-	-	-	288	90.9	0.220	66.4[h]	288	372.0	472.0	422.0	-	-	267.5	A.36
316L	GTA	-	-	10.0	400	1,000	-	-	288	-	-	-	288	423.0	509.0	466.0	-	-	125.0	A.36
316L	GTA	-	-	10.0	400	5,000	-	-	288	-	-	-	288	271.0	482.0	376.5	-	-	108.8	A.36
316L	GTA	-	-	10.0	400	10,000	-	-	288	-	-	-	288	415.0	536.0	475.5	-	-	82.5	A.36
316L	GTA	-	-	14.0	-	-	-	-	25	177.5	0.320	93.8	25	516.0	633.0	267.5	30.0	67.0	267.5	A.36
316L	GTA	-	-	14.0	-	-	-	-	25	172.5	0.300	113.7	25	516.0	633.0	267.5	30.0	67.0	267.5	A.36
316L	GTA	-	-	14.0	300	5,000	-	-	25	-	-	-	25	468.0	644.0	186.3	36.5	74.0	186.3	A.36
316L	GTA	-	-	14.0	300	20,000	-	-	25	-	-	-	25	462.0	661.0	217.5	32.0	68.0	217.5	A.36
316L	GTA	-	-	14.0	400	1,000	-	-	25	-	-	-	25	535.0	683.0	225.0	29.5	75.0	225.0	A.36
316L	GTA	-	-	14.0	400	5,000	-	-	25	-	-	-	25	499.0	696.0	192.5	37.0	79.0	192.5	A.36
316L	GTA	-	-	14.0	400	10,000	-	-	25	-	-	-	25	444.0	692.0	262.5	34.5	77.0	262.5	A.36
316L	GTA	-	-	14.0	-	-	-	-	288	161.9	0.240	117.9	288	392.0	496.0	444.0	-	-	408.8	A.36
316L	GTA	-	-	14.0	-	-	-	-	288	159.5	0.270	111.2	288	392.0	496.0	444.0	-	-	408.8	A.36
316L	GTA	-	-	14.0	-	-	-	-	288	145.6	0.320	93.8[h]	288	392.0	496.0	444.0	-	-	408.8	A.36
316L	GTA	-	-	14.0	400	1,000	-	-	288	-	-	-	288	386.0	518.0	452.0	-	-	325.0	A.36
316L	GTA	-	-	14.0	400	5,000	-	-	288	-	-	-	288	378.0	530.0	454.0	-	-	185.0	A.36
316L	GTA	-	-	14.0	400	10,000	-	-	288	-	-	-	288	387.0	533.0	460.0	-	-	233.8	A.36
308	SA	304L plate	L-01	-	-	-	315	0.08	320	144.0	0.590	57.0[i]	-	-	-	-	-	-	-	A.37

[h] Tested at 288°C in high-purity water with 300 ppb DO after soaking for 2000 h at 288°C.

[i] Tested in low-DO water at 320°C.

Table B2. Fracture Toughness J-R Curve data for unaged and aged, unirradiated and irradiated, austenitic stainless steel welds.

Δa (mm)	J (kJ/m^2)	Δa (mm)	J (kJ/m^2)	Δa (mm)	J (kJ/m^2)	Δa (mm)	J (kJ/m^2)	Δa (mm)	J (kJ/m^2)	Δa (mm)	J (kJ/m^2)	Δa (mm)	J (kJ/m^2)	Δa (mm)	J (kJ/m^2)	Δa (mm)	J (kJ/m^2)
Gudas & Anderson		Gudas & Anderson		Gudas & Anderson		Gudas & Anderson		Gudas & Anderson		Gudas & Anderson		Picker et al.		Picker et al.		Picker et al.	
CF8A SMA Weld		CF8A SMA Weld		CF8A SMA Weld		CF8A SMA Weld		CF8A SMA Weld		CF8A SMA Weld		316 MMA Weld		316 MMA Weld		316 MMA Weld	
Unaged		Unaged		Unaged		Unaged		Unaged		Unaged		PWHT 2 h @650°C		PWHT 2 h @650°C		PWHT 2 h @650°C	
Unirradiated		Unirradiated		Unirradiated		Unirradiated		Unirradiated		Unirradiated		As above		1340 h @370°C		6050 h @370°C	
FUC-6	***24°C***	**FUC-7**	***24°C***	**FUC-9**	***149°C***	**FUC-5**	***149°C***	**FUC-12**	***288°C***	**FUC-10**	***288°C***	**-**	***370°C***	**-**	***370°C***	**-**	***370°C***
-0.047	15.71	0.019	12.57	-0.035	3.16	0.005	15.81	0.005	10.9	0.006	38.7	0.002	43.36	0.232	106.16	0.249	119.71
0.019	40.84	0.058	40.84	-0.074	41.11	-0.035	37.95	0.062	30.4	0.052	61.0	0.032	61.89	0.014	41.96	0.117	93.24
0.058	65.97	0.164	72.25	0.268	101.20	0.044	98.04	0.052	58.2	0.040	77.6	0.035	46.85	0.092	67.84	0.133	107.98
0.045	100.52	0.19	109.95	0.662	129.67	0.189	129.67	0.144	113.7	0.075	102.7	0.071	49.30	0.291	145.77	0.321	164.97
0.124	128.79	0.348	163.35	1.07	158.13	0.4	167.62	0.235	147.1	0.144	130.4	0.089	64.69	0.307	129.62	0.437	147.25
0.203	160.21	0.414	194.76	1.11	167.62	0.584	192.92	0.453	191.5	0.235	149.9	0.146	58.39	0.567	210.37	0.674	225.86
0.23	207.33	0.599	241.88	1.544	173.94	0.728	208.73	0.761	227.5	0.350	177.6	0.174	81.12				
0.44	245.02	0.822	273.29	1.478	183.43	0.847	224.54	0.898	246.9	0.362	205.4	0.192	104.20	**C**	288.65	**C**	246.31
0.585	282.72	1.007	304.71	2.043	192.92	1.044	237.19	1.127	269.1	0.567	227.6	0.211	96.15	**n**	0.622	**n**	0.445
0.664	320.41	1.165	336.12	2.359	199.24	1.281	249.84	1.275	288.5	0.659	247.0	0.218	91.26	**FS**		**FS**	
1.007	361.25	1.573	364.39	2.832	205.57	1.531	265.66	1.503	310.6	0.750	274.8	0.220	97.55	**Jic**		**Jic**	
1.165	402.08	1.837	386.38	3.345	240.35	1.675	275.14	1.709	318.9	0.910	302.5	0.281	130.42				
1.494	439.78	2.179	408.37	3.95	265.66	1.754	284.63	1.960	335.5	1.116	324.7	0.509	144.06	13000 h @370°C		0.4 dpa @370°C	
1.903	468.05	2.377	442.92	4.938	290.96	2.004	300.44	2.507	365.9	1.322	341.3	0.559	218.53	**-**	***370°C***	**-**	***370°C***
2.258	502.61	2.692	483.76	5.857	316.26	2.621	338.39	3.123	379.6	1.550	355.1	0.887	323.08	0.099	85.23	0.056	84.30
2.535	543.44	3.353	556.01	6.66	325.74	3.241	373.18	3.705	398.8	1.641	366.2	1.017	319.93	0.178	119.13	0.089	85.02
2.865	596.84	3.879	647.11	7.475	335.23	3.899	404.81	4.321	412.5	1.801	380.0			0.211	90.06	0.099	66.47
3.365	672.24	4.63	694.23			4.727	430.11	4.811	429.0	2.234	399.4	**C**	302.61	0.263	105.82	0.185	90.98
3.919	753.91	5.38	735.06			5.265	461.73	5.085	448.4	2.508	410.4	**n**	0.718	0.294	88.04	0.227	102.72
4.735	813.59	6.106	772.76			5.7	502.85			2.851	435.3	**FS**				0.391	115.97
5.446	860.71	6.843	797.89			6.251	521.82			3.205	476.9	**Jic**					
6.157	895.27	7.475	823.02							3.729	501.7			**C**	108.10	**C**	133.67
7.000	907.83									4.140	521.0			**n**	0.067	**n**	0.205
										4.517	537.6			**FS**		**FS**	
C	367.03	**C**	297.61	**C**	154.81	**C**	236.05	**C**	252.39	4.973	545.7			**Jic**		**Jic**	
n	0.482	**n**	0.518	**n**	0.373	**n**	0.395	**n**	0.370	5.520	548.3						
FS*	489.0	**FS**	489.0	**FS**	489.0	**FS**	489.0	**FS**	362.6								
Jic	153.5	**Jic**	153.5	**Jic**	91.9	**Jic**	141.2	**Jic**	164.3	**C**	292.51						
										n	0.406						
										FS	362.6						
										Jic	186.1						

* Used flow stress data for 308L MMA weld from Ould et al, 1986. Room temperature values also used for 149°C data.

Table B2. (Contd.)

Δa (mm)	J (kJ/m^2)	Δa (mm)	J (kJ/m^2)	Δa (mm)	J (kJ/m^2)	Δa (mm)	J (kJ/m^2)	Δa (mm)	J (kJ/m^2)	Δa (mm)	J (kJ/m^2)	Δa (mm)	J (kJ/m^2)	Δa (mm)	J (kJ/m^2)	Δa (mm)	J (kJ/m^2)
Picker et al.		Picker et al.		Picker et al.		Picker et al.		Picker et al.		Garwood		Garwood		Slama et al.		Vassilaros et al. et al.	
316 MMA Weld		316 MMA Weld		316 MMA Weld		316 MMA Weld		316 MMA Weld		316 SMA Weld		316 MMA Weld		308L Weld		304 SMA Weld	
PWHT 2 h @650°C		As welded		As welded		PWHT 2 h @1050°C		PWHT 2 h @1050°C		As welded		PWHT 2 h @650°C		-		As welded	
2.0 dpa @370°C		As above		1340 h @370°C		As above		1340 h @370°C		As above		1340 h @370°C		Weld B FN=6.0		As above	
-	***370°C***	**-**	***370°C***	**-**	***370°C***	**-**	**370C**	**-**	***370°C***	**-**	***370°C***	**-**	***540°C***	**-**	***20°C***	**-**	***24°C***
0.053	74.01	0.015	43.92	0.049	50.68	0.013	84.17	0.112	131.12	0.480	190.59	0.376	84.08	0.320	207.8	0.107	38.2
0.178	75.48	0.006	55.74	0.055	64.19	0.097	111.69	0.259	211.51	0.497	230.01	0.397	109.83	0.650	252.6	0.207	135.7
0.262	91.64	0.059	67.57	0.133	76.35	0.176	131.12	0.587	328.06	0.826	224.59	0.796	168.16	0.960	348.7	0.314	224.7
0.305	97.83	0.111	53.38	0.162	89.19	0.351	271.94	0.854	396.04	0.729	304.5	1.438	265.76	1.320	500.8	0.513	402.8
0.332	83.81	0.412	113.51	0.328	143.58	1.118	550.90	0.896	404.14	2.506	620.1	2.101	401.42	1.400	496.3	0.620	466.4
0.320	60.86			0.425	168.58			1.267	542.81	3.521	729.75	3.649	734.38	2.510	639.3	0.812	542.8
				0.556	238.51			1.411	587.59							0.934	585.2
C	102.18															1.057	657.3
n	0.067	**C**	126.50	**C**	298.96	**C**	512.92	**C**	455.30	**C**	324.28	**C**	213.93	**C**	380.70	1.241	729.3
FS		**n**	0.263	**n**	0.625	**n**	0.995	**n**	0.993	**n**	0.651	**n**	0.883	**n**	0.600	1.424	780.2
Jic		**FS**		**FS**		**FS**		**FS**		**FS**	399.0	**FS**	428.5	**FS**	572.5	1.562	839.6
		Jic		**Jic**		**Jic**		**Jic**		**Jic**	145.17	**Jic**	59.49	**Jic**	176.2	1.716	877.8
																1.915	937.1
4.0 dpa @370°C		0.4 dpa @370°C				0.4 dpa @370°C						As above		Weld D FN=7.5		2.167	1026.2
-	***370°C***	**-**	***370°C***			**-**	***370°C***					**-**	***370°C***	**-**	***20°C***	2.428	1,085.5
0.044	22.94	0.074	69.93			0.156	150.54					0.842	118.93	0.337	183.3	2.756	1,149.1
0.382	31.28	0.164	96.62			0.222	195.32					1.417	206.42	0.856	263.8	3.101	1,212.7
0.730	54.33	0.169	102.70			0.267	223.92					2.525	323.20	0.910	335.3	3.310	1,272.1
0.984	32.53	0.165	107.77			0.363	242.27					3.057	399.49	1.141	413.5	3.653	1,352.7
0.984	39.03	0.183	71.96			0.549	306.47					4.655	487.31			3.967	1,407.8
		0.457	132.09			0.764	421.94					5.155	931.87	**C**	343.60	4.211	1,471.4
														n	0.614	4.465	1,530.8
C	40.59	**C**	168.80			**C**	469.48					**C**	138.93	**FS**	572.5	4.686	1,602.9
n	0.180	**n**	0.333			**n**	0.986					**n**	0.982	**Jic**	152.6	5.070	1,619.8
FS		**FS**				**FS**						**FS**	399.0			5.613	1,628.3
Jic		**Jic**				**Jic**						**Jic**	31.36			6.081	1,632.5
																C	627.33
																n	0.585
																FS	538.5
																Jic	345.3

Table B2. (Contd.)

Δa (mm)	J (kJ/m^2)	Δa (mm)	J (kJ/m^2)	Δa (mm)	J (kJ/m^2)	Δa (mm)	J (kJ/m^2)	Δa (mm)	J (kJ/m^2)	Δa (mm)	J (kJ/m^2)	Δa (mm)	J (kJ/m^2)	Δa (mm)	J (kJ/m^2)	Δa (mm)	J_m (kJ/m^2)
Picker et al.		Picker et al.		Picker et al.		Picker et al.		Picker et al.		Slama et al.		Garwood		Garwood		Hiser et al.	
316 MMA Weld		316 MMA Weld		316 MMA Weld		316 MMA Weld		316 MMA Weld		308L Weld		316 SMA Weld		316 MMA Weld		A508 Cl3 SA Weld	
PWHT 2 h @650°C		As welded		As welded		PWHT 2 h @1050°C		PWHT 2 h @1050°C		-		As welded		PWHT 2 h @650°C		Linde 80 weld metal	
2.0 dpa @370°C		As above		1340 h @370°C		As above		1340 h @370°C		Weld B FN=6.0		As above		1340 h @370°C		62W-21 4T-CT	
-	***370°C***	**-**	***370°C***	**-**	***370°C***	**-**	***370°C***	**-**	***370°C***	**-**	***20°C***	**-**	***370°C***	**-**	***540°C***	**-**	***200°C***
0.053	74.01	0.015	43.92	0.049	50.68	0.013	84.17	0.112	131.12	0.320	207.8	0.480	190.59	0.376	84.08	0.062	64.2
0.178	75.48	0.006	55.74	0.055	64.19	0.097	111.69	0.259	211.51	0.650	252.6	0.497	230.01	0.397	109.83	0.090	82.9
0.262	91.64	0.059	67.57	0.133	76.35	0.176	131.12	0.587	328.06	0.960	348.7	0.826	224.59	0.796	168.16	0.144	104.5
0.305	97.83	0.111	53.38	0.162	89.19	0.351	271.94	0.854	396.04	1.320	500.8	0.729	304.5	1.438	265.76	0.226	128.5
0.332	83.81	0.412	113.51	0.328	143.58	1.118	550.90	0.896	404.14	1.400	496.3	2.506	620.1	2.101	401.42	0.277	150.7
0.320	60.86			0.425	168.58			1.267	542.81	2.510	639.3	3.521	729.75	3.649	734.38	0.397	171.7
				0.556	238.51			1.411	587.59							0.523	195.7
C	102.18															0.613	216.2
n	0.067	**C**	126.50	**C**	298.96	**C**	512.92	**C**	455.30	**C**	380.70	**C**	324.28	**C**	213.93	0.757	240.7
FS	-	**n**	0.263	**n**	0.625	**n**	0.995	**n**	0.993	**n**	0.600	**n**	0.651	**n**	0.883	0.869	266.4
Jic	-	**FS**	-	**FS**	-	**FS**	-	**FS**	-	**FS**	572.5	**FS**	399.0	**FS**	428.5	1.034	293.3
		Jic	-	**Jic**	-	**Jic**	-	**Jic**	-	**Jic**	176.2	**Jic**	145.17	**Jic**	59.49	1.208	320.8
																1.625	372.3
4.0 dpa @370°C		0.4 dpa @370°C				0.4 dpa @370°C				Weld D FN=7.5				As above		1.895	402.7
-	***370°C***	**-**	***370°C***			**-**	***370°C***			**-**	***20°C***			**-**	***370°C***	2.461	458.3
0.044	22.94	0.074	69.93			0.156	150.54			0.337	183.3			0.842	118.93	2.763	475.2
0.382	31.28	0.164	96.62			0.222	195.32			0.856	263.8			1.417	206.42	3.516	537.9
0.730	54.33	0.169	102.70			0.267	223.92			0.910	335.3			2.525	323.20	3.995	568.3
0.984	32.53	0.165	107.77			0.363	242.27			1.141	413.5			3.057	399.49	4.909	631.0
0.984	39.03	0.183	71.96			0.549	306.47							4.655	487.31	5.388	663.4
		0.457	132.09			0.764	421.94			**C**	343.60			5.155	931.87	5.959	703.3
										n	0.614					6.575	735.6
C	40.59	**C**	168.80			**C**	469.48			**FS**	572.5			**C**	138.93	7.100	769.8
n	0.180	**n**	0.333			**n**	0.986			**Jic**	152.6			**n**	0.982	8.927	851.5
FS	-	**FS**	-			**FS**	-							**FS**	399.0	10.479	925.7
Jic	-	**Jic**	-			**Jic**	-							**Jic**	31.36	12.626	1,013.1
																15.160	1,108.1
																C	279.2
																n	0.512
																FS	465.7
																Jic	144.9

Table B2. *(Contd.)*

Δa (mm)	**J_m (kJ/m^2)**	**Δa (mm)**	**J_m (kJ/m^2)**	**Δa (mm)**	**J_m (kJ/m^2)**	**Δa (mm)**	**J_m (kJ/m^2)**	**Δa (mm)**	**J_m (kJ/m^2)**	**Δa (mm)**	**J_m (kJ/m^2)**	**Δa (mm)**	**J_m (kJ/m^2)**	**Δa (mm)**	**J_m (kJ/m^2)**	**Δa (mm)**	**J_m (kJ/m^2)**
Hiser et al.		Hiser et al.		Hiser et al.		Hiser et al.		Hiser et al.		Hiser et al.		Hiser et al.		Hiser et al.		Hiser et al.	
A508 Cl3 SA Weld		A508 Cl3 SA Weld		A508 Cl3 SA Weld		A508 Cl3 SA Weld		A508 Cl3 SA Weld		A508 Cl3 SA Weld		A508 Cl3 SA Weld		A508 Cl3 SA Weld		A508 Cl3 SA Weld	
Linde 80 weld metal		Linde 80 weld metal		Linde 80 weld metal		Linde 80 weld metal		Linde 80 weld metal		Linde 80 weld metal		Linde 80 weld metal		Linde 80 weld metal		Linde 80 weld metal	
62W-32 1.6T-CT		62W-30 1.6T-CT		62W-47 0.8T-CT		62W-160 0.5T-CT		62W-20 0.5-CT		62W-20 4.0T-CT[a]		62W-34 1.6T-CT[a]		62W-42 0.8T-CT[a]		62W-118 0.5T-CT[a]	
-	***200°C***	**-**	***200°C***	**-**	***200°C***	**-**	***200°C***	**-**	***200°C***	**-**	***200°C***	**-**	***200°C***	**-**	***200°C***	**-**	***200°C***
-0.014	14.3	0.008	4.1	0.047	7.7	0.003	1.7	0.003	1.5	0.098	61.3	0.006	25.5	0.002	4.1	0.003	2.3
0.079	72.6	-0.032	17.4	0.028	30.6	0.018	24.2	0.008	12.0	0.133	72.9	0.034	39.2	0.055	4.1	0.020	9.3
0.140	87.5	0.034	51.8	0.038	52.5	0.041	35.4	0.048	18.9	0.191	83.6	0.076	55.9	0.009	11.2	0.027	20.3
0.187	103.3	0.099	65.7	0.038	73.9	0.052	48.3	0.057	40.8	0.202	96.6	0.125	74.7	0.017	20.9	0.065	33.8
0.211	115.6	0.132	82.1	0.130	97.9	0.087	62.2	0.125	51.0	0.294	108.2	0.284	95.4	0.019	28.5	0.131	51.0
0.283	131.5	0.134	98.5	0.218	124.0	0.101	76.4	0.181	62.8	0.332	122.5	0.326	106.9	0.047	40.2	0.232	66.5
0.339	146.9	0.184	116.5	0.248	135.7	0.125	91.1	0.167	75.1	0.392	134.6	0.390	118.2	0.033	53.4	0.406	84.0
0.477	181.2	0.265	135.0	0.329	148.0	0.145	106.6	0.260	85.9	0.479	153.9	0.595	135.5	0.085	66.2	0.653	98.0
0.694	217.6	0.317	154.5	0.318	152.6	0.261	121.7	0.323	98.8	0.618	174.0	0.685	148.6	0.107	83.5	0.817	108.0
0.817	242.2	0.388	174.5	0.387	162.3	0.313	136.9	0.438	111.2	0.746	191.9	0.930	173.2	0.139	99.2	1.052	118.0
1.011	265.2	0.496	195.1	0.392	175.5	0.425	152.4	0.566	122.3	0.888	208.5	1.248	199.0	0.202	114.0	1.218	124.5
1.361	314.5	0.736	235.7	0.533	186.8	0.525	164.1	0.631	134.3	1.048	224.1	1.506	211.5	0.271	130.8	1.449	133.0
1.580	338.6	0.915	258.8	0.621	201.2	0.620	180.9	0.765	146.7	1.218	242.5	1.732	224.9	0.382	148.1	1.651	139.3
1.787	362.7	1.102	284.0	0.828	231.3	0.698	196.5	0.860	157.5	1.443	259.5	2.037	237.7	0.476	162.3	1.809	146.5
2.079	389.9	1.609	337.1	1.025	253.4	0.900	212.1	0.977	169.3	1.595	274.3	2.257	250.5	0.565	180.7	2.137	156.5
2.407	420.7	1.953	362.3	1.223	269.3	1.117	225.5	1.152	179.8	1.854	296.2	2.625	260.9	0.718	199.5	2.469	166.3
2.876	459.2	2.291	390.2	1.418	294.4	1.206	238.0	1.285	191.0	2.102	314.2	3.151	283.1	0.868	218.8	2.751	176.2
3.316	495.1	2.762	425.5	1.591	307.7	1.408	254.9	1.444	202.1	2.407	333.4	3.696	299.2	1.049	238.2	3.112	189.7
3.928	539.3	3.910	484.3	1.741	320.1	1.881	300.3	1.642	213.6	2.661	319.3	4.366	315.8	1.195	255.5	3.622	202.6
4.510	585.1	4.634	516.3	1.870	331.3	2.082	315.4	1.775	223.2	3.040	338.0	5.188	333.8	1.374	273.3	4.071	218.4
5.170	622.7	5.311	548.3	2.117	348.8	2.330	334.9	2.155	244.1	3.533	364.6	5.953	349.9	1.581	295.7	4.573	235.4
5.971	681.6	6.239	586.7	2.391	367.3	2.565	323.3	2.410	259.8	3.988	383.2	6.824	363.5	1.886	317.0	5.041	250.2
7.024	738.9	7.246	622.5	2.564	383.8	2.892	341.8	2.654	274.1	4.595	408.5	7.627	3759	2.189	342.5	5.603	271.8
8.155	804.3	8.411	667.4	2.852	406.8	3.197	359.1	2.904	293.2	5.088	428.5	8.574	390.1	2.557	376.5	6.221	294.7
9.522	881.2	9.655	704.5	3.190	429.1	3.642	384.1	3.224	311.3	5.733	445.8	9.387	401.9	3.045	415.1	6.746	316.3
11.015	964.7	11.040	754.4	3.555	452.8	4.119	409.7	3.714	340.4	6.567	467.0	10.343	414.3	3.639	452.4		
12.901	1,058.0	12.755	807.0	3.916	479.1	4.646	434.7	4.115	364.0	7.173	484.3	11.098	424.8	4.275	492.4	**C**	116.7
			871.0	4.353	504.8	5.105	441.1	4.528	385.9	8.121	501.6	11.997	438.5	5.024	532.5	**n**	0.455
C	263.1	**C**	942.7	4.787	534.5	5.591	471.2	4.962	412.3	9.750	534.9	12.820	449.0	5.845	576.9	**FS**	596.6
n	0.538	**n**	1,020.9	5.121	549.4	6.155	504.5	5.662	458.3	11.986	576.2					**Jic**	59.2
FS	465.7	**FS**	1,097.7									**C**	171.6	**C**	237.2		
Jic	130.0	**Jic**		**C**	248.3	**C**	218.9	**C**	166.6	**C**	210.4	**n**	0.400	**n**	0.501		
			251.1	**n**	0.494	**n**	0.456	**n**	0.555	**n**	0.412	**FS**	596.6	**FS**	596.6		
			0.465	**FS**	465.7	**FS**	465.7	**FS**	465.7	**FS**	596.6	**Jic**	97.1	**Jic**	118.4		
			465.7	**Jic**	130.0	**Jic**	119.2	**Jic**	73.5	**Jic**	118.8						
			137.5														

[a] Irradiated at 260-293°C to 1.6 to 2.1 x 10^{19} n/cm^2 (E>1 MeV) in the Bulk Shielded Reactor, ORNL..

Table B2. (Contd.)

Δa (mm)	**J (kJ/m^2)**	**Δa (mm)**	**J (kJ/m^2)**	**Δa (mm)**	**J (kJ/m^2)**	**Δa (mm)**	**J (kJ/m^2)**	**Δa (mm)**	**J (kJ/m^2)**	**Δa (mm)**	**J (kJ/m^2)**	**Δa (mm)**	**J (kJ/m^2)**	**Δa (mm)**	**J (kJ/m^2)**	**Δa (mm)**	**J (kJ/m^2)**
Vassilaros et al. et		Vassilaros et al. et		Vassilaros et al. et		Vassilaros et al. et		Nakagaki et al.		Nakagaki et al.		Nakagaki et al.		Nakagaki et al.		Landes & McCabe	
304 SMA Weld		304 SMA Weld		304 SMA Weld		304 SMA Weld		308L TIG Weld		308L TIG Weld		308L TIG Weld		308L TIG Weld		308 SMA Weld	
As welded		As welded		As welded		As welded		As welded		As welded		As welded		As welded		As welded	
As above		As above		As above		As above		3.0T A46-1		1.5T A46-2		0.5T A46-WM1		0.5T A46-WM2		As above	
-	***200°C***	**-**	***149°C***	**-**	***288°C***	**-**	***288°C***	**-**	***288°C***	**-**	***288°C***	**-**	***288°C***	**-**	***288°C***	**-**	***24°C***
0.062	64.2	0.100	17.0	0.153	67.8	0.115	42.4	0.00	731.2	-0.05	1,095.1	0.00	581.0	0.06	648.5	0.047	116.1
0.090	82.9	0.368	97.5	0.360	195.1	0.230	114.5	-0.05	1,028.4	0.00	1,267.4	0.41	718.2	0.00	817.8	0.071	186.5
0.144	104.5	0.513	352.0	0.437	262.9	0.521	195.1	2.57	1,321.8	0.86	1,423.7	0.71	862.2	0.46	935.7	0.166	252.9
0.226	128.5	0.681	474.9	0.582	330.7	0.797	237.5	7.36	1,647.4	1.76	1,529.4	1.16	1,024.6	0.97	1,813.6	0.356	294.3
0.277	150.7	0.896	559.7	0.827	385.9	0.957	271.4	9.57	1,858.1	2.77	1,612.1	1.67	1,165.5	1.41	1,108.1	0.592	348.2
0.397	171.7	1.555	640.3	1.486	458.0	1.363	292.6	11.44	2,040.4	3.88	1,679.6	2.52	1,324.9	1.76	1,184.7	0.782	410.4
0.523	195.7	1.815	716.6	1.953	504.6	1.455	339.2	13.90	2,117.0	4.89	1,740.1	3.43	1,455.9	2.52	1,293.5	0.900	480.8
0.613	216.2	1.876	759.0	2.198	538.5	1.539	347.7	16.38	2,164.5	5.89	1,781.4	4.29	1,561.6	3.03	1,324.9	1.445	551.3
0.757	240.7	1.945	814.1	2.497	572.4	1.677	364.7	18.73	2,248.0	6.96	1,819.7	5.08	1,644.3	3.38	1,370.1	1.801	609.3
0.869	266.4	2.137	852.3	2.972	644.5	1.807	407.1	21.05	2,327.6	8.16	1,845.8	5.94	1,734.0	3.83	1,417.6	2.062	708.8
1.034	293.3	2.213	890.5	3.216	678.5	1.976	453.7	22.91	2,375.1	9.37	1,851.9	6.80	1,819.7	4.69	1,462.0	2.441	804.2
1.208	320.8	2.397	971.0	3.721	716.6	2.305	491.9	25.39	2,385.1	11.99	1,861.1	8.06	1,906.3	4.99	1,497.2	2.962	891.2
1.625	372.3	2.565	1,017.7	3.967	750.5	2.664	542.8	30.41	2608.8	14.50	1,842.0	8.36	2,177.5	5.85	1,494.2	3.460	974.1
2.461	458.3	2.903	1102.5	4.465	763.3	2.911	597.9			16.87	1,829.7	8.91	1,999.0	6.20	1,526.4	4.123	974.1
2.461	458.3	3.277	1,149.1	4.732	780.2	3.292	627.6	**C**	1001.0	19.44	1,858.1	8.47	2,037.3	6.61	1,557.8		
2.763	475.2	3.538	1,212.7	5.055	805.7	3.553	678.5	**n**	0.277					7.26	1,573.8	**C**	505.82
3.516	537.9	3.891	1,255.1	5.306	852.3	3.884	725.1	**FS**	372.5	**C**	1493.2	**C**	960.30	8.01	1,576.9	**n**	0.449
3.995	568.3	4.188	1,327.2	6.586	835.4	4.082	750.5	**Jic**	953.9	**n**	0.085	**n**	0.345			**FS**	-
4.909	631.0	4.595	1,369.6			4.542	776.0			**FS**	372.5	**FS**	372.5	**C**	1232.4	**Jic**	
5.388	663.4	5.583	1,348.4	**C**	379.79	4.879	801.4			**Jic**	1518.6	**Jic**	887.5	**n**	0.112		
5.959	703.3			**n**	0.469	5.339	818.4							**FS**	372.5		
6.575	735.6	**C**	553.97	**FS**	395.0	6.373	822.6							**Jic**	1236.4		
7.100	769.8	**n**	0.587	**Jic**	230.9												
8.927	851.5	**FS**	416.0			**C**	280.98										
10.479	925.7					**n**	0.648										
12.626	1,013.1					**FS**	395.0										
15.160	1,108.1					**Jic**	122.43										
C	279.2																
n	0.512																
FS	465.7																
Jic	144.9																

Table B2. (Contd.)

Δa (mm)	J (kJ/m^2)	Δa (mm)	J (kJ/m^2)	Δa (mm)	J (kJ/m^2)	Δa (mm)	J (kJ/m^2)	Δa (mm)	J (kJ/m^2)	Δa (mm)	J (kJ/m^2)	Δa (mm)	J (kJ/m^2)	Δa (mm)	J (kJ/m^2)	Δa (mm)	J (kJ/m^2)
Landes & McCabe		Landes & McCabe		Landes & McCabe		Landes & McCabe		Landes & McCabe		Landes & McCabe		Landes & McCabe		Wilkowski et al.		Wilkowski et al.	
308 SMA Weld		308 SA Weld		308 SA Weld		308 TIG Weld		308 TIG Weld		316 SA Weld		316 SA Weld		308L GTA Weld		308L GTA Weld	
As welded		As welded		As welded		As welded		As welded		As welded		As welded		As welded		As welded	
As above		As above		As above		As above		As above		As above		As above		1T-CT		1T-CT	
-	***288°C***	**-**	***24°C***	**-**	***288°C***	**-**	***24°C***	**-**	**288°C**	**-**	***24°C***	**-**	***288°C***	**-**	***24°C***	**-**	***149°C***
0.047	58.0	0.112	35.1	0.112	23.4	0.112	156.3	0.089	171.9	0.095	95.8	0.071	37.5	5.870	1,626.9	5.412	1,355.9
0.095	149.2	0.201	78.1	0.268	50.7	0.223	281.3	0.112	359.4	0.190	120.8	0.142	83.3	5.398	1,625.1	4.409	1,358.3
0.213	174.1	0.335	132.7	0.491	89.8	0.357	453.1	0.179	515.6	0.379	158.3	0.616	154.2	4.850	1,623.	3.997	1,320.9
0.426	199.0	0.580	202.9	0.670	128.8	0.714	578.1	0.558	640.6	0.521	191.7	1.019	187.5	4.454	1,609.	3.694	1,262.4
0.664	219.7	0.871	273.2	1.161	160.0	0.714	718.8	0.759	734.4	0.664	220.8	1.540	225.0	4.249	1,530.	3.358	1,204.1
0.829	252.9	1.161	331.7	1.540	187.3	1.004	890.6	0.960	812.5	0.806	254.2	1.943	258.3	3.990	1,474.7	3.099	1,148.5
0.948	294.3	1.451	374.6	2.098	222.4	1.161	1,078.1	1.205	906.3	1.090	283.3	2.346	283.3	3.752	1,404.	2.709	1,096.2
1.588	339.9	1.786	425.4	2.344	249.8	1.384	1,234.4	1.339	953.1	1.327	325.0	2.796	300.0	3.438	1,348.	2.417	1,020.0
1.967	385.5	2.143	472.2	2.679	273.2	1.741	1,390.6	1.451	1062.5	1.588	370.8	3.152	325.0	3.108	1,269.	2.222	967.2
2.393	431.1	2.433	534.6	2.946	304.4	1.875	1,546.9	1.830	1156.3	1.943	412.5	3.460	341.7	2.897	1,211.	2.088	899.5
3.223	476.7	2.812	581.5	3.259	343.4	1.920	1,703.1	2.210	1234.4	2.322	462.5	4.265	345.8	2.578	1,146.	2.001	858.3
3.626	522.3	3.214	643.9	3.661	382.4	2.121	1,875.0	2.433	1328.1	2.654	504.2			2.270	1,088.	1.828	814.3
3.697	526.4	3.549	698.5	4.129	429.3	2.411	2,046.9	2.589	1421.9	3.009	545.8	**C**	181.43	2.010	1,015.	1.758	779.0
		3.839	753.2	4.777	460.5	3.013	2,187.5	2.924	1500.0	3.365	579.2	**n**	0.510	1.773	947.6	1.710	740.7
		4.174	831.2	5.536	464.4	3.192	2,375.0	3.237	1593.8	3.531	579.2	**FS**	-	1.594	888.9	1.429	637.8
C	292.58	4.531	835.1			2.991	2,375.0	3.683	1671.9			**Jic**		1.416	833.1	0.618	491.9
n	0.430							3.951	1765.6	**C**	289.70			1.297	777.2	0.376	317.9
FS	-	**C**	268.69	**C**	138.92	**C**	934.16	4.799	1781.3	**n**	0.530			1.124	727.3	0.156	120.3
Jic		**n**	0.792	**n**	0.752	**n**	0.823			**FS**	-			0.919	659.8	0.308	108.1
		FS	-	**FS**	-	**FS**	-	**C**	863.95	**Jic**				0.811	600.9		
		Jic		**Jic**		**Jic**		**n**	0.495					0.704	544.9	**C**	583.60
								FS	-					0.558	468.4	**n**	0.570
								Jic						0.440	394.7	**FS**	416.1
														0.289	300.4	**Jic**	351.8
														0.312	226.4		
														0.209	226.6		
														0.166	135.0		
														C	662.1		
														n	0.572		
														FS	538.2		
														Jic	378.4		

Table B2. (Contd.)

Δa (mm)	J (kJ/m^2)	Δa (mm)	J (kJ/m^2)	Δa (mm)	J (kJ/m^2)	Δa (mm)	J (kJ/m^2)	Δa (mm)	J (kJ/m^2)	Δa (mm)	J (kJ/m^2)	Δa (mm)	J (kJ/m^2)	Δa (mm)	J (kJ/m^2)	Δa (mm)	J (kJ/m^2)
Wilkowski et al.		Wilkowski et al.		Wilkowski et al.		Wilkowski et al.		Wilkowski et al.		Michel & Gray		Michel & Gray		Michel & Gray		Michel & Gray	
308L GTA Weld		308L GTA Weld		308L GTA Weld		308L GTA Weld		308L GTA Weld		308 ?? Weld		308 ?? Weld		308 ?? Weld		308 ?? Weld	
As welded		As welded		As welded		As welded		Fusion Line		As welded W10-10		As welded W10-12		As welded W10-3		As welded W10-9	
1T-CT		1T-CT		2T-CT		2T-CT		1T-CT		Unirradiated		Unirradiated		11.1 dpa @		11.1 dpa @ 427°C	
-	***288°C***	**-**	***288°C***	**-**	***288°C***	**-**	***288°C***	**-**	***288°C***	**-**	***427°C***	**-**	***427°C***	**-**	***427°C***	**-**	***427°C***
6.454	829.7	6.254	815.4	5.632	2,157.6	6.372	1,677.0	4.596	1,366.4	0.044	19.8	0.011	7.7	0.061	4.6	0.016	1.1
5.174	832.9	5.218	818.0	5.280	2,105.7	4.877	1,680.1	4.398	1,335.4	0.036	32.7	0.119	79.1	0.016	14.0	0.024	15.5
4.974	803.8	4.774	795.4	5.144	2,047.3	4.582	1,618.9	4.257	1,279.6	0.073	47.0	0.088	79.1	0.104	25.1	0.049	29.2
4.644	777.9	4.427	766.6	4.753	1,980.1	4.350	1,551.3	3.902	1,248.8	0.090	62.1	0.146	112.3	0.566	32.7	0.174	38.6
4.346	752.0	3.961	747.0	4.384	1,860.3	4.049	1,477.8	3.648	1,196.2	0.054	79.1	0.203	148.5	0.883	33.2	0.357	46.2
3.879	741.3	3.766	720.9	4.022	1,774.5	3.907	1,410.1	3.564	1,137.2	0.128	93.0	0.373	181.7	1.164	41.4	0.678	50.0
3.592	712.4	3.430	680.3	3.460	1,661.3	3.397	1,346.2	3.344	1,090.8	0.139	110.4	0.394	201.0	1.700	49.6	1.054	56.1
3.115	675.1	3.170	633.6	3.234	1,569.1	3.284	1,259.9	2.858	1,078.7	0.123	128.5	0.468	216.9			1.378	58.9
2.867	631.4	2.807	587.1	3.126	1,473.5	2.853	1,183.5	2.655	1,032.2	0.172	144.4	0.563	211.6	**C**	53.20	1.964	60.4
2.417	588.1	2.558	549.3	2.717	1,378.5	2.365	1,088.7	2.407	964.0	0.195	162.5	0.580	267.4	**n**	0.250	2.308	63.7
2.136	538.5	2.223	499.8	2.627	1,304.5	2.320	993.0	1.973	917.7	0.212	182.9	0.695	280.3	**FS**	485.0		
1.876	500.7	1.903	453.3	2.139	1,228.2	2.212	912.9	1.770	849.5	0.238	204.8	0.733	312.7	**Jic**	36.4	**C**	39.20
1.404	469.3	1.752	412.2	1.918	1,151.4	1.844	848.7	1.617	793.7	0.292	227.0	0.889	343.7			**n**	0.354
0.749	376.2	1.611	374.1	1.918	1,083.4	1.702	777.9	1.290	741.2	0.266	244.0	1.024	356.9			**FS**	485.0
0.522	329.4	1.498	350.7	1.895	1,015.5	1.481	688.7	1.183	685.3	0.297	274.8	1.116	385.2	11.1	**Jic**	22.6	
0.349	267.7	1.341	330.4	1.697	944.8	1.191	621.3	0.963	635.8	0.379	274.2	1.313	410.1	**-**	***427°C***		
0.285	193.9	1.276	301.0	1.464	756.8	1.197	541.0	0.822	586.2	0.468	307.4	1.395	437.3	0.035	5.2		
0.091	76.0	0.897	278.2	1.396	701.3	0.936	458.1	0.613	546.0	0.558	338.8	1.525	0.035	0.035	9.3		
		0.724	240.2	1.180	646.1	0.624	375.2	0.512	443.5	0.545	373.9	1.678	0.068	0.068	19.5		
C	398.80	0.486	202.3	0.908	581.7	0.267	230.7	0.388	353.6	0.621	352.7	1.793	0.462	0.462	28.3		
n	0.436	0.177	123.2	0.789	495.4	0.125	122.8	0.338	300.8	0.721	398.0	1.995	2.009	2.009	35.7		
FS	395.1			0.471	384.8			0.180	217.1	0.973	419.2	2.199	540.0				
Jic	256.0	**C**	303.80	0.250	283.3	**C**	538.30	0.033	164.4	0.992	451.6			**C**	30.60		
		n	0.596	0.114	190.8	**n**	0.702	0.163	133.2	1.277	474.7	**C**	349.40	**n**	0.298		
		FS	395.1	0.091	51.8	**FS**	395.1			1.612	497.7	**n**	0.594	**FS**	485.0		
		Jic	146.0			**Jic**	267.5	**C**	610.90	1.706	524.9	**FS**	1113.0	**Jic**	19.2		
				C	674.60			**n**	0.516	2.217	545.2	**Jic**	147.1				
				n	0.670			**FS**	395.1	2.252	563.4						
				FS	395.1			**Jic**	408.3								
				Jic	394.9					**C**	410.80						
										n	0.470						
										FS	1113.0						
										Jic	213.3						

Table B2. (Contd.)

Δa (mm)	J (kJ/m²)	Δa (mm)	J (kJ/m²)	Δa (mm)	J (kJ/m²)	Δa (mm)	J (kJ/m²)	Δa (mm)	J (kJ/m²)	Δa (mm)	J (kJ/m²)	Δa (mm)	J (kJ/m²)	Δa (mm)	J (kJ/m²)	Δa (mm)	J (kJ/m²)
Mills 1987		Mills 1987		Mill 1988		Mills 1988		Mills 1988		Mills 1988		Mills 1988		Faure et al.		Faure et al.	
308 GTA Weld		308 SMA Weld		16-8-2 GTA Weld		16-8-2 SA Weld		308 GTA Weld		308 SA Weld		308 SMA Weld		316L GTA Weld		316L GTA Weld	
As welded		As welded		As welded		As welded		As welded		As welded		As welded		As welded		As welded	
As above		As above		5.7% ferrite		9.0% ferrite		9.9% ferrite		10.7% ferrite		6.8% ferrite		As above		As above	
-	***427***	**-**	***427°C***	**-**	***24°C***	**-**	***24°C***	**-**	***427°C***	**-**	***24°C***	**-**	***427***	**-**	***100°C***	**-**	***100°C***
0.294	309.4	0.245	150.4	0.493	501.3	0.589	255.0	0.370	295.9	0.400	216.3	0.060	94.7	0.012	17.2	0.026	25.8
0.381	360.5	0.599	272.7	0.696	565.4	0.534	265.6	0.520	371.4	0.680	255.5	0.240	161.3	0.026	38.7	0.026	64.5
0.426	397.6	1.076	409.1	1.135	767.2	0.659	314.5	0.530	439.2	0.670	290.8	0.580	278.7	0.026	98.9	0.088	77.4
0.669	491.4	1.463	496.9	1.369	684.4	1.233	394.5	0.830	519.3	1.180	364.1	0.600	322.7	0.044	137.6	0.079	98.9
0.755	445.8	1.776	599.2	1.510	756.6	1.703	471.3	1.330	661.9	1.530	390.8	0.740	394.7	0.088	167.7	0.044	137.6
0.957	644.8	1.907	593.7	1.552	998.5	1.960	434.3	1.460	719.6	1.760	445.1	1.070	407.9	0.123	202.2	0.096	137.6
1.175	636.3	2.282	653.3									1.420	469.3	0.246	228.0	0.149	167.7
1.500	710.0	2.463	784.1									1.940	502.8	0.298	266.7	0.184	215.1
1.574	826.8			**C**	682.80	**C**	350.40	**C**	573.50	**C**	331.20	1.300	606.8	0.404	296.8	0.219	258.1
1.767	988.7	**C**	389.90	**n**	0.845	**n**	0.438	**n**	0.605	**n**	0.475	1.700	676.0	0.526	335.5	0.298	296.8
		n	0.694	**FS**	514.0	**FS**	514.0	**FS**	377.5	**FS**	517.5	1.800	601.4	0.596	365.6	0.474	352.7
C	618.80	**FS**	397.5	**Jic**	267.7	**Jic**	207.0	**Jic**	342.7	**Jic**	183.6	1.930	597.4	0.667	404.3	0.588	395.7
n	0.578	**Jic**	172.3									2.320	649.4	0.746	438.7	0.693	438.7
FS	377.5			-		-			-			2.500	784.0	0.833	468.8	0.816	481.7
Jic	396.2	10,000		As		As				As				0.886	498.9	0.982	537.6
		-	***427***	**-**	***427°C***	**-**	***427°C***			**-**	***427°C***	**C**	423.10	0.974	529.0	1.158	580.7
10,000		0.250	148.0	0.610	387.7	0.476	154.4			0.145	68.5	**n**	0.565			1.377	628.0
-	***427***	286.8	286.8	0.830	494.6	0.790	184.9			0.326	113.6	**FS**	397.5	**C**	512.06	1.632	683.9
0.414	358.0	315.4	315.4	0.910	594.7	0.884	239.1			0.478	144.0	**Jic**	232.3	**n**	0.524	1.798	731.2
0.644	392.1	386.1	386.1	1.500	671.0	1.245	249.7			0.824	142.4			**FS**	507.0	2.018	782.8
0.821	511.4	499.9	499.9	1.780	771.2	1.148	303.2			1.298	189.1			**Jic**	292.9	2.202	834.4
1.031	593.7					2.244	355.5			1.396	314.2						
1.430	610.7	**C**	360.55	**C**	554.20	2.309	411.1			2.223	301.1					**C**	535.72
		n	0.631	**n**	0.585											**n**	0.555
C	539.00	**FS**	-	**FS**	387.5	**C**	238.80			**C**	197.00					**FS**	507.0
n	0.486	**Jic**	(155.0)	**Jic**	330.5	**n**	0.591			**n**	0.584					**Jic**	297.6
FS	-					**FS**	387.5			**FS**	409.0						
Jic	(269.0)					**Jic**	110.5			**Jic**	88.5						

Table B2. (Contd.)

Δa (mm)	J (kJ/m²)	Δa (mm)	J (kJ/m²)	Δa (mm)	J (kJ/m²)	Δa (mm)	J (kJ/m²)	Δa (mm)	J (kJ/m²)	Δa (mm)	J (kJ/m²)	Δa (mm)	J (kJ/m²)	Δa (mm)	J (kJ/m²)	Δa (mm)	J (kJ/m²)
Faure et al.		Faure et al.		Faure et al.		Faure et al.		Faure et al.		Faure et al.		Faure et al.		Faure et al.		Faure et al.	
316L GTA Weld		508-ERNiCr3 GTA		508-ERNiCr3 GTA		508-ERNiCr3 GTA		508-ERNiCr3 GTA		508-ERNiCr3 GTA		316L GTA Weld		316L GTA Weld		316L GTA Weld	
As welded		508 Cl3. interface		508 Cl3. interface		508 Cl3. interface		508 Cl3. interface		508 Cl3. interface		As welded		As welded		As welded	
As above		As above		As above		As above		As above		As above		As above		As above		As above	
-	***300°C***	**-**	***100°C***	**-**	***100°C***	**-**	***100°C***	**-**	***300°C***	**-**	***300°C***	**-**	***100°C***	**-**	***100°C***	**-**	***300°C***
0.014	12.8	0.023	25.4	1.590	724.2	0.691	440.0	0.010	28.2	0.010	28.2	0.012	17.2	0.026	25.8	0.014	12.8
0.020	28.9	0.034	49.7	1.605	766.1	0.748	438.6	0.014	68.7	0.014	68.7	0.026	38.7	0.026	64.5	0.020	28.9
0.052	48.2	0.044	79.8	1.640	759.5	0.821	483.5	0.087	95.1	0.087	95.1	0.026	98.9	0.088	77.4	0.052	48.2
0.045	67.4	0.065	111.4	1.746	797.8	0.831	467.1	0.136	130.4	0.136	130.4	0.044	137.6	0.079	98.9	0.045	67.4
0.079	93.1	0.070	146.8	1.840	780.1	0.885	500.6	0.178	198.8	0.178	198.8	0.088	167.7	0.044	137.6	0.079	93.1
0.124	128.4	0.087	187.9	1.855	796.3	0.938	527.6	0.196	143.3	0.196	143.3	0.123	202.2	0.096	137.6	0.124	128.4
0.169	167.0	0.122	194.6	1.899	818.3	0.976	529.0	0.294	167.7	0.294	167.7	0.246	228.0	0.149	167.7	0.169	167.0
0.293	208.7	0.158	224.7	1.948	855.1	0.991	534.0	0.303	210.2	0.303	210.2	0.298	266.7	0.184	215.1	0.293	208.7
0.451	250.5	0.240	235.8			1.165	580.3	0.362	216.4	0.362	216.4	0.404	296.8	0.219	258.1	0.451	250.5
0.654	298.6	0.249	271.1	**C**	563.62	1.383	630.1	0.462	252.7	0.462	252.7	0.526	335.5	0.298	296.8	0.654	298.6
0.823	343.6	0.278	307.8	**n**	0.564	1.636	683.5	0.662	300.4	0.662	300.4	0.596	365.6	0.474	352.7	0.823	343.6
0.981	391.7	0.324	293.1	**FS**	490.4	1.805	732.0	0.834	347.0	0.834	347.0	0.667	404.3	0.588	395.7	0.981	391.7
1.252	436.7	0.351	340.9	**Jic**	317.7	2.022	781.8	0.988	395.7	0.988	395.7	0.746	438.7	0.693	438.7	1.252	436.7
1.511	484.9	0.385	339.5			2.131	836.6	1.264	439.8	1.264	439.8	0.833	468.8	0.816	481.7	1.511	484.9
1.782	526.6	0.420	384.3			2.193	836.6	1.519	487.0	1.519	487.0	0.886	498.9	0.982	537.6	1.782	526.6
2.098	558.7	0.495	374.8	**Secon**				1.794	531.0	1.794	531.0	0.974	529.0	1.158	580.7	2.098	558.7
		0.531	391.0	0.012	23.5	**C**	531.77	1.994	564.2	1.994	564.2			1.377	628.0		
C	386.66	0.623	430.7	0.031	64.1	**n**	0.555	2.104	564.2	2.104	564.2	**C**	512.06	1.632	683.9	**C**	386.66
n	0.529	0.665	416.7	0.048	138.8	**FS**	490.4	2.849	649.7	2.849	649.7	**n**	0.524	1.798	731.2	**n**	0.529
FS	442.8	0.714	467.5	0.079	106.1	**Jic**	297.7					**FS**	507.0	2.018	782.8	**FS**	442.8
Jic	211.5	0.773	452.8	0.101	170.9			**C**	384.29	**C**	384.29	**Jic**	292.9	2.202	834.4	**Jic**	211.5
		0.769	499.1	0.131	204.4			**n**	0.527	**n**	0.527						
		0.886	515.3	0.155	172.3			**FS**	455.2	**FS**	455.2			**C**	535.72		
		0.959	497.6	0.172	209.3			**Jic**	209.0	**Jic**	209.0			**n**	0.555		
		1.052	537.4	0.186	216.5									**FS**	507.0		
		1.103	577.8	0.222	257.8									**Jic**	297.6		
		1.203	631.5	0.238	232.8												
		1.291	613.3	0.300	267.7												
		1.279	666.8	0.340	299.8												
		1.346	646.2	0.403	301.9												
		1.386	689.6	0.479	353.2												
		1.410	680.1	0.547	333.9												
		1.498	703.6	0.590	367.4												
		1.549	726.4	0.664	405.1												
		continued		continued													

Table B2. *(Contd.)*

Δa (mm)	**J (kJ/m²)**	**Δa (mm)**	**J (kJ/m²)**	**Δa (mm)**	**J (kJ/m²)**	**Δa (mm)**	**J (kJ/m²)**	**Δa (mm)**	**J (kJ/m²)**	**Δa (mm)**	**J (kJ/m²)**	**Δa (mm)**	**J (kJ/m²)**	**Δa (mm)**	**J (kJ/m²)**	**Δa (mm)**	**J (kJ/m²)**
Hale & Garwood		Hale & Garwood		Matti Valo		Matti Valo		Matti Valo		Matti Valo		Matti Valo		Matti Valo		Matti Valo	
19-9L MMA Weld		19-9L MMA Weld		BWR 308L Weld		BWR 308L Weld		BWR 308L Weld		BWR 308L Weld		BWR 308L Weld		BWR 308L Weld		BWR 308L Weld	
As welded		As welded		Riser pipe		Riser pipe		Riser pipe		Control rod handle		Control rod handle		Control rod handle		Control rod handle	
As above		10 h @ 400°C		RP-W1 0.8 dpa		RP-W3 0.6 dpa		RP-W5 0.7 dpa		CRH-W1 12 dpa		CRH-W2 12 dpa		CRH-W3 12 dpa		CRH-W4 12 dpa	
-	***300°C***	**-**	***300°C***	**-**	***20°C***	**-**	***199°C***	**-**	***249°C***	**-**	***259°C***	**-**	***25°C***	**-**	***25°C***	**-**	***259°C***
0.550	128.7	0.336	44.8	0.000	10.1	0.000	10.6	-0.012	5.9	0.000	4.6	0.006	1.2	-0.019	0.6	-0.021	3.3
1.252	212.7	0.611	78.4	0.015	26.9	0.021	24.9	0.022	3.4	-0.040	3.8	0.043	2.0	0.025	10.6	-0.043	5.8
2.473	307.8	0.947	111.9	0.024	47.8	0.012	40.8	0.007	25.9	-0.074	13.9	0.139	9.5	0.065	3.9	-0.018	14.1
3.664	369.4	1.374	151.1	0.043	66.3	0.040	55.9	0.026	48.5	0.000	12.1	0.195	12.8	0.069	12.2	0.025	2.5
4.550	403.0	1.924	184.7	0.111	87.3	0.105	71.9	0.017	69.3	0.053	9.5	0.577	24.1	0.072	20.6	0.340	40.7
5.618	436.6	2.412	207.1	0.166	105.7	0.166	89.5	0.082	91.8	0.069	18.8	1.003	30.2	0.103	24.7	0.546	61.4
6.534	459.0	3.328	240.7	0.215	126.7	0.277	118.1	0.076	113.5	0.235	29.5	1.336	35.7	0.175	36.3	1.454	62.2
7.115	470.2	3.939	268.7	0.317	147.7	0.438	146.7	0.111	135.2	0.538	53.4	1.638	37.8	0.346	64.5	1.620	63.1
				0.388	170.3	0.573	171.9	0.222	163.4	0.875	72.3	1.869	37.5	0.461	91.1		
C	184.18	**C**	120.98	0.487	191.3	0.755	194.6	0.359	186.6	1.003	91.5			0.747	111.8	**C**	58.59
n	0.504	**n**	0.593	0.588	213.1	0.857	214.8	0.406	210.0	1.116	105.6	**C**	29.14	1.215	115.6	**n**	0.222
FS	544.9	**FS**	557.6	0.662	231.6	0.993	228.3	0.502	239.1	1.416	112.8	**n**	0.659	1.528	124.6	**FS**	820.0
Jic	90.0	**Jic**	49.6	0.727	250.9	1.104	242.6	0.676	261.4	1.656	118.3	**FS**	1009.0	1.730	137.0	**Jic**	41.6
				0.826	269.4	1.202	256.0	0.862	272.1	2.020	113.6	**Jic**	10.2	1.965	143.5		
1 h @				0.921	287.8	1.335	263.6	0.974	286.2								
-	***300°C***			1.011	304.6	1.440	273.7	1.185	290.1	**C**	84.12			**C**	107.84		
0.702	117.5			1.106	323.1	1.616	280.5	1.222	307.6	**n**	0.665			**n**	0.574		
1.344	162.3			1.205	339.0	1.755	292.3	1.387	321.6	**FS**	820.0			**FS**	1009.0		
2.107	195.9			1.307	356.6	1.894	299.9	1.542	329.0	**Jic**	29.7			**Jic**	44.1		
2.809	218.3			1.402	368.4	2.057	303.3	1.681	343.9								
3.511	240.7			1.495	381.8			1.697	328.0								
4.244	251.9			1.618	391.0	**C**	223.63	1.821	347.1								
4.916	263.1			1.729	399.4	**n**	0.466	1.935	350.3								
5.557	268.7			1.841	406.2	**FS**	361.0	1.954	358.6								
6.321	274.3			1.930	416.2	**Jic**	124.9	2.205	341.7								
				2.050	417.1												
C	142.05							**C**	280.75								
n	0.387			**C**	295.95			**n**	0.358								
FS	561.2			**n**	0.533			**FS**	431.9								
Jic	81.3			**FS**	566.0			**Jic**	183.8								
				Jic	145.6												

Table B2. *(Contd.)*

Δa (mm)	**J (kJ/m²)**	**Δa (mm)**	**J (kJ/m²)**	**Δa (mm)**	**J (kJ/m²)**	**Δa (mm)**	**J (kJ/m²)**	**Δa (mm)**	**J (kJ/m²)**	**Δa (mm)**	**J (kJ/m²)**	**Δa (mm)**	**J (kJ/m²)**	**Δa (mm)**	**J (kJ/m²)**	**Δa (mm)**	**J (kJ/m²)**
Gavenda et al.		Gavenda et al.		Gavenda et al.		Gavenda et al.		Gavenda et al.		Gavenda et al.		O'Donnell et al.		O'Donnell et al.		O'Donnell et al.	
308L SMA		308L SMA		308L SMA		308 SMA		308 SMA		308 SMA		316 MMA Weld		316 MMA Weld		316 MMA Weld	
As welded		7,700 h @400°C		7,700 h @400°C		As welded		10,000 h @400°C		10,000 h @400°C		As welded		As welded		As welded	
PWWO-01		PWWO-04		PWWO-02		PWCE-01		PWCE-03		PWER-01		As above		50,000h @ 400°C		2.0 dps fast MTR	
-	**290°C**	**-**	**290°C**	**-**	**290°C**	**-**	**290°C**	**-**	**290°C**	**-**	**290°C**	**-**	***370°C***	**-**	***370°C***	**-**	***370°C***
0.026	72.9	0.052	47.7	0.082	46.9	0.199	37.3	0.061	142.7	0.141	12.8	0.033	42.5	0.204	69.7	0.088	44.2
0.086	111.3	-0.090	92.1	-0.016	104.5	0.233	61.3	0.075	203.9	-0.006	63.4	0.062	46.8	0.408	99.1	0.228	46.2
0.137	150.7	0.231	144.6	0.294	141.6	0.202	87.7	0.206	268.2	0.130	91.2	0.110	48.6	0.707	161.5	0.378	31.4
0.307	190.8	0.330	193.8	0.392	190.1	0.101	126.1	0.374	340.6	0.025	127.7	0.062	62.1	0.762	209.2	0.393	53.5
0.322	230.6	0.546	236.0	0.722	245.4	0.350	177.9	0.516	384.5	0.123	198.5	0.136	60.3			0.301	57.4
0.317	271.8	0.704	287.4	0.581	280.5	0.050	238.2	0.548	418.1	0.375	279.4	0.143	67.8	**C**	226.86	0.363	65.3
0.581	311.9	0.811	328.0	0.930	321.9	0.560	322.4	0.545	461.1	0.390	360.8	0.212	80.1	**n**	0.782		
0.722	350.2	1.167	366.7	1.166	359.0	0.235	407.1	0.765	526.2	0.952	437.5	0.246	94.7	**FS**	-	**C**	72.10
1.041	387.0	1.501	402.8	1.410	396.3	0.686	490.7	1.020	586.6	1.164	512.0	0.220	102.2	**Jic**	-	**n**	0.219
1.299	459.8	1.949	435.6	1.936	428.6	0.975	568.3	1.107	649.2	1.628	583.7	0.334	84.9			**FS**	-
1.576	495.2	2.282	467.5	2.161	502.7	0.860	635.4	1.149	715.4	2.102	647.9	0.355	86.2			**Jic**	-
1.667	530.2	2.720	497.5	2.844	563.1	1.145	762.1	1.530	769.6	2.342	718.8	0.319	129.3				
1.954	563.1	3.185	524.1	3.679	574.7	1.424	816.0	1.593	831.4	3.057	771.0	0.546	137.3	50,000 h @		4.0 dps fast MTR	
2.169	592.2	3.701	581.3	3.786	599.4	1.569	874.1	2.085	878.7	3.112	841.6	0.656	160.7	**-**	***370°C***	**-**	***370°C***
2.681	671.7	4.548	630.5	4.111	627.9	1.762	933.1	2.131	938.4	3.633	896.6	0.601	208.1	0.204	58.7	0.066	9.8
2.979	706.3	5.075	644.6	4.900	666.7	1.793	996.5	2.471	987.2	4.008	950.2	0.353	248.7	0.326	154.1	0.389	12.7
3.416	732.3	5.752	682.9	5.465	676.8	1.894	1057.6	2.754	1035.5	4.474	997.6	1.316	256.7	0.544	132.1	0.751	24.5
3.699	762.7	6.426	696.7	5.931	696.3	2.090	1111.9	2.815	1094.8	4.809	1,048.6	1.034	308.4	0.571	165.1	1.001	18.6
4.240	779.0	6.778	716.8	6.703	700.3	2.409	1157.6	3.321	1187.7	5.142	1,096.7	0.917	312.7	0.898	179.8		
4.590	801.0	7.516	745.2	7.407	723.9	2.664	1266.4	4.118	1254.2	5.667	1,129.4			1.061	183.5	**C**	21.30
5.055	855.5	8.077	772.3	8.253	733.3	3.127	1357.3	4.845	1356.8	5.981	1,175.7	**C**	240.70	1.333	212.8	**n**	0.319
5.621	909.7	8.752	790.3	8.942	744.5	3.650	1443.5	5.550	1448.2	6.856	1,231.7	**n**	0.663			**FS**	-
6.024	933.3	9.474	797.6	9.637	750.0	3.923	1568.0	6.257	1529.0	7.370	1,250.5	**FS**	-	**C**	193.75	**Jic**	-
6.265	961.4	10.248	795.7	10.129	764.0	4.328	1712.2	7.063	1584.5	7.885	1,322.9	**Jic**	-	**n**	0.549		
7.142	983.8	10.905	808.7	10.829	775.0	4.950	1883.6	7.753	1641.9	8.779	1,344.4			**FS**	-		
7.773	1018.1	11.461	824.0	11.521	776.0	5.533	1949.1	8.745	1684.6	9.470	1,375.0			**Jic**	-		
8.705	1043.6	12.190	821.3	12.596	786.8	5.924	2027.8	9.717	1696.5	9.874	1,381.0						
9.409	1080.8	12.959	856.3	13.065	792.0	6.867	2149.2	10.432	1736.1	10.176	1,394.5						
10.004	1117.6	13.396	867.5	13.728	776.0	7.485	2306.6	11.095	1771.2								
										C	459.4						
C	400.9	**C**	338.8	**C**	330.2	**C**	648.3	**C**	614.2	**n**	0.509						
n	0.481	**n**	0.505	**n**	0.621	**n**	0.713	**n**	0.611	**FS**	409.0						
FS	397.5	**FS**	409.0	**FS**	409.0	**FS**	373.0	**FS**	406.03	**Jic**	276.6						
Jic	242.9	**Jic**	189.3	**Jic**	154.5	**Jic**	363.0	**Jic**	363.5								

Table B2. (Contd.)

Δa (mm)	J (kJ/m^2)	Δa (mm)	J (kJ/m^2)	Δa (mm)	J (kJ/m^2)	Δa (mm)	J (kJ/m^2)	Δa (mm)	J (kJ/m^2)	Δa (mm)	J (kJ/m^2)	Δa (mm)	J (kJ/m^2)	Δa (mm)	J (kJ/m^2)	Δa (mm)	J (kJ/m^2)
O'Donnell et al.		Hojo et al.		Hojo et al.		Hojo et al.		Hojo et al.		Hojo et al.		Hojo et al.		Hojo et al.		Hojo et al.	
316 TIG Weld		308L SMA Weld		308L SMA Weld		308L SMA Weld		308L SMA Weld		316L SMA Weld		316L SMA Weld		316L SMA Weld		316L SMA Weld	
As welded		As welded (ID = K)		As welded (ID = K)		As welded (ID = K)		As welded (ID = K)		As welded (ID = J)		As welded (ID = J)		As welded (ID = J)		As welded (ID = J)	
As above		Unaged		10,000 h @400°C		20,000 h @400°C		40,000 h @400°C		Unaged		Unaged		40,000 h @300°C		60,000 h @300°C	
-	***370°C***	**-**	***325°C***	**-**	***325°C***	**-**	***325°C***	**-**	***325°C***	**-**	***325°C***	**-**	***325°C***	**-**	***325°C***	**-**	***325°C***
0.379	287.1	0.140	107.5	0.012	40.0	0.611	125.4	0.208	64.4	0.058	46.7	3.819	837.6	3.083	616.6	0.392	220.9
0.591	360.6	0.245	172.0	0.185	82.8	0.852	143.6	0.577	168.5	0.047	99.5	4.130	878.1	3.336	719.3	1.278	376.6
0.908	455.5	0.383	214.9	0.622	134.6	1.277	170.7	0.796	192.9	0.185	93.3	4.314	924.8	3.681	731.9	1.508	401.6
0.861	506.3	0.683	269.9	0.691	146.8	1.828	203.9	1.094	204.8	0.288	146.2	4.553	735.2	3.807	750.6	3.496	657.2
0.719	545.4	1.223	324.6	0.979	171.1	2.012	209.8	1.530	222.7	0.231	171.1	4.705	968.5	3.830	716.4	4.013	672.9
1.178	631.6	1.303	321.5	1.323	204.5	2.471	230.8	1.875	234.6	0.197	208.4	5.279	1,012.2	3.991	766.2	4.507	679.3
1.240	702.2	1.649	379.5	1.587	216.5	2.873	248.8	2.001	249.8	0.312	267.5	5.266	788.3	4.128	725.8	4.794	701.1
		1.832	388.5	1.920	234.6	3.102	257.7	2.207	246.5	0.405	323.5	5.989	838.3	4.301	778.7	5.047	747.8
C	572.00	2.131	431.2	2.379	246.3	3.355	266.6	2.391	258.6	0.657	249.0	6.747	882.1	4.405	800.5	5.219	713.7
n	0.719	2.614	455.2	2.138	222.0	3.527	294.1	3.114	282.3	0.646	295.6			4.600	806.8	5.368	735.5
FS	-	2.694	482.8	2.678	252.1	3.860	309.1	3.355	288.2	0.520	382.6	Upper curve		4.405	4.714	781.9	757.3
Jic	-	3.154	531.5	2.781	264.3	4.204	287.1	4.216	324.0	0.841	317.4	**C**	481.94	4.772	828.6	5.817	776.1
		3.337	512.8	3.011	273.2	4.365	299.2	4.537	326.7	0.818	351.6	**n**	0.449	5.036	794.5	5.770	745.0
		3.557	574.1	3.584	281.7	3.940	269.0	5.008	356.9	0.727	441.8	Lower curve		4.772	4.968	841.1	760.6
		4.038	567.3	3.998	321.2	4.605	302.0	5.329	359.6	0.854	500.9	**C**	329.70	5.186	866.0	6.207	776.2
		4.028	610.4	4.423	336.1	4.904	317.0	4.755	308.0	1.105	329.9	**n**	0.544	5.347	878.5	6.459	770.0
		4.636	615.8	4.756	351.1	5.157	356.7	5.443	319.5	1.301	404.6			5.289	816.3	6.517	785.6
		4.614	652.8			5.111	322.9	5.879	328.1	1.439	401.6	40,000 h @300°C		5.347	5.564	828.8	770.2
		5.233	664.3	**C**	171.28	5.535	334.7	5.708	371.4	1.199	563.2	**-**	***325°C***	5.702	844.4	7.045	785.8
		5.234	688.9	**n**	0.434	5.536	371.6	6.029	383.3	1.508	442.0	0.507	248.9	5.519	891.0	7.286	776.5
		5.739	725.2	**FS**	-			6.189	333.9	1.658	466.9	0.681	354.7	5.646	912.8	7.355	789.0
		6.026	755.7	**Jic**	-	**C**	153.93	6.315	343.0	1.647	619.3	1.278	382.9	5.921	916.0	7.745	770.4
		6.048	706.4			**n**	0.466	6.557	391.9	2.002	473.3	1.578	501.1	5.967	857.0	7.941	814.0
		6.588	745.7			**FS**	-	6.844	400.8	2.083	491.9	1.715	429.6	6.196	872.6	8.205	773.7
		7.185	781.9			**Jic**	-			2.473	544.9	1.853	451.4	6.185	928.5	8.629	783.2
		7.599	812.2					**C**	176.01	2.669	545.0	1.807	529.2	6.450	941.1	9.089	805.1
								n	0.413	2.222	678.6	2.037	566.6	6.553	950.4		
		C	304.91					**FS**	-	2.659	731.5	2.301	513.8			**C**	356.63
		n	0.475					**Jic**	-	2.761	573.0	2.359	604.0	Upper curve		**n**	0.410
		FS	-							2.876	601.0	2.543	616.5	**C**	412.41	**FS**	-
		Jic	-							3.243	613.6	2.727	635.2	**n**	0.446	**Jic**	-
										3.210	787.7	2.842	650.8	Lower curve			
										3.657	675.9	2.980	675.7	**C**	340.12		
										3.795	675.9	3.198	700.6	**n**	0.522		

Table B1. (Contd.)

Δa (mm)	J (kJ/m^2)	Δa (mm)	J (kJ/m^2)	Δa (mm)	J (kJ/m^2)	Δa (mm)	J (kJ/m^2)	Δa (mm)	J (kJ/m^2)	Δa (mm)	J (kJ/m^2)	Δa (mm)	J (kJ/m^2)	Δa (mm)	J (kJ/m^2)	Δa (mm)	J (kJ/m^2)
Hojo et al.		Hojo et al.		Hojo et al.		Hojo et al.		Hojo et al.		Hojo et al.		Hojo et al.		Hojo et al.		Hojo et al.	
316L SMA Weld		316L SMA Weld		316L SMA Weld		316L SMA Weld		308L SMA Weld		316L TIG Weld		316L TIG Weld		316L TIG Weld		316L TIG Weld	
As welded (ID = J)		As welded (ID = J)		As welded (ID = J)		As welded (ID = J)		As welded (ID = K)		As welded (ID = H)		As welded (ID = H)		As welded (ID = H)		As welded (ID = H)	
40,000 h @350°C		60,000 h @350°C		10,000 h @400°C		20,000 h @400°C		40,000 h @400°C		Unaged		Unaged		40,000 h @300°C		60,000 h @300°C	
-	***325°C***	**-**	***325°C***	**-**	***325°C***	**-**	***325°C***	**-**	***325°C***	**-**	***325°C***	**-**	***325°C***	**-**	***325°C***	**-**	***325°C***
0.334	206.8	0.553	197.4	0.092	59.4	1.619	216.1	1.210	228.5	0.012	-	5.950	1,385.0	3.940	842.8	0.444	292.1
0.853	294.5	0.703	247.5	0.423	128.3	1.904	241.2	1.494	231.7	0.001	38.1	6.544	1,454.5	4.074	868.2	0.687	333.3
0.899	275.7	0.922	222.4	0.264	128.2	2.109	256.9	1.631	250.5	0.159	47.6	7.235	1,520.8	4.230	833.1	0.966	364.9
1.394	357.1	1.118	297.6	0.539	237.7	2.326	266.4	1.802	253.7	0.099	85.7			4.292	880.8	0.991	409.3
1.590	354.0	1.348	256.9	0.847	284.6	2.531	291.4	2.099	294.4	0.101	136.6	**C**	562.54	4.413	899.7	1.173	418.8
1.912	404.1	1.889	282.0	0.961	322.2	2.941	332.2	2.223	275.7	0.138	171.5	**n**	0.514	4.436	861.6	1.367	447.2
2.258	432.3	2.143	397.9	0.914	240.9	3.215	351.0	2.748	322.7	0.248	193.7			4.655	918.7	1.500	456.7
2.362	448.0	2.500	316.4	0.708	153.3	3.545	363.6	2.964	341.6	0.249	238.2	*40,000 h @ 300°C*		4.801	934.5	1.731	494.7
2.535	438.6	2.535	429.2	0.959	162.8	3.727	385.5	3.909	360.6	0.324	304.9	**-**	***325°C***	4.956	896.2	1.888	494.6
2.719	469.9	3.145	344.6	1.118	178.5	3.966	407.5	4.603	392.1	0.386	362.1	0.530	327.0	5.078	915.2	2.094	529.4
2.961	479.3	3.802	529.5	1.232	209.8	4.274	423.2	4.811	551.5	0.569	425.5	0.555	355.6	5.055	950.2	2.385	557.8
3.387	532.6	4.009	379.1	1.414	203.6	4.525	445.2	5.698	564.3	0.595	470.0	0.774	399.9	5.152	966.0	2.469	538.7
3.571	535.7	4.850	551.4	1.314	337.9	4.798	460.9	7.474	580.5	0.788	482.6	0.945	460.2	5.272	931.0	2.870	598.8
3.952	570.2	5.415	388.5	1.189	322.3	4.980	479.7	8.407	590.1	0.877	590.6	1.236	501.3	5.370	984.9	3.388	569.9
4.251	582.7	5.899	563.9	1.178	359.7	5.265	498.5	5.502	411.1	0.814	536.6	1.309	514.0	5.467	1,000.8	3.342	658.9
4.055	598.4	6.509	410.4	1.577	400.5	5.572	511.1	6.754	427.1	1.044	542.8	1.430	536.2	5.514	949.9	3.609	687.3
4.539	595.2	6.912	579.6	1.691	391.2	5.971	530.0	7.971	430.6	1.312	599.8	1.613	571.0	5.768	968.8	3.997	718.9
4.793	607.8	7.638	416.7	2.010	435.0	6.290	545.7	9.325	440.4	1.327	707.9	1.795	599.5	5.733	1,013.3	4.162	598.0
5.127	623.4	8.894	429.2	2.329	466.4	6.586	558.3			1.519	656.9	2.013	628.0	5.866	1,029.1	4.650	769.3
5.230	642.2	7.823	579.6	3.150	538.5			**C**	214.82	1.436	704.6	2.243	659.6	5.998	981.4	4.880	788.2
5.737	670.4			3.743	607.4	**C**	153.18	**n**	0.357	1.666	717.2	2.375	627.7	5.988	1,041.8	5.135	803.9
5.830	683.0	**C**	279.39	4.392	657.6	**n**	0.699			1.717	822.0	2.438	694.4	6.036	1,057.6	5.486	841.9
6.175	695.5	**n**	0.405	4.745	676.5					2.006	771.0	2.666	659.3	6.230	1,073.4	4.887	626.1
				5.109	698.5					2.249	828.0	2.872	691.0	6.204	997.1	5.540	657.5
C	308.17			3.321	560.4					2.540	875.5	2.777	722.8	6.337	1,016.1	5.970	860.6
n	0.436			5.930	758.1					2.470	929.6	3.030	716.3	6.352	1,089.2	6.333	892.2
				6.488	795.8					2.760	932.6	3.019	754.4	6.449	1,105.0	6.828	895.0
										2.991	983.3	3.297	744.7	6.642	1,120.8	6.290	676.1
				C	254.36					3.113	1,034.0	3.261	767.0	Upper curve		7.100	691.5
				n	0.621					3.853	1,128.9	3.335	792.4	**C**	454.26	7.680	719.7
										4.435	1,217.5	3.587	766.8	**n**	0.463	8.308	725.7
										5.271	1,302.8	3.565	811.3	Lower curve		9.059	776.0
												3.721	789.0	**C**	448.35	7.275	901.1
												3.891	811.1	**n**	0.434	7.795	913.5

Table B2. *(Contd.)*

Δa (mm)	J (kJ/m²)	Δa (mm)	J (kJ/m²)	Δa (mm)	J (kJ/m²)	Δa (mm)	J (kJ/m²)	Δa (mm)	J (kJ/m²)	Δa (mm)	J (kJ/m²)	Δa (mm)	J (kJ/m²)	Δa (mm)	J (kJ/m²)	Δa (mm)	J (kJ/m²)
Hojo et al.		Hojo et al.		Hojo et al.		Hojo et al.		Hojo et al.		Hojo et al.		Tavassoli et al.		Tavassoli et al.		Yiren Chen	
316L TIG Weld		316L TIG Weld		316L TIG Weld		316L TIG Weld		316L TIG Weld		316L TIG Weld		316LN SA Weld		308L SA Weld		308 SMA Weld	
As welded (ID = H)		As welded (ID = H)		As welded (ID = H)		As welded (ID = H)		As welded (ID = H)		As welded (ID = H)		As welded		As welded		Low-DO environment	
60,000 h @300°C		40,000 h @350°C		60,000 h @350°C		10,000 h @400°C		20,000 h @400°C		20,000 h @400°C		5.0 dpa @ xxx°C		4.8 dpa @ xxx°C		0.08 dpa @ 320°C	
-	***325°C***	-	***325°C***	-	***325°C***	-	***325°C***	-	***325°C***	-	***325°C***	-	***xxx°C***	-	***xxx°C***	-	***320°C***
8.254	919.5	0.506	266.5	0.577	316.1	0.559	299.5	0.934	302.2	6.789	723.6	0.21	123.6	0.22	22.0	0.004	2.0
8.738	925.6	0.729	322.3	1.362	443.0	0.854	373.4	1.146	326.8	7.083	738.8	0.37	135.5	0.66	28.0	0.012	5.5
9.064	931.7	1.057	343.9	1.842	498.7	1.183	397.9	1.381	354.4			0.60	145.3	1.10	31.4	0.022	8.5
9.511	953.7	1.432	402.7	2.298	486.1	1.454	453.3	1.711	375.7	*Upper*		0.88	154.2	1.64	34.4	0.028	12.5
		1.642	424.3	2.661	523.2	1.712	449.9	2.122	397.0	**C**	318.75	1.25	162.9	2.50	37.3	0.043	17.5
Upper		1.923	449.0	3.387	572.6	2.136	486.7	1.512	413.0	**n**	0.436	1.95	174.2	3.50	40.7	0.065	25.3
C	390.92	2.216	470.6	3.750	600.4	2.265	498.9	2.463	412.1	*Lower*		2.52	180.6			0.094	31.9
n	0.305	2.626	486.0	4.849	631.1	2.500	511.1	2.582	492.4	**C**	341.83	2.99	185.5	**C**	30.70	0.13	41.2
Lower		3.141	520.0	5.025	668.2	2.724	551.1	2.722	439.7	**n**	0.391			**n**	0.221	0.174	50.2
C	399.30	3.340	535.4	5.470	677.4	2.806	535.5	2.829	507.7			**C**	157.20			0.232	60.5
n	0.409	3.691	572.5	5.996	686.5	3.030	569.3	2.945	461.2			**n**	0.152			0.311	72.0
		4.042	584.8	6.277	680.2	3.394	590.7	3.158	525.9							0.393	81.1
		4.440	600.2	6.441	711.2	3.664	599.7	3.344	473.2							0.467	90.7
		4.709	621.8	6.874	720.4	4.017	633.4	3.358	541.2							0.551	101.0
		5.002	637.2	7.096	701.7	4.252	657.9	3.475	553.5							0.634	110.7
		5.446	658.8	7.412	748.1	4.334	642.4	3.662	494.5							0.71	119.3
		5.645	671.1	7.693	726.3	4.640	660.6	3.687	574.9							0.787	130.3
		6.031	692.7	8.313	729.2	4.722	669.8	3.850	509.8							0.916	139.6
		6.359	711.2	9.062	787.9	4.922	685.1	4.051	590.0							1.025	148.8
		6.780	726.6			5.005	706.7	4.120	531.2							1.159	158.9
		7.096	738.9	**C**	389.70	5.121	678.7	4.461	546.4							1.31	167.4
				n	0.315	5.251	697.2	4.474	605.1							1.902	174.9
		C	347.41			5.345	718.7	4.673	567.8							2.226	175.9
		n	0.377			5.416	737.2	4.943	583.0							2.393	173.2
						5.663	755.6	5.015	644.8								
						5.604	721.6	5.190	598.3							**C**	144.00
						5.910	767.7	5.378	610.5							**n**	0.590
						5.968	736.7	5.426	663.0							**FS**	-
						6.122	783.0	5.650	681.3							**Jic**	57.0
						6.332	751.8	5.590	625.7								
								5.966	653.2								
						C	374.55	6.037	693.4								
						n	0.382	6.343	711.6								

Table B2. (Contd.)

Δa (mm)	J (kJ/m^2)	Δa (mm)	J (kJ/m^2)	Δa (mm)	J (kJ/m^2)	Δa (mm)	J (kJ/m^2)	Δa (mm)	J (kJ/m^2)	Δa (mm)	J (kJ/m^2)	Δa (mm)	J (kJ/m^2)	Δa (mm)	J (kJ/m^2)	Δa (mm)	J (kJ/m^2)
Lucas et al.		Lucas et al.		Lucas et al.		Lucas et al.		Lucas et al.		Lucas et al.		Lucas et al.		Lucas et al.		Matti Valo	
316 GTA Weld		316 GTA Weld		316 GTA Weld		316 GTA Weld		316 GTA Weld		316 GTA Weld		316 GTA Weld		316 GTA Weld		BWR 308L Weld	
Low ferrite (# 84)		Low ferrite (# 92)		Low ferrite (# 112)		Low ferrite (# 102)		High ferrite (# 144)		High ferrite (# 211)		High ferrite (# 193)		High ferrite (# 238)		Riser pipe	
As above		As above		As above		Low-DO environment		As above		As above		As above		Low-DO environment		RP-W1 0.8 dpa	
-	***25°C***	-	***288°C***	-	***288°C***	-	***288°C***	-	***25°C***	-	***288°C***	-	***288°C***	-	***288°C***	-	***20°C***
0.229	55.1	0.155	34.3	0.137	35.7	0.023	10.8	0.142	28.7	0.162	60.6	0.151	49.0	0.034	8.3	0.000	10.1
0.269	71.2	0.215	54.4	0.190	53.3	0.043	17.4	0.200	51.5	0.189	77.1	0.178	60.9	0.103	32.6	0.015	26.9
0.295	88.8	0.274	75.5	0.269	78.5	0.088	27.9	0.271	72.6	0.200	90.4	0.207	76.2	0.178	52.0	0.024	47.8
0.312	93.1	0.329	90.4	0.338	92.4	0.124	39.6	0.320	94.0	0.282	112.1	0.252	91.2	0.247	74.2	0.043	66.3
0.329	97.2	0.388	102.2	0.408	106.1	0.178	50.1	0.387	116.8	0.349	123.2	0.306	106.3	0.305	87.6	0.111	87.3
0.355	104.5	0.438	109.8	0.463	112.5	0.226	59.2	0.443	134.3	0.450	138.8	0.376	119.4	0.385	102.4	0.166	105.7
0.386	114.4	0.477	116.0	0.528	118.0	0.276	66.8	0.493	144.6	0.559	150.4	0.437	127.7	0.488	115.5	0.215	126.7
0.436	119.8	0.554	122.1	0.611	124.5	0.347	74.6	0.594	158.5	0.714	158.8	0.538	141.9	0.600	127.1	0.317	147.7
0.485	132.5	0.658	130.3	0.669	127.8	0.421	82.1	0.735	169.1	0.896	164.6	0.619	149.9	0.679	134.3	0.388	170.3
0.554	140.7	0.772	135.1	0.749	131.3	0.490	85.3	0.851	178.3	1.067	171.3	0.735	155.4	0.802	144.9	0.487	191.3
0.650	148.7	0.907	138.2	0.803	133.1	0.594	89.2	0.976	189.1	1.240	176.6	0.864	161.3	0.939	152.4	0.588	213.1
0.731	153.5	1.025	142.5	0.841	134.7	0.740	91.7	1.127	196.3	1.473	181.9	0.997	167.1	1.107	160.2	0.662	231.6
0.837	158.5	1.116	145.0	0.939	138.4	0.954	93.1	1.257	202.5	1.608	184.4	1.182	170.2	1.258	164.6	0.727	250.9
1.004	166.0	1.237	147.8	1.023	141.6	1.243	95.6	1.509	208.3	1.845	187.5	1.339	175.2	1.387	168.5	0.826	269.4
1.167	172.4	1.364	147.3	1.101	144.3	1.530	95.2	1.771	213.5	1.999	190.5	1.484	186.1	1.526	172.2	0.921	287.8
1.347	177.2	1.503	150.1	1.193	146.6	1.705	96.8	2.023	217.8	2.130	191.6	1.593	181.9	1.619	173.8	1.011	304.6
1.545	177.9	1.635	148.2	1.280	148.2	2.036	102.0	2.275	220.8	2.253	188.0	1.904	185.5	1.823	175.8	1.106	323.1
1.790	180.0	1.749	148.2	1.341	149.8	2.226	100.9	2.509	223.3	2.421	188.9	1.932	188.3	2.085	180.2	1.205	339.0
1.999	183.9	1.837	150.3	1.446	149.4	2.498	100.0					2.143	191.6	2.182	182.5	1.307	356.6
2.204	188.4	1.956	150.5	1.522	150.7			**C**	177.50	**C**	161.90	2.330	193.5	2.375	182.7	1.402	368.4
2.375	192.6	1.997	151.4	1.643	149.6	**C**	90.90	**n**	0.320	**n**	0.240	2.511	193.5	2.518	183.6	1.495	381.8
2.499	194.8	2.084	150.3	1.742	152.6	**n**	0.220	**FS**	573.9	**FS**	433.4					1.618	391.0
		2.199	153.9	1.883	153.0	**FS**	431.9	**Jic**	113.8	**Jic**	118.0	**C**	159.50	**C**	145.60	1.729	399.4
C	153.90	2.297	153.7	2.026	154.9	**Jic**	65.6					**n**	0.270	**n**	0.320	1.841	406.2
n	0.300	2.388	153.9	2.075	156.5							**FS**	433.4	**FS**	433.4	1.930	416.2
FS	557.8	2.498	151.2	1.904	156.7							**Jic**	110.0	**Jic**	93.9	2.050	417.1
Jic	101.0			2.194	152.1												
		C	132.30	2.289	151.9											**C**	295.95
		n	0.220	2.414	152.6											**n**	0.533
		FS	431.9	**C**	134.60											**FS**	566.0
		Jic	98.1	**n**	0.220											**Jic**	145.6
				FS	431.9												
				Jic	99.9												

Table B2. (Contd.)

Δa (mm)	J (kJ/m^2)	Δa (mm)	J (kJ/m^2)	Δa (mm)	J (kJ/m^2)	Δa (mm)	J (kJ/m^2)	Δa (mm)	J (kJ/m^2)	Δa (mm)	J (kJ/m^2)	Δa (mm)	J (kJ/m^2)	Δa (mm)	J (kJ/m^2)	Δa (mm)	J (kJ/m^2)
Matti Valo		Matti Valo		Matti Valo		Matti Valo		Matti Valo		Matti Valo							
BWR 308L Weld		BWR 308L Weld		BWR 308L Weld		BWR 308L Weld		BWR 308L Weld		BWR 308L Weld							
Riser pipe		Riser pipe		Control rod handle		Control rod handle		Control rod handle		Control rod handle							
RP-W3 0.6 dpa		RP-W5 0.7 dpa		CRH-W1 12 dpa		CRH-W2 12 dpa		CRH-W3 12 dpa		CRH-W4 12 dpa							
-	***199°C***	-	***249°C***	-	***259°C***	-	***25°C***	-	***25°C***	-	***259°C***						
0.000	10.6	-0.012	5.9	0.000	4.6	0.006	1.2	-0.019	0.6	-0.021	3.3						
0.021	24.9	0.022	3.4	-0.040	3.8	0.043	2.0	0.025	10.6	-0.043	5.8						
0.012	40.8	0.007	25.9	-0.074	13.9	0.139	9.5	0.065	3.9	-0.018	14.1						
0.040	55.9	0.026	48.5	0.000	12.1	0.195	12.8	0.069	12.2	0.025	2.5						
0.105	71.9	0.017	69.3	0.053	9.5	0.577	24.1	0.072	20.6	0.340	40.7						
0.166	89.5	0.082	91.8	0.069	18.8	1.003	30.2	0.103	24.7	0.546	61.4						
0.277	118.1	0.076	113.5	0.235	29.5	1.336	35.7	0.175	36.3	1.454	62.2						
0.438	146.7	0.111	135.2	0.538	53.4	1.638	37.8	0.346	64.5	1.620	63.1						
0.573	171.9	0.222	163.4	0.875	72.3	1.869	37.5	0.461	91.1								
0.755	194.6	0.359	186.6	1.003	91.5			0.747	111.8	**C**	58.59						
0.857	214.8	0.406	210.0	1.116	105.6	**C**	29.14	1.215	115.6	**n**	0.222						
0.993	228.3	0.502	239.1	1.416	112.8	**n**	0.659	1.528	124.6	**FS**	820.0						
1.104	242.6	0.676	261.4	1.656	118.3	**FS**	1009.0	1.730	137.0	**Jic**	41.6						
1.202	256.0	0.862	272.1	2.020	113.6	**Jic**	10.2	1.965	143.5								
1.335	263.6	0.974	286.2														
1.440	273.7	1.185	290.1	**C**	84.12			**C**	107.84								
1.616	280.5	1.222	307.6	**n**	0.665			**n**	0.574								
1.755	292.3	1.387	321.6	**FS**	820.0			**FS**	1009.0								
1.894	299.9	1.542	329.0	**Jic**	29.7			**Jic**	44.1								
2.057	303.3	1.681	343.9														
		1.697	328.0														
C	223.63	1.821	347.1														
n	0.466	1.935	350.3														
FS	361.0	1.954	358.6														
Jic	124.9	2.205	341.7														
		C	280.75														
		n	0.358														
		FS	431.9														
		Jic	183.8														

APPENDIX C REFERENCES

The source of the experimental data on Charpy-impact, tensile, and fracture toughness properties of austenitic stainless steel welds in the as welded and/or aged condition as well as with or without neutron irradiation, are listed below.

A.1. Hawthorne, J.R., and B.H. Menke, “Influence of Delta Ferrite Content and Welding Variables on Notch Toughness of Austenitic Stainless Steel Weldments,” in *Structural Materials for Service at Elevated Temperatures in Nuclear Power Generation*, G.V. Smith, ed., MPC–1, ASME, New York, pp. 351–364, 1975.

A.2. Chipperfield, C.G., “A Toughness and Defect Size Assessment of Welded Stainless Steel Components,” *Tolerance of Flaws in Pressurized Components*, Inst. Mech. Eng. pp. 125–137, 1978.

A.3. Gudas, J.P., and D.R. Anderson, “J-R Curve Characteristics of Piping Material and Welds,” in *Proc. 9th Water Reactor Safety Research Information Meeting*, U.S. Nuclear Regulatory Commission, October 1981.

A.4. Picker, C., A.L. Stott, and H. Cocks, “Effects of Low-Dose Fast Neutron Irradiation on the Fracture Toughness of Type 316 Stainless Steel and Weld Metal,” Proc. Specialists Meeting on Mechanical Properties of Fast Reactor Structural Materials, Chester, UK, Paper IWGFR 49/440-4, 1983.

A.5. Slama, G., P. Petrequin, and T. Mager, “Effect of Aging on Mechanical Properties of Austenitic Stainless Steel Castings and Welds,” presented at SMIRT Post-Conference Seminar 6, *Assuring Structural Integrity of Steel Reactor Pressure Boundary Components*, Aug. 29–30, Monterey, CA, 1983.

A.6. Garwood, S.J., “Fracture Toughness of Stainless Steel Weldments at Elevated Temperatures,” in *Fracture Mechanics: 15th Symposium*, R. J. Sanford, ed., ASTM STP 833, American Society for Testing and Materials, Philadelphia, PA, pp. 333–359, 1984.

A.7. Hiser, A.L., Loss, F.J., and Menke, B.H., "J-R Curve Characterization of Irradiated Low Upper Shelf Welds," Report No. NUREG/CR-3506, April 1984.

A.8. Vassilaros, M. G., R.A. Hays, and J.P. Gudas, “Investigation of the Ductile Fracture Properties of Type 304 Stainless Steel Plate, Welds, and 4-inch Pipe,” in *Proc. 12th Water Reactor Safety Research Information Meeting*, NUREG/CP-0058, Vol. 4, U.S. Nuclear Regulatory Commission, pp. 176–189, 1985.

A.9. Bernard, J., and G. Verzeletti, “Elasto-Plastic Fracture Mechanics Characterization of Type 316H Irradiated Stainless Steel up to 1 dpa,” Effects of Radiation on Materials: 12th Intl. Symp., ASTM STP 870, F.A. Garner and J.S. Perrin, eds., American Society for Testing and Materials, Philadelphia, PA, pp. 619–641, 1985.

A.10. Mills, W.J., L.A. James, and L.D. Blackburn, “Results of Fracture Mechanics Tests on PNC SU 304 Plate,” Westinghouse Hanford Report HEDL-7544, Hanford Engineering Development Laboratory, Richland, WA, 1985.

A.11. Nakagaki, M., C. Marshall, and F. Brust, "Analysis of Cracks in Stainless Steel TIG Welds," NUREG/CR-4806, BMI-2144, December 1986.

A.12. Horn, R.M., H.S. Mehta, W.R. Andrews, and S. Ranganath, "Evaluation of the Toughness of Austenitic Stainless Steel Pipe Weldments," EPRI NP-4668, Electric Power Research Institute, Palo Alto, CA, June 1986.

A.13. Landes, J.D., and D.E. McCabe, "Toughness of Austenitic Stainless Steel Pipe Welds," EPRI NP-4768, Electric Power Research Institute, Palo Alto, CA, October 1986.

A.14. Wilkowski, G., et al., "Analysis of Experiments on Stainless Steel Flux Welds," NUREG/CR-4878, BMI-2151, April 1987.

A.15. Michel, D.J., and R.A. Gray, "Effects of Irradiation on the Fracture Toughness of FBR Structural Materials," *J. Nucl. Mater*. 148, 194–203, 1987.

A.16. Mills, W.J., "Fracture Toughness of Aged Stainless Steel Primary Piping and Reactor Vessel Materials," *J. Pres. Ves. Technol. (Trans ASME)* 109, 440–448, 1987.

A.17. Mills, W.J., "Fracture Toughness of Irradiated Stainless Steel Alloys," Nucl. Technol. 82, 290–303, 1988.

A.18. Mills, W.J., "Fracture Toughness of Stainless Steel Welds," in Fracture Mechanics: Nineteenth Symposium, STP 969, ASTM, Philadelphia, PA, 330–355, 1988.

A.19. Ould, P., P. Balladon, and Y. Meyzaud, "Fracture Toughness Properties of Austenitic Stainless Steel Welds," Bull. Cercle Etud. Metaux 15, 31.1–31.12, 1988.

A.20. Faure, F., B. Houssin, and P. Balladon, "Mechanical Properties of Automatic TIG/GTA Welds of Stainless Steel Piping in Nuclear Reactors," in *Trends in Welding Research*, ASM Conf., Gatlinburg, May 14–18, 1989.

A.21. Hale, G.E., and S.J. Garwood, "Effect of Aging on Fracture Behaviour of Cast Stainless Steel and Weldments," *Mater. Sci. Technol.*, 6, 230–236, 1990.

A.22. Commission of the European Communities, *Mechanical Testing of Austenitic Steel Welded Joints*, Joint Final Report–Vol. 2, Ispra, Italy, 1990.

A.23. Strangewood, M., and S.G. Druce, "Aging Effects in Welded Cast CF–3 Stainless Steel," *Mater. Sci. Technol.*, 6, 237–248, 1990.

A.24. Vitek, J.M., S.A. David, D.J. Alexander, J.R, Keiser, and R.K. Nanstad, "Low Temperature Aging Behavior of Type 308 Stainless Steel Weld Metal," *Acta Metall.*, 39, 503–516, 1991.

A.25. Sindelar, R.L., G.R. Caskey, Jr., J.K. Thomas, J.R. Hawthorne, A.L. Hiser, R.A. Lott, J.A. Begley, and R.P. Shogan, "Mechanical Properties of 1950s Vintage Type 304 Stainless Steel Weldment Components after Low Temperature Neutron Irradiation," 16th Intl. Symp. on Effects of Radiation on Materials, ASTM STP 1175, American Society of Testing and Materials, Philadelphia, PA, pp. 714–746, 1993.

A.26. Valo, M. “Fracture toughness and Tensile Properties of Irradiated Austenitic Stainless Steel Components removed from Service,” DNo REA 35/91, VTT Reactor Laboratory, ESPOO, Finland, September 1993.

A.27. Gavenda, D.J., W.F. Michaud, T.M. Galvin, W.F. Burke, and O.K. Chopra, “Effects of Thermal Aging on Fracture Toughness and Charpy-Impact Strength of Stainless Steel Pipe Welds,” NUREG/CR-6428 ANL-95/47, May 1996.

A.28. O’Donnell, I.J., H. Huthmann, and A.A. Tavassoli, “The Fracture Toughness Behaviour of Austenitic Steels and Weld Metal Including the Effects of Thermal Aging and Irradiation,” *Intl. J. Pres. Ves. and Piping* 65 (3), 209–220, 1996.

A.29. Alexander, D.J., J.E. Pawel, L.M. Grossbeck, A.F. Rowcliffe, and K. Shiba, “Fracture Toughness of Irradiated Candidate Materials for ITER First Wall/Blanket Structures,” Effect of Radiation on Materials: 17th Intl. Symp., ASTM STP 1270, American Society of Testing and Materials, Philadelphia, PA, pp. 945–970, 1996.

A.30. Hojo, K., I. Muroya, S. Kawaguchi, K. Koyama, and K. Sakai, “Application of the Two-Criteria Approach to the Austenitic Cast Stainless Steel Pipe,” 5th International Conference on Nuclear Engineering (ICONE-5), ICONE5-2379, May 26–30, American Society of Mechanical Engineers, New York, 1997.

A.31. Alexander D.J., K.B. Alexander, M.K. Miller, R.K. Nanstad, and Y.A. Davidov, “The Effect of Aging at 343°C on the Microstructure and Mechanical Properties of Type 308 Stainless Steel Weldments,” NUREG/CR-6628, ORNL/TM-13767, November 2000.

A.32. Kim C., R. Lott, S. Byrne, M. Burke, and G. Gerzen, “Embrittlement of Cast Austenitic Stainless Steel Reactor Internals Components,” in *Proc. 6th Intl. Symp. on Contribution of Materials Investigations to Improve the Safety and Performance of LWRs*, Vol. 1, Fontevraud 6, French Nuclear Energy Society, SFEN, Fontevraud Royal Abbey, France, September 18–22, 2006.

A.32. JNES-SS Report, “Investigation Report on the Integrity of Thermally-Embrittled Cast Stainless Steel Pipe,” Nuclear Energy System Safety Division, Japan Nuclear Energy Safety Organization, Report JNES-SS-0602, 2006.

A.33. Tavassoli, A.A., “The Influence of Radiation on the Properties of Welds and Joints,” *J. Nucl. Sci. and Technol.* 155-157 105-112. 1988.

A.34. Tavassoli, A.A., J.L. Bertin, and P. Nicolino, “Effect of low and medium dose neutron irradiation on toughness of austenitic stainless steel welded joints,” Technical note, FR/MWG/P(91)777,AGT9A-9A0207 & PSM 2/7, final report, 1989.

A.35. Lucas, T., R.G. Ballinger, H. Hanninen, and T. Saukkonen, "Effect of Thermal Aging on SCC, Material Properties and Fracture Toughness of Stainless Steel Weld Metals," 15th Intl. Conf. on Environmental Degradation of Materials in Nuclear Power Systems - Water Reactors, Jeremy T. Busby, Gabriel Ilevbare, and Peter L. Andresen, eds., The Minerals, Metals & Materials Society, Warrendale, PA, pp. 883–900, 2011.

A.36. Lucas, Timothy R., "The Effect of Thermal Aging and Boiling Water reactor Environment on Type 316L Stainless Steel Welds," Doctoral Thesis, Massachusetts Institute of Technology, Cambridge, MA, May 2011.

A.37. Chen, Y., B. Alexandreanu, and K. Natesan, “Crack Growth Rate and Fracture Toughness Tests on Irradiated Cast Stainless Steels,” NUREG/CR-7184, ANL-12/56, July 2015.

A.37. Hutchinson, J.W., and P.C. Paris, "The Theory of Stability Analysis of J-Controlled Crack Growth," ASTM STP 668, pp. 37-64, March 1979.

A.37. Albrecht, P., et. al., "Tentative Test Procedure for Determining the Plane Strain JI-R Curve," Journal of Testing and Evaluation, Vol. 10, No.6, pp. 245-251, Nov. 1982.

A.37. Ernst, H.A., “Material Resistance and Instability Beyond J-Controlled Crack Growth," *Elastic-Plastic Fracture: Second Symp. Vol. I: Inelastic Crack Analysis,* ASTM STP 803, American Society for Testing and Materials, Philadelphia, PA, 1983.

APPENDIX D PREVIOUS DOCUMENTS IN SERIES

Effects of Thermal Aging on Fracture Toughness and Charpy-Impact Strength of Stainless Steel Pipe Welds, NUREG/CR-6428, ANL-95/47, May 1996.

NRC FORM 335 (12-2010) NRCMD 3.7 U.S. NUCLEAR REGULATORY COMMISSION **BIBLIOGRAPHIC DATA SHEET** *(See instructions on the reverse)*	1. REPORT NUMBER (Assigned by NRC, Add Vol., Supp., Rev., and Addendum Numbers, if any.) NUREG/CR-6428, Rev. 1 ANL/EVS-17/3
2. TITLE AND SUBTITLE Effects of Thermal Aging on Fracture Toughness and Charpy-Impact Strength of Stainless Steel Pipe Welds	3. DATE REPORT PUBLISHED MONTH: August YEAR: 2018
	4. FIN OR GRANT NUMBER
5. AUTHOR(S) Omesh K. Chopra	6. TYPE OF REPORT Technical
	7. PERIOD COVERED (Inclusive Dates)

8. PERFORMING ORGANIZATION - NAME AND ADDRESS (If NRC, provide Division, Office or Region, U. S. Nuclear Regulatory Commission, and mailing address; if contractor, provide name and mailing address.)

Environmental Science Division
Argonne National Laboratory
Argonne, IL 60439

9. SPONSORING ORGANIZATION - NAME AND ADDRESS (If NRC, type "Same as above", if contractor, provide NRC Division, Office or Region, U. S. Nuclear Regulatory Commission, and mailing address.)

Engineering Division
Office of Nuclear Regulatory Research
U.S. Nuclear Regulatory Commission
Washington, DC 20555-0001

10. SUPPLEMENTARY NOTES

11. ABSTRACT (200 words or less)

The effect of thermal aging on the degradation of fracture toughness and Charpy-impact properties of austenitic stainless steel (SS) welds has been characterized at reactor temperatures. The solidification behavior and the distribution and morphology of the ferrite phase in SS welds are described. Thermal aging of the welds results in moderate decreases in Charpy-impact strength and fracture toughness. The upper-shelf Charpy-impact energy of aged welds decreases by 50–80 J/cm^2. The decrease in fracture toughness J-R curve, or J_{Ic} is relatively small. Thermal aging has minimal effect and the welding process has a significant effect on the tensile strength. Fracture properties of SS welds are controlled by the distribution and morphology of second-phase particles. Failure occurs by the formation and growth of microvoids near hard inclusions. Differences in fracture resistance of the welds arise from differences in the density and size of inclusions. The approach used for evaluating thermal and neutron embrittlement of austenitic SS welds relies on establishing a lower-bound fracture toughness J-R curve for unaged and aged, and non-irradiated and irradiated, SS welds. The existing fracture toughness J-R curve data for SS welds have been reviewed and evaluated to define lower-bound J-R curve for austenitic SS welds in the unaged and aged conditions.

12. KEY WORDS/DESCRIPTORS (List words or phrases that will assist researchers in locating the report.)	13. AVAILABILITY STATEMENT unlimited
Thermal Embrittlement, Neutron Embrittlement, Fracture Properties, J-R Curves, Stainless Steel Welds, Cast Austenitic Stainless Steel (CASS), Thermal Aging	14. SECURITY CLASSIFICATION *(This Page)* unclassified *(This Report)* unclassified
	15. NUMBER OF PAGES
	16. PRICE

UNITED STATES
NUCLEAR REGULATORY COMMSSION
WASHINGTON, DC 20555-0001

OFFICIAL BUSINESS

@NRCgov

NUREG/CR-6428, Rev. 1

Effects of Thermal Aging on Fracture Toughness and Charpy-Impact
Strength of Stainless Steel Pipe Welds

August 2018